

Titre: Solids behaviour in fluidized beds
Title:

Auteur: Navid Mostoufi
Author:

Date: 1999

Type: Mémoire ou thèse / Dissertation or Thesis

Référence: Mostoufi, N. (1999). Solids behaviour in fluidized beds [Thèse de doctorat, École
Citation: Polytechnique de Montréal]. PolyPublie. <https://publications.polymtl.ca/8911/>

 **Document en libre accès dans PolyPublie**
Open Access document in PolyPublie

URL de PolyPublie: <https://publications.polymtl.ca/8911/>
PolyPublie URL:

**Directeurs de
recherche:** Jamal Chaouki
Advisors:

Programme: Non spécifié
Program:

UNIVERSITÉ DE MONTRÉAL

SOLIDS BEHAVIOUR IN FLUIDIZED BEDS

NAVID MOSTOUFI

DÉPARTEMENT DE GÉNIE CHIMIQUE

ÉCOLE POLYTECHNIQUE DE MONTRÉAL

THÈSE PRÉSENTÉE EN VUE DE L'OBTENTION DU DIPLÔME

DE PHILOSOPHIAE DOCTOR (Ph.D.)

(GÉNIE CHIMIQUE)

DÉCEMBRE 1999



National Library
of Canada

Acquisitions and
Bibliographic Services

395 Wellington Street
Ottawa ON K1A 0N4
Canada

Bibliothèque nationale
du Canada

Acquisitions et
services bibliographiques

395, rue Wellington
Ottawa ON K1A 0N4
Canada

Your file Votre référence

Our file Notre référence

The author has granted a non-exclusive licence allowing the National Library of Canada to reproduce, loan, distribute or sell copies of this thesis in microform, paper or electronic formats.

The author retains ownership of the copyright in this thesis. Neither the thesis nor substantial extracts from it may be printed or otherwise reproduced without the author's permission.

L'auteur a accordé une licence non exclusive permettant à la Bibliothèque nationale du Canada de reproduire, prêter, distribuer ou vendre des copies de cette thèse sous la forme de microfiche/film, de reproduction sur papier ou sur format électronique.

L'auteur conserve la propriété du droit d'auteur qui protège cette thèse. Ni la thèse ni des extraits substantiels de celle-ci ne doivent être imprimés ou autrement reproduits sans son autorisation.

0-612-53540-1

UNIVERSITÉ DE MONTRÉAL
ÉCOLE POLYTECHNIQUE DE MONTRÉAL

Cette thèse intitulée :

SOLIDS BEHAVIOUR IN FLUIDIZED BEDS

présentée par : MOSTOUFI Navid

en vue de l'obtention du diplôme de : Philosophiae Doctor

a été dûment acceptée par le jury d'examen constitué de :

M. TANGUY Philippe, Ph.D., président

M. CHAOUKI Jamal, Ph.D., membre et directeur de recherche

M. GUY Christophe, Ph.D., membre

M. DE LASA Hugo I., Ph.D., membre

In the name of God

Dedicated to

my parents, my wife Fereshteh,

and my children Kourosh and Soroush

ACKNOWLEDGMENTS

I am grateful to many people for their helpful contributions during my study in École Polytechnique. I am particularly indebted to:

My supervisor, professor Jamal Chaouki, for his leadership, constant support, encouragement, helpful discussions, bright ideas, and friendship.

Dr. Rahmat Sotudeh-Gharebaagh for all his helps and useful discussions throughout my study.

Dr. Faiçal Larachi and Dr. Larin Godfroy for teaching me how to use radioactive particle tracking facilities and their valuable hints during the data processing at the beginning.

Dr. Gregory Kennedy and Mr. Jean St. Pierre for activating the tracers.

Mr. Giordano Malossi for his assistance during the experiments.

Ms. Mariam Sepehr for translating the abstract and extended abstract into French.

The technicians of the department, Jean Huard, Robert Delisle, Daniel Duma, Carol Painchaud, and Luc Parent.

I am especially indebted to my wife and my children for their help, understanding, and patience during my study. I also would like to thank my parents and parents-in-law for their help and support at the time I needed it most.

Last, but not least, I wish to thank the Ministry of Culture and Higher Education of the Islamic Republic of Iran for making my graduate study possible.

RÉSUMÉ

Malgré le nombre faramineux de publications sur la fluidisation gaz-solide, il y a très peu d'entre elles qui se sont intéressées à la caractérisation du mouvement des particules. Ce mouvement a bien sûr une importance capitale dans plusieurs types d'opérations, par exemple les réactions catalytiques en général et particulièrement celles où le catalyseur se désactive, le séchage. Le présent travail tente de combler ce fossé.

Le mouvement de particules dans les lits fluidisés a été examiné à différents niveaux, en employant la technique du Traçage d'une Particule Radioactive (TPR). D'abord, nous avons caractérisé le coefficient de traînée d'une particule en présence de plusieurs autres ayant des propriétés similaires ou différentes. Ensuite, nous avons estimé les diffusivités des particules. Enfin, nous avons caractérisé le mouvement des particules.

Plus spécifiquement, et dans un premier temps, le mouvement d'une seule particule a été étudié dans un lit fluidisé solide-liquide. Le liquide utilisé était de l'eau. Ainsi, neuf différents types de particules ont été utilisés comme particules fluidisées. Un traceur radioactif est introduit dans le lit fluidisé afin de mesurer la vitesse de chute. Les rayons γ émis du traceur ont été détectés par huit détecteurs du scintillement NaI, placés autour du lit. Le nombre de rayons γ a ensuite été utilisé pour estimer d'abord les coordonnées du traceur en fonction du temps, ensuite les vitesses du traceur et enfin les coefficients de

traînée. Le facteur correcteur, i.e. le rapport du coefficient de traînée en présence de plusieurs particules et celui d'une seule particule est connu pour être fonction de la porosité et du nombre de Reynolds terminal de la particule. Grâce à cette étude, il a été trouvé que ce facteur est aussi fonction du nombre d'Archimède des particules fluidisées. Une corrélation a été développée pour calculer ce facteur correcteur. Celle-ci fait intervenir le nombre de Reynolds terminal de la particule, le nombre d'Archimède des particules fluidisées et d'un paramètre géométrique qui est le rapport du diamètre de la particule sur le diamètre des particules fluidisées. De plus, nous avons montré que les modèles qui calculent la poussée d'Archimède en utilisant la densité du fluide peuvent prédire la vitesse de la particule dans le lit fluidisé d'une meilleure façon que ceux qui l'évaluent en utilisant la densité moyenne du lit.

Dans un deuxième temps, le comportement local des lits fluidisés a été examiné dans un lit fluidisé gaz-solide à température ambiante et à pression atmosphérique. Le gaz utilisé est de l'air. Quant au solide employé, il s'agit de sable ou de particules FCC. Les expériences ont été effectuées à la fois dans les régimes à bulles et turbulent. Les diffusivités locales axiale et radiale du solide ont été calculées à partir de la position et du temps obtenus dans des expériences TPR, faisant appel à seize détecteurs. Les résultats obtenus montrent que les diffusivités augmentent avec la vitesse superficielle du gaz et sont corrélées linéairement au gradient de vitesse du solide axial. La diffusivité du solide dans un lit de FCC est plus

haute que celle mesurée dans un lit de sable avec la même vitesse superficielle d'excès de gaz (différence de la vitesse superficielle et la vitesse minimale de fluidisation).

Dans un troisième temps, le comportement global des particules du lit fluidisé a été étudié dans la direction axiale en utilisant les données obtenues par TPR. Ainsi, la dispersion globale, le mouvement axial restreint (vers le haut ou vers le bas), et le mouvement axial global ont été étudiés dans cette partie en utilisant les mêmes données expérimentales que pour la partie précédente. La valeur du coefficient de dispersion des particules a été évaluée à partir de la dispersion globale du solide. Nous avons trouvé qu'elle était constante dans la plage des conditions expérimentales de ce travail. Le test de variance développé par Levenspiel et Fitzgerald a été appliqué sur la distribution des temps de séjour (DTS) du solide pour les déplacements restreints vers le haut et bas. Les résultats du test de variance ont montré clairement qu'un déplacement ascendant du solide peut être expliqué par un mécanisme de type diffusif, tandis que le mécanisme du déplacement descendant doit être considéré comme convectif. Le test de variance du déplacement axial non-restreint du solide a montré que ce type de mouvement ne peut être expliqué par aucun des deux mécanismes mentionnés ci-dessus. Pour le modéliser, nous avons supposé que les particules se déplacent selon les deux mécanismes diffusif et convectif. En comparant la DTS avec cette formulation, nous avons pu estimer une vitesse efficace (plus grand que la vitesse moyenne du solide mais moins que la vitesse d'une seule particule) du solide qui ne dépend que de la vitesse superficielle du gaz et des propriétés des particules. Ainsi, nous avons montré que

celle-ci était plus faible que la vitesse d'une seule particule se déplaçant dans un lit fluidisé aux mêmes conditions. Ceci peut être expliqué par le fait que les particules ne se déplacent pas séparément dans le lit fluidisé mais sous forme d'agglomérats qui exercent une plus grande force résistante à leurs déplacements que celle d'une particule isolée.

ABSTRACT

The movement of solids in fluidized beds was investigated at different levels by employing the Radioactive Particle Tracking technique (RPT). In the first step, the movement of a single particle in liquid fluidized beds has been studied. The liquid was water and nine different types of particles were used as fluidized particles. A radioactive tracer was dropped into the fluidized bed in order to measure its settling velocity. Emitted γ -rays from the tracer were detected by eight NaI scintillation detectors placed around the bed. The number of counts of γ -rays were then used to calculate the coordinates of the tracer from which the velocity of the tracer and then the effective drag coefficient were calculated. The correction factor, i.e., the ratio of effective drag coefficient over standard drag coefficient, is known to be a function of the porosity and terminal Reynolds number of the falling particle and was found from the present study to be also a function of Archimedes number of the fluidized particles. A correlation has been developed for calculating the correction factor as a function of terminal Reynolds number of the falling particle, Archimedes number of the fluidized particles and a geometric parameter which is the ratio of diameters of the falling particle to the fluidized particles. It was shown in this study that the models which calculate the buoyancy force exerted on a single particle based on the fluid density can predict the slip velocity of particle in the fluidized bed better than those evaluate the buoyancy force based on the bulk density of the bed.

In the second step, the local behavior of fluidized beds was investigated in a gas-solid fluidized bed. The gas was air at room temperature and atmospheric pressure and the solids were sand or FCC powder. The experiments were done in both bubbling and turbulent regimes of fluidization. Local axial and radial diffusivity of solids were calculated from the time-position data obtained in RPT experiments employing sixteen detectors. The results showed that the diffusivities increase with gas superficial velocity and are linearly correlated to the axial solid velocity gradient. Solid diffusivity in a bed of FCC was higher than that of a bed of sand at the same excess gas superficial velocity.

In the third step, the global behavior of fluidized beds in axial direction was studied. The RPT data of the previous section were also used for calculations of this part. A variety of solids behaviors, including natural dispersion, restricted axial movement, and unrestricted axial movement of solids, was studied in this section by processing the data in an appropriate manner. The value of dispersion coefficient of solids was evaluated from the natural dispersion of solids and was found to be constant under the experimental conditions of this work. The variance test was performed on the Residence Time Distribution (RTD) of solids in the restricted upward and downward movement. The results of the variance test clearly showed that upward movement of solids could be explained by a diffusive mechanism while the mechanism of downward movement of solids should be considered as convective. The variance test for unrestricted axial movement of solids showed that this type of movement can be explained by neither of the two above mentioned mechanisms. In order to model the

axial movement of the solids, it was assumed that solids move according to the two diffusive and convective mechanisms. By comparing the RTD of unrestricted movement of solids with the unsteady state formulation of the solid movement it was found that the solid velocity in the convective term of the model have to be less than the velocity of a single particle moving in a fluidized bed at the same condition. This fact confirms that the solid particles do not move separately in the fluidized bed, but move as a part of a solid aggregate which exercises a drag force greater than that of a single particle and therefore, move at a lower velocity.

CONDENSÉ EN FRANÇAIS

Malgré le nombre faramineux de publications sur la fluidisation gaz-solide, il y a très peu d'entre elles qui se sont intéressées à la caractérisation du mouvement des particules. Ce mouvement a bien sûr une importance capitale dans plusieurs types d'opérations, par exemple les réactions catalytiques en général et particulièrement celles où le catalyseur se désactive, le séchage. Le présent travail tente de combler ce fossé.

Le mouvement de particules dans les lits fluidisés a été examiné à différents niveaux, en employant la technique du Traçage d'une Particule Radioactive (TPR). D'abord, nous avons caractérisé le coefficient de traînée d'une particule en présence de plusieurs autres ayant des propriétés similaires ou différentes. Ensuite, nous avons estimé les diffusivités des particules. Enfin, nous avons caractérisé le mouvement des particules.

La technique du traçage de particule radioactive (TPR) a été employée dans l'étude présente pour caractériser le mouvement d'un traceur radioactif dans le lit fluidisé. C'est une technique expérimentale non-intrusive utilisant la détection de rayons γ issus d'un isotope artificiel. Un des principaux buts qu'elle permet d'atteindre est la cartographie en 3 dimensions de l'écoulement des phases solides dans les lits fluidisés.

La TPR est la variante la plus puissante des méthodes dynamiques non-intrusives (Chaouki et al, 1997). Son principe est basé sur la détection de rayons γ énergétiques émis par une particule radioactive introduite dans le réacteur et dynamiquement similaire à la phase à tracer (Larachi et al., 1994, 1995). Le mouvement de cette particule est suivi par un réseau de détecteurs à scintillation stratégiquement localisés autour du réacteur. Les rayons (γ) utilisés sont généralement du ^{46}Sc , ^{198}Au and ^{99}Mo qui sont obtenus par l'activation de neutron dans le réacteur nucléaire Slowpoke de l'École Polytechnique.

Dans la première partie de cette étude, les vitesses d'un traceur radioactif ont été mesurées dans un lit fluidisé liquide-solide avec différentes particules. La colonne est faite d'un tube Plexiglas avec un diamètre interne de 100 mm et une hauteur de 1500 mm. L'eau à 25°C a été introduite dans le lit à travers un distributeur qui assure l'écoulement axisymétrique de l'eau à travers le lit fluidisé. Dans le distributeur, l'eau traverse un cône d'une hauteur de 150 mm rempli avec des billes de verre de 4 mm de diamètre, une plaque perforée et finalement un lit d'une hauteur de 210 mm rempli avec des billes de verre de 2 mm de diamètre. Le débit de l'eau a été mesuré par un rotamètre. Neuf différentes particules, avec un nombre d'Archimède variant de 7.92×10^2 à 2.72×10^5 , ont été utilisées. Deux traceurs de 3 mm, presque identiques, ont été utilisés dans ces expériences. Les traceurs sont composés d'un mélange de poudre de la lime du soda et de l'oxyde du scandium (10 – 12 % de Sc) fondu à de hautes températures. L'isotope ^{46}Sc produit émet des rayons γ qui ont été comptés par huit détecteurs placés sur les rails glissants.

Avant de commencer l'expérience du traçage de la particule, le débit de l'eau et les hauteurs du lit ont été mesurés dans les deux états de repos et fluidisé. Puis le traceur a été introduit dans le lit par le haut du lit, presque au centre de la colonne, et immédiatement les détecteurs ont commencé à compter le nombre des rayons γ . Après un certain temps passé dans le lit fluidisé, le traceur atteint une vitesse de chute constante. Seulement la partie constante a été considérée dans le calcul de la vitesse terminale. Cette partie est située entre 500 mm et 100 mm au-dessus du sommet du distributeur. Cette précaution a été appliquée pour s'assurer que le traceur a atteint une vitesse constante où l'effet probable du bout dû au distributeur n'est pas pris en compte. À chaque fois que le traceur touche le distributeur, il est récupéré du fond de la colonne. La vitesse de chute du traceur pour chaque condition expérimentale, i.e., différentes particules fluidisées et différents débits d'eau a été mesurée trois fois avec la méthode décrite ci-dessus. La moyenne arithmétique de ces trois vitesses a été considérée comme vitesse terminale du traceur pour cette condition expérimentale. Les expériences ont montré une bonne reproductibilité dans la partie du lit mentionnée ci-dessus. La vitesse terminale du traceur a été mesurée pour différentes particules fluidisées et différents débits de l'eau.

Basée sur les données obtenues dans ce travail et d'autres données de la littérature, une nouvelle corrélation a été développée pour prédire le facteur de correction. Le facteur correcteur, i.e. le rapport du coefficient de traînée en présence de plusieurs particules et celui d'une seule particule est connu pour être fonction de la porosité et du nombre de Reynolds

terminal de la particule. Grâce à cette étude, il a été trouvé que ce facteur est aussi fonction du nombre d'Archimède des particules fluidisées. Une corrélation a été développée pour calculer ce facteur correcteur. Celle-ci fait intervenir le nombre de Reynolds terminal de la particule, le nombre d'Archimède des particules fluidisées et d'un paramètre géométrique qui est le rapport du diamètre de la particule sur le diamètre des particules fluidisées.

Dans la première partie de ce travail, nous nous sommes attaqués à une autre question fondamentale qui est la méthode du calcul de la poussée d'Archimède agissant sur une particule dans un lit fluidisé. L'évaluation de cette force est un sujet de discorde. Quelques auteurs affirment qu'elle devrait être calculée en se basant sur la densité moyenne du lit. D'autres croient qu'elle devrait être basée seulement sur la densité du fluide. Dans ce travail, nous avons conclu qu'un modèle utilisant la densité moyenne n'est pas capable de prédire correctement la vitesse de la particule dans les cas où la densité moyenne du lit est très différente de la densité du fluide. Cependant, le modèle de la densité du fluide est capable de prédire la vitesse de la particule dans des lits fluidisés sans prendre en compte la densité moyenne du lit. Dans le cas d'un lit fluidisé très dilué (porosité supérieure à 0.8), les deux méthodes sont pratiquement équivalentes.

Dans la deuxième partie de cette étude, le comportement local des solides a été étudié. Les expériences dans cette partie ont été réalisées dans un lit fluidisé gaz-solide. La colonne a été faite d'un tube plexiglas avec un diamètre interne de 152 mm et une hauteur de 1500 mm.

L'air à température ambiante est introduit dans le lit à travers une partie conique. Le distributeur d'air est de type tuyère. Le débit d'air a été mesuré par une plaque à orifice connectée à un manomètre d'eau. Un cyclone placé à la sortie de l'air de la colonne retourne les solides au lit.

Le solide utilisé dans les expériences est du sable. Dans quelques expériences, pour avoir une comparaison, nous avons également utilisé du FCC. La hauteur initiale du lit est de 0.22 m (1.5 fois le diamètre de la colonne). Les traceurs ont été faits d'un mélange de poudre d'or et de la résine époxy. La proportion d'or et de la résine d'époxy dans le mélange a été choisie de manière à ce que la densité de la particule soit égale à celle du sable. Les traceurs ainsi fabriqués avaient des dimensions de 420, de 500, et de 600 μm . L'isotope ^{198}Au produit émet des rayons γ qui sont comptés par seize détecteurs sur des rails glissants situés autour du lit. Deux ordinateurs enregistrent simultanément le nombre de rayons γ détectés par chaque détecteur pour une période d'échantillonnage de 20 ms. Dans chaque expérience, un seul traceur a été placé dans le lit pour se déplacer librement avec les autres particules à l'intérieur du lit. Chaque expérience dure approximativement 5 heures. Ainsi pour chaque expérience, le traceur est localisé 820,000 fois. À la fin de chaque expérience, le lit est vidé et le traceur est récupéré des solides pour être utilisé dans une expérience ultérieure. Les vitesses superficielles de l'air sont de 0.9 à 2 m/s pour des expériences avec du sable, et elles sont de 0.44 à 0.9 m/s pour des expériences avec de la poudre FCC.

Les résultats de ces expériences montrent que les solides ne se déplacent pas indépendamment dans un lit fluidisé mais comme des agrégats soit dans le sillage d'une bulle ou dans la phase émulsion. Toutes les quantités évaluées dans la présente étude (les vitesses des particules, la diffusivité du solide...) montrent qu'elles changent seulement avec la vitesse superficielle du gaz et elles sont indépendantes de la dimension du traceur (dans la gamme des diamètres de particules utilisées). En d'autres termes, les particules ne se déplacent pas individuellement. Chaque particule est attachée à un agrégat de solides dans le lit dense, dans le nuage ou le sillage des bulles, et elle se déplace avec lui jusqu'à ce qu'elle s'en détache. Alors la particule entre dans un autre ensemble de solides et continue son mouvement avec celui-ci.

Le taux de cisaillement axial, dV_z/dr , a un effet considérable sur la diffusivité des solides. La diffusivité des particules est une fonction linéaire de leur gradient de vitesse axial. Le gradient de vitesse radiale, dV_r/dr , a un effet moindre (au moins un ordre de grandeur plus petit). Deux corrélations ont été développées dans cette étude pour prédire la diffusivité axiale et radiale des particules à un taux de cisaillement nul. Nous devons remarquer que la diffusivité des solides change plus rapidement à la paroi, où le taux de cisaillement est important, et elle change moins au centre de la colonne, où la valeur du taux de cisaillement tend vers zéro. Par conséquent, dans les réacteurs industriels où l'effet de paroi est négligeable, la valeur de diffusivité des particules à un taux de cisaillement nul peut être considérée comme une valeur moyenne raisonnable.

La diffusivité axiale des particules à un taux de cisaillement nul dans un lit de particules FCC a été obtenue, et elle est identique à celle des particules du sable. (Signalons que la taille de la particule poursuivie est cependant beaucoup plus grosse que les particules de FCC). Par contre, la diffusivité radiale dans un lit de FCC est plus grande que celle des particules du sable à une vitesse superficielle d'excès de gaz donnée. Ce qui explique que le mélange radial des particules FCC est plus efficace que celui du sable.

Dans la troisième partie de ce travail, le mouvement global des particules a été étudié dans les lits fluidisés. Les mêmes expériences de la deuxième partie de l'étude présente ont été réexaminées pour déterminer les mécanismes de mélange et pour estimer les propriétés du mouvement global des particules.

Le coefficient global de la dispersion du solide, obtenu par l'injection de particules en bas ou en haut du lit, montre une valeur constante d'à peu près $0.05 \text{ m}^2/\text{s}$ dans la gamme de la vitesse superficielle du gaz employée dans ce travail. Il est plus élevé que celui prédit par les corrélations existantes dans la littérature. De plus, le coefficient de la dispersion des particules injectées en haut du lit est légèrement plus grand que celui obtenu pour des particules injectées proche du distributeur. Cependant, les données expérimentales montrent clairement que le modèle de type diffusif (hypothèse pour l'estimation de ce coefficient) n'est pas adéquat pour rendre compte de l'écoulement complexe des particules.

Le mouvement restreint des particules se déplaçant exclusivement d'un bout à l'autre du lit (soit du bas en haut ou du haut vers le bas) a aussi été étudié. En utilisant le test de variance, développé par Levenspiel et Fitzgerald (1983), sur les courbes de la distribution de temps de séjour (DTS), on a montré que le mouvement ascendant de particules dans le lit dense est de type diffusif alors que leur mouvement descendant est plutôt convectif. Ce comportement peut être justifié par la forte fréquence d'interactions entre les bulles qui obligent les particules à interagir entre elles. D'autre part, le solide descend comme des agrégats avec peu d'interactions entre eux.

En analysant la DTS des particules en ne tenant pas compte de la direction de leur écoulement (mouvement sans restriction), nous avons montré qu'elle ne peut être décrite ni par un modèle de type convectif ni diffusif seul. Un modèle diffusif-convectif a été alors proposé pour décrire le mouvement axial des particules dans lequel la vitesse de la particule a été remplacée par une vitesse effective qui tient compte de la formation d'agrégats dans le lit. Ce modèle est capable de prédire le comportement des particules à partir de faibles vitesses superficielles du gaz, où le mélange de particules a eu lieu seulement grâce à la diffusion, jusqu'aux très hautes vitesses superficielles du gaz, où toutes les particules se déplacent indépendamment les unes des autres. La vitesse effective du solide a été estimée en tenant compte des courbes DTS. Elle est nulle à des vitesses superficielles du gaz proche de la vitesse minimale de fluidisation. Elle est égale à la vitesse de la particule seule aux très hautes vitesses superficielles du gaz. Dans les expériences avec FCC, la vitesse effective n'a

pas pu être évaluée à cause de la grosseur de la particule poursuivie.

Les expériences réalisées dans ce travail couvrent une large gamme de vitesses superficielles de gaz allant de la fluidisation à bulles au régime turbulent. Tous les paramètres que nous avons estimés dans ce travail sont soit constants (par exemple la dispersion du solide), soit augmentent d'une manière monotone avec la vitesse superficielle du gaz (par exemple la vitesse effective). On peut conclure alors que la transition du régime à bulles au régime turbulent n'est pas brusque. En d'autres termes, cette transition est essentiellement graduelle et le comportement du lit en régime turbulent peut être considéré comme une interpolation entre le régime à bulles et le régime circulant.

TABLE OF CONTENTS

DEDICATION	iv
ACKNOWLEDGMENTS	v
RÉSUMÉ	vii
ABSTRACT	xi
CONDENSÉ EN FRANÇAIS	xiv
TABLE OF CONTENT	xxiii
LIST OF TABLES	xxvi
LIST OF FIGURES	xxviii
LIST OF APPENDICES	xxxviii
LIST OF ABBREVIATIONS AND SYMBOLS	xxxix
CHAPTER 1 : INTRODUCTION	1
1. Introduction	1
2. Objectives	6
3. Thesis Structure	7
CHAPTER 2 : PREDICTION OF EFFECTIVE DRAG COEFFICIENT IN FLUIDIZED BEDS	9
2.1 Abstract	10
2.2 Introduction	11
2.3 Theory	13

2.4	Experimental	15
2.4.1	Experimental Set-up	16
2.4.2	Radioactive Particle Tracking System	17
2.4.3	Experimental Procedure	17
2.5	Results and Discussion	18
2.5.1	Analysis of Experimental Data	19
2.5.2	Comparison of New Correlation with Experimental Data	20
2.6	Statistical Analysis of the New Correlation	24
2.8	Prediction of Slip Factor	24
2.6	Conclusions	26
2.9	References	27
CHAPTER 3 : LOCAL SOLID MIXING IN GAS-SOLID FLUIDIZED BEDS		43
3.1	Context	44
3.2	Abstract	45
3.3	Introduction	46
3.4	Theory	48
3.5	Experimental	50
3.6	Results and Discussion	52
3.7	Conclusions	60
3.8	References	62

CHAPTER 4 : ON THE AXIAL MOVEMENT OF SOLIDS IN GAS-SOLID FLUIDIZED	
BEDS	80
4.1 Context	81
4.2 Abstract	81
4.3 Introduction	82
4.4 Experimental	84
4.5 Treatment of Data	86
4.5.1 Overall Dispersion of Solids	86
4.5.2 Restricted Axial Movement of Solids	90
4.5.3 Unrestricted Axial Movement of Solids	97
4.6 Conclusions	107
4.7 Calculation of the Single Particle Velocity	110
4.8 References	111
CONCLUSIONS	133
RECOMMENDATIONS	138
GENERAL BIBLIOGRAPHY	140
APPENDICES	150

LIST OF TABLES

Table 2.1	Fluidized particles used throughout the experiments	32
Table 2.2	Radioactive tracers used in the experiments	32
Table 2.3	Original experimental data obtained in this work	33
Table 3.1	Properties of the solids	65
Table 3.2	Summary of experimental conditions	66
Table 4.1	Properties of the solids	116
Table 4.2	Summary of experimental conditions	117
Table 4.3	The constants of Eqs. (4.7) and (4.8)	118
Table B.1	Size distribution of the bed materials	184
Table B.2	The values of parameters in Eqs. (B.27-B.31) ($r/R = 0$)	185

Table C.1 Size distribution of the bed materials 217

LIST OF FIGURES

Figure 2.1	Velocities of different components in a system of a particle falling in a fluidized bed	34
Figure 2.2	Schematic of the experimental set-up. 1- Fluidized bed, 2- Stainless steel screen, 3- 2 mm glass beads, 4- Perforated plate, 5- 4 mm glass beads, 6- Water inlet, 7- Detector	35
Figure 2.3	Axial coordinate of the tracer falling in a fluidized bed of glass beads, calculated based on the count rate of the detectors at every 20 ms. Only one out of five points is shown in this figure	36
Figure 2.4	Experimental m vs Ar , based on the data presented in Table 2.3	37
Figure 2.5	Parity plot of calculated m against experimental m	38
Figure 2.6	Comparison between experimental slip velocity and calculated slip velocity (Data from Table 2.3)	39

Figure 2.7	Comparison between experimental slip velocity and calculated slip velocity (Data from Van der Wielen et al., 1996)	40
Figure 2.8	Comparison between experimental slip velocity and calculated slip velocity (Data from Martin et al., 1981)	41
Figure 2.9	Comparison between experimental and calculated slip factor. Calculated based on this work: black keys; Calculated from the correlation presented in Patience et al. (1992): white keys.	42
Figure 3.1	Experimental set-up and typical configuration of the detectors	67
Figure 3.2	Particle size distribution of the solids employed in this work	68
Figure 3.3	Sample trajectory of the tracer (Sand, $U_0 = 1$ m/s, $d_T = 420$ μ m). Solid lines are the parts that initiate their move from the cell: 150 mm $< z < 200$ mm , 19.1 mm $< r < 28.6$ mm	69
Figure 3.4	Self diffusion of 1000 tracers virtually injected in the imaginary compartment 150 mm $< z < 200$ mm , 19.1 mm $< r < 28.6$ mm (Sand, $U_0 = 1$ m/s, $d_T = 420$ μ m)	70

Figure 3.5a	Mean square displacement of 1000 tracers virtually injected in the imaginary compartment $150 \text{ mm} < z < 200 \text{ mm}$, $19.1 \text{ mm} < r < 28.6 \text{ mm}$ (sand, $U_0 = 1 \text{ m/s}$, $d_T = 420 \text{ }\mu\text{m}$): (a) axial displacement	71
Figure 3.5b	Mean square displacement of 1000 tracers virtually injected in the imaginary compartment $150 \text{ mm} < z < 200 \text{ mm}$, $19.1 \text{ mm} < r < 28.6 \text{ mm}$ (sand, $U_0 = 1 \text{ m/s}$, $d_T = 420 \text{ }\mu\text{m}$): (b) radial displacement	72
Figure 3.6a	Solid diffusivity as a function of radial position (sand, $d_T = 420 \text{ }\mu\text{m}$): (a) axial solid diffusivity	73
Figure 3.6b	Solid diffusivity as a function of radial position (sand, $d_T = 420 \text{ }\mu\text{m}$): (b) radial solid diffusivity	74
Figure 3.7	Eulerian velocity field of solids at different gas superficial velocities (sand, $d_T = 420 \text{ }\mu\text{m}$)	75
Figure 3.8	Axial and radial solid velocity gradient (sand, $d_T = 420 \text{ }\mu\text{m}$)	76

Figure 3.9	Axial solid diffusivity as a function of axial solid velocity gradient (sand, $d_T = 420 \mu\text{m}$)	77
Figure 3.10a	Solid diffusivity in the absence of velocity gradient: (a) axial solid diffusivity	78
Figure 3.10b	Solid diffusivity in the absence of velocity gradient: (b) radial solid diffusivity	79
Figure 4.1	Experimental set-up and typical configuration of the detectors	119
Figure 4.2	Overall diffusion of 1000 tracers injected to the top of the bed (sand, $U_0 = 1 \text{ m/s}$, $d_T = 420 \mu\text{m}$)	120
Figure 4.3	Calculated dispersion coefficient based on overall dispersion of solids	121
Figure 4.4a	Restricted movement of solids (sand, $U_0 = 1 \text{ m/s}$, $d_T = 420 \mu\text{m}$): (a) Upward	122
Figure 4.4b	Restricted movement of solids (sand, $U_0 = 1 \text{ m/s}$, $d_T = 420 \mu\text{m}$): (b) Downward	123

Figure 4.5	Evolution of restricted upward movement of solids (sand, $U_0 = 1$ m/s, $d_T = 420$ μ m). The RTD of solids was studied between the two dashed lines	124
Figure 4.6	Performing the variance test on the RTD curve of restricted axial movement of solids in the dense bed (sand, $U_0 = 1$ m/s, $d_T = 420$ μ m)	125
Figure 4.7	Dispersion coefficient of solids in strictly upward movement	126
Figure 4.8a	Unrestricted movement of solids (sand, $U_0 = 1$ m/s, $d_T = 420$ μ m): (a) Upward	127
Figure 4.8b	Unrestricted movement of solids (sand, $U_0 = 1$ m/s, $d_T = 420$ μ m): (b) Downward	128
Figure 4.9	Performing the variance test on the RTD curve of unrestricted axial movement of solids in the dense bed (sand, $U_0 = 1$ m/s, $d_T = 420$ μ m)	129
Figure 4.10	Ratio of effective solid velocity to single particle velocity as a function of excess gas superficial velocity for experiments with sand	130

Figure 4.11	Relative cluster size in dense bed as a function of excess gas superficial velocity.	131
Figure 4.12	Comparison between calculated and experimental mean residence time of solids at 300 mm distance from the injection point.	132
Figure A.1	The plexiglas column - Side view	153
Figure A.2	The plexiglas column - Top view	154
Figure A.3	The nozzle-type distributor	154
Figure A.4	The nozzles of the distributor	155
Figure A.5	Arrangement of the cyclone	156
Figure A.6	The cyclone	157
Figure B.1	Probability distribution model of the local voidage ε	186

- Figure B.2 Change in the minimum voidage of the emulsion phase, ϵ_{min} and the maximum voidage of the bubble phase, ϵ_{max} with U_g for FCC and sand particles ($r/R = 0$ and $r/R = 5/6$) 187
- Figure B.3 Evolution of the probability distribution function of the local voidage with U_g at $r/R = 0$. (a) FCC; (b) sand 188
- Figure B.4 Comparison between the probability distribution functions of the local voidage at different radial positions and different U_g . (a1), (b1), (c1) FCC; (a2), (b2), (c2) sand 189
- Figure B.5 Change in the probability density function of the local voidage with U_g at $r/R = 0$. (a) FCC; (b) sand 190
- Figure B.6 Comparison between the probability density functions of the local voidage at different radial positions. (a1), (b1) FCC; (a2), (b2) sand; (a1), (a2) for the same U_g ; (b1), (b2) for the same time-averaged voidage 191
- Figure B.7 Change in the emulsion phase fraction, the time-averaged voidage, and the mean voidages of the bubble phase and the emulsion phase with U_g at $r/R = 0$; (a) FCC; (b) sand 192

- Figure B.8 Change in the mean variance of voidage fluctuations, and the variances of voidage fluctuations in the emulsion phase and the bubble phase with U_g at $r/R = 0$. (a) FCC; (b) sand 193
- Figure B.9 Comparison between experimental and simulated probability density functions of the local voidage ($r/R = 0$) 194
- Figure B.10 Changes in the probability density function of the local voidage with increasing gas velocity ($r/R = 0$; dash line: bubbling regime; line: turbulent regime) 195
- Figure B.11 Changes in the probability of the local voidage $\varepsilon = \varepsilon_{mf}$ for the FCC particles and of the local voidage $\varepsilon = 1$ for the sand particles 196
- Figure B.12 Spatiotemporal voidage distribution between two centres of an emulsion phase element and its neighboring bubble phase at time scale ($r/R = 0$) 197
- Figure C.1 Comparison of the voidage fluctuations for the FCC and sand particles ($r/R = 0$) 218

Figure C.2	Changes in the probability density functions of local voidages with U_g ($r/R = 0$; a for the FCC; b for the sand)	219
Figure C.3	Changes in the emulsion phase fraction, the time-averaged voidage, and the mean voidages of bubble phase and emulsion phase with U_g and r/R (a1, b1 FCC; a2, b2 for the sand)	220
Figure C.4	Changes in the mean variances of voidage fluctuations, and the variance of voidage fluctuations in emulsion phase and bubble phase with U_g and r/R (a1, b1 for the FCC; a2, b2 for the sand)	221
Figure C.5	Changes in the time-mean voidages ε_r , and the two bed voidages with U_g and r/R (a1, b1 for FCC; a2, b2 for sand)	222
Figure C.6	Superficial gas velocities for the equal gas distribution between two phases at different bed positions for two particles	223
Figure C.7	Ratio of bed voidages of emulsion phase to those of bubble phase and the dependence on U_g and bed positions (a for the FCC; b for the sand)	224

Figure C.8	Changes in bed solid volume concentrations of emulsion phase and bubble phase with U_g (a for the FCC; b for the sand)	225
Figure C.9	Ratios of solid distributions of bubble phase to those of emulsion phase (a for the FCC; b for the sand)	226

LIST OF APPENDIXES

APPENDIX A	DETAILS OF THE GAS-SOLID FLUIDIZED BED SET-UP	150
APPENDIX B	CHARACTERIZATION OF DYNAMIC GAS-SOLID DISTRIBUTION IN FLUIDIZED BEDS	158
APPENDIX C	ON THE DISTRIBUTION OF GAS AND SOLIDS BETWEEN BUBBLE AND EMULSION IN FLUIDIZED BEDS	198

LIST OF ABBREVIATIONS AND SYMBOLS

CHAPTER 2 NOMENCLATURE

Ar	Archimedes number [$d^3 \rho_f (\rho - \rho_f) g / \mu_f^2$]
C_D	effective drag coefficient
$C_{D,o}$	standard drag coefficient
d	particle diameter, m
e	dimensionless voidage, defined in Eq. (2.12)
f	correction factor for drag coefficient
g	acceleration of gravity, m/s^2
k	number of data points
m	exponent in Eq. (2.7)
n	Richardson & Zaki index
R	matrix of correlation coefficients
Re	Reynold number [$d \rho_f V / \mu_f$]
V	linear velocity, m/s
U	superficial velocity, m/s
z	axial coordinate, m

Greek letters

δ	mean relative error
ϵ	volume fraction
μ	viscosity, Pa.s
ρ	density, kg/m ³
φ	slip factor

Subscripts

b	bulk
cal	calculated
exp	experimental
f	fluid
g	gas
mf	minimum fluidization
p	falling particle
s	fluidized solid
sl	slip
t	terminal

CHAPTER 3 NOMENCLATURE

a	constant defined in Eq. (3.8), m^2
C	number of photopeak counts of the detector
d_s	mean particle diameter, m
d_T	diameter of tracer, m
D_r	radial diffusivity, m^2/s
$D_{r,0}$	radial diffusivity at zero velocity gradient, m^2/s
D_z	axial diffusivity, m^2/s
$D_{z,0}$	axial diffusivity at zero velocity gradient, m^2/s
N	number of labelled particles
N_D	number of detectors
$Pe_{r,0}$	radial Peclet number at zero shear rate $[(U_0 - U_{mf})d_s/D_{r,0}]$
$Pe_{z,0}$	axial Peclet number at zero shear rate $[(U_0 - U_{mf})d_s/D_{z,0}]$
r	radial coordinate, m
r_0	reference radial coordinate, m
R	excess radial displacement, m
t	time, sec.
U_0	superficial velocity, m/s
U_c	superficial velocity at onset of turbulent fluidization, m/s
U_{mf}	minimum fluidization velocity, m/s

V_r	radial velocity, m/s
V_z	axial velocity, m/s
z	axial coordinate, m
z_0	reference axial coordinate, m
Z	excess axial displacement, m

Greek letters

$\dot{\gamma}_z$	axial velocity gradient $[dV_z/dr]$, s^{-1}
ϵ	porosity
ρ_s	solid density, kg/m^3
σ_z	standard deviation of calculated axial coordinate, m

CHAPTER 4 NOMENCLATURE

a	constant in Eq. (4.8)
A	constant in Eq. (4.7)
Ar	Archimedes number $[d_s^3 \rho_g (\rho_s - \rho_g) g / \mu^2]$
b	constant in Eq. (4.8)
c	constant in Eq. (4.8)
C	concentration of solid tracer
C_0	initial concentration of solid tracer

C_D	effective drag coefficient
$C_{D,0}$	standard drag coefficient
d_c	equivalent spherical cluster diameter, m
d_p	particle diameter, m
d_s	mean particle diameter of fluidized solids, m
d_T	diameter of tracer, m
D_{sz}	axial solid dispersion coefficient, m^2/s
D_{sup}	axial solid dispersion coefficient for strictly upward movement, m^2/s
$D_{z,0}$	axial solid diffusivity at zero shear rate, m^2/s
f	correction factor for drag coefficient
g	acceleration of gravity, m/s^2
H	height of the bed, m
L	length of the vessel, m
m	exponent in Eq. (4.15)
n	vessel length exponent in relation (4.9)
N	number of labelled particles
p	constant in Eq. (4.7)
$Pe_{z,0}$	axial Peclet number at zero shear rate $[(U_0 - U_{mf})d_p/D_{z,0}]$
Re_s	Reynolds number $[d_s\rho_s(U_0 - U_{mf})/\mu]$
Re_t	terminal Reynolds number $[d_s\rho_s U_f/\mu]$
t	time, sec.

U_0	superficial velocity, m/s
U_c	superficial velocity at onset of turbulent fluidization, m/s
U_{mf}	minimum fluidization velocity, m/s
U_t	terminal velocity of solid particle, m/s
V_p	single particle velocity, m/s
V_s	effective solid velocity, m/s
V_{sl}	slip velocity, m/s
z	axial coordinate, m

Greek letters

β	ratio of effective solid velocity to single particle velocity
δ	height of injection layer, m
ϵ	porosity
ϵ_{mf}	porosity at minimum fluidization
μ	gas viscosity, Pa.s
ρ_s	solid density, kg/m ³
ρ_g	gas density, kg/m ³
σ_t	standard deviation of the RTD curve, sec.
σ_θ	dimensionless standard deviation of the RTD curve

APPENDIX B NOMENCLATURE

- $A_{f(i)}$ parameter of Eq. (B.27) ($i=1,2,3$)
- $A_{\rho(i)}$ parameter of Eq. (B.32) ($i=1,2$)
- $A_{var-b(i)}$ parameter of Eq. (B.30) ($i=1,2,3$)
- $A_{var-e(i)}$ parameter of Eq. (B.31) ($i=1,2,3$)
- $A_{void-b(i)}$ parameter of Eq. (B.28) ($i=1,2,3$)
- $A_{void-e(i)}$ parameter of Eq. (B.29) ($i=1,2,3$)
- d_p average particle diameter, μm
- f dense phase (emulsion phase) fraction
- f^0 dense phase fraction for the two extreme phases
- k_{div0} parameter of Eq. (B.14)
- k_{div1} parameter of Eq. (B.14)
- $k_{max(1)}$ parameter of Eq. (B.13)
- $k_{max(2)}$ parameter of Eq. (B.13)
- $k_{max(n)}$ parameter of Eq. (B.13)
- k_{min} parameter of Eq. (B.12)
- m_1 number of samples for emulsion phase
- m_2 number of samples for bubble phase
- n number of scopes of equality probability in total
- $Pr^0(\varepsilon)$ probability distribution function of local voidages for the two extreme phases

- $Pr_b^0(\varepsilon)$ probability distribution function of local voidages for pure bubble phase
- $Pr_e^0(\varepsilon)$ probability distribution function of local voidages for saturated emulsion phase
- $Pr(\varepsilon)$ probability distribution function of local voidages for the two phases
- $Pr_b(\varepsilon)$ probability distribution function of local voidages for dynamic bubble phase
- $Pr_e(\varepsilon)$ probability distribution function of local voidages for dynamic emulsion phase
- $pr(\varepsilon)$ probability density function of local voidages for the two phases
- $pr_b(\varepsilon)$ probability density function of local voidages for dynamic bubble phase
- $pr_e(\varepsilon)$ probability density function of local voidages for dynamic emulsion phase
- r/R dimensionless radial position of bed
- U_c transition superficial gas velocity from bubbling to turbulent fluidization, m/s
- U_g superficial gas velocity, m/s
- U_{mf} minimum fluidization gas velocity, m/s (0.003 m/s for FCC; 0.24 m/s for sand)
- Y vector of voidages and positions

Greek letters

- α_i parameter in Beta distribution ($i=e, b$)
- β_i parameter in Beta distribution ($i=e, b$)
- ε local voidage from ε_{mf} to 1
- ε_b mean voidage of bubble phase
- ε_{div} division local voidage between bubble phase and emulsion phase

ε_e	mean voidage of emulsion phase
ε_i	local voidage corresponding to time coordinate i/n between two centres
ε_{max}	maximum local voidage
ε_{mf}	minimum fluidization voidage (0.45 for FCC; 0.42 for sand)
ε_{min}	minimum local voidage
ε_r	time-averaged voidage at arbitrary radial position
ρ_p	particle density, kg/m^3
σ_b	variance of voidage fluctuations in bubble phase
σ_e	variance of voidage fluctuations in emulsion phase

Subscripts

b	bubble phase
e	emulsion phase

APPENDIX C NOMENCLATURE

$A_{void(i)}$	parameter of Eqs. (C.5) ($i=1,2,3$)
$A_{var(i)}$	parameter of Eqs. (C.6) ($i=1,2,3$)
d_p	average particle diameter, μm
f	emulsion phase fraction

N_1	the number of samples for emulsion phase
N_2	the number of samples for bubble phase
r/R	dimensionless radial position of bed
U_g	superficial gas velocity, m/s
U_{mf}	minimum fluidization gas velocity, m/s, (0.003m/s for the FCC; 0.24 for the sand)

Greek letters

β_g	ratio of bed voidage of emulsion phase to that of bubble phase
β_p	ratio of bed solid concentration of emulsion phase to that of bubbles
ε	local voidage
ε_b	mean voidage of bubble phase
ε_e	mean voidage of emulsion phase
ε_{gb}	bed voidage of gases in bubble phase
ε_{ge}	bed voidage of gases in emulsion phase
ε_{lim}	local voidage at the transition point between bubble and emulsion phase
ε_{max}	maximum local voidage of flow structure
ε_{mf}	minimum fluidization voidage (0.45 for the FCC; 0.42 for the sand)
ε_{min}	minimum local voidage of flow structure
ε_r	average voidage at arbitrary radial position
ϕ_r	time-averaged solid volume concentration

- ϕ_{pb} bed solid volume concentration of bubble phase
- ϕ_{pe} bed solid volume concentration of emulsion phase
- ρ_p particle density, kg/m³

Subscripts

- b* bubble phase
- e* emulsion phase

CHAPTER 1 : INTRODUCTION

1.1 Introduction

Solid movement is recognized as an influential factor in the design of many physical and chemical processes involving fluidized beds. The mixing of solids in a fluidized bed has a crucial effect on the rate of mass and heat transfer in processes such as drying. In the case of fluidized reactors, the solid mixing can even control the final conversion of the chemical reaction carried out in the bed. A weak mixing in a fluidized bed may result in bypassing the fluids and formation of dead zones. In the case of exothermic reactions being carried out in a fluidized bed, improper solid mixing may cause creation of hot spots in the bed which in turn can affect the overall conversion and may damage the solids. In the case of two competing reactions taking place in a fluidized reactor, the desired reaction being the catalytic one and the undesired reaction being the homogeneous one, bad mixing can result in progress of the undesired homogeneous reaction rather than the desired catalytic one. Consequently, reliable knowledge of the mechanism of solid mixing and solid movement in the fluid beds will help in designing a more efficient unit. It has been tried in this study to investigate the movement of solids and solid mixing in three different levels, i.e., movement of a single particle, local behavior of solids, and global behavior of solids in the fluidized bed.

Several experimental techniques have been employed for studying the behaviour of solids in fluidized beds. Some of these methods are (Kunii and Levenspiel, 1991; Louge, 1997):

- Spread of a thin layer of the tracer solid
- Capacitance probe
- Fiber optic
- Residence Time Distribution (RTD)
- Axial heat flow
- Tomography
- Radioactive Particle Tracking (RPT)

Some of these instruments, such as fiber optics and capacitance probes, are able to provide local information about solids in the bed. However, these methods are intrusive, i.e., they change the local hydrodynamic of the bed at the time of data acquisition and, therefore, introduce an uncertainty in the measurement to some extent. On the other hand, techniques such as RTD or axial heat flow measurements can be done in non-intrusive form. However, these methods can only provide global information about the solids at the cross section of the bed. The Radioactive Particle Tracking (RPT) technique has this advantage over the above mentioned techniques that it is able to provide local information about the solids while is a non-intrusive method.

The experimental data in this work were obtained by the RPT technique. In this technique, a radioactive tracer, which emits γ -rays, is being pursued as long as desired by several scintillation detectors which are placed outside the bed. Therefore, the local position of the tracer can be provided by this technique without disturbing the hydrodynamic of the fluidized bed. The instantaneous, as well as time-averaged, quantities of the tracer (e.g., position,

velocity, etc.) are obtained from the results of the RPT experiments. If the density and size of the tracer is the same as the solid particles in the bed, its movement can be considered to represent the movement of all other solid particles in the bed.

The movement of a particle in a fluidized bed can be described by having a precise knowledge of the forces acting on it. These forces are gravitational, buoyancy, and drag. When the particle moves with a constant velocity, these three forces are in dynamic equilibrium with each other. In this condition the drag force is equal to the apparent weight of the particle which is the gravitational force minus the buoyancy force exerted on the particle. This simple relation can be considered as the definition of the drag force and the way it should be calculated in practice. On the other hand, in order to model the movement of a single particle, it is easier to benefit from the drag coefficient in the calculations. Thus, for calculating the effective drag coefficient in the fluidized beds, it is essential to have a good estimate of the gravity and buoyancy forces in the fluidized condition. The gravitational force is well defined by the Newton's second law. However, there is an ongoing debate between researchers on the way the buoyancy force in a fluidized bed should be evaluated. In early 1980's, Gibilaro and Foscolo claimed that the correct method of calculating the buoyancy force exerted on a single particle moving a fluidized bed is to evaluate it based on the mixture density of the bed (Foscolo et al., 1983; 1984). This definition faced strong protests from others who believed that the buoyancy force in the fluidized beds have to be determined based on the fluid density alone (Clift et al., 1987; Fan et al., 1987). There are still need for more experimental evidences on this subject to test the

validity of these two approaches.

The effective drag coefficient exerted on a single particle moving in a swarm of other particles of different type is known to be a strong function of the porosity of the bed. The researchers usually employ a Richardson-Zaki type equation for relating the effective drag coefficient (in the fluidized bed) to the standard drag coefficient (in the fluid alone). In this type of correlation, the physical properties of the falling particle is used to determine the Richardson-Zaki index. However, in the RPT experiments it is not required to see the tracer visually and therefore, it is possible to use different particles as tracer and fluidized solids and study the effect of the both type of the solids on the effective drag coefficient.

Mixing of solids in a gas-solid fluidized bed is caused by different mechanisms. Global mixing of solids occurs by gross circulation of solids due to rising gas bubbles which is called bubble-induced mixing. In this mechanism, the solids are carried up to the surface, as bubble wakes and clouds, where they are dispersed by bursting bubbles and then descend to the bottom of the bed through the emulsion. In addition to this global mixing of particles, local mixing of solids happens, while the bubbles rise, within the bubble wakes and between the wakes and the emulsion. While the first mechanism (global) is characterized by the movement of the bubbles, the second one (local) can be attributed to the random movement of the solid particles. Both these mechanisms can be described by the Fick's law of diffusion with different diffusion coefficients which are called *dispersion coefficient* for the former and *particle diffusivity* for the latter.

Local mixing of solids bed plays an important role in many physical and chemical processes carried out in a fluidized bed. For example, in the case of very rapid reactions where the reactants may convert to products before the bubble reaches the surface or interacts with the other bubbles in the bed, an undesired rate of local solid mixing results in low overall conversion and/or selectivity of the desired product and/or creating hot spots in the bed. Measurement of the local mixing rate of the solids in a fluidized bed is not an easy task to carry out because when some labelled particles are released in the bed, they will be mixed with other bed materials according to both local and global mixing mechanisms. Since the global mixing rate is usually more significant than the local, it is practically impossible to observe the local mixing rate of the solids. Consequently, most of the data reported in the literature are related to the global mixing of the solids resulting in calculation of the dispersion coefficient. However, the radioactive particle tracking technique provides the instantaneous location of a tracer for a long time from which the diffusivity of this tracer according to the random walk theory can be evaluated.

There are two types of the models for representing the global movement of the solids in the axial direction of the fluidized beds. The first type is based on the assumption that the solid mixing in a fluidized bed occurs based on a diffusion-type mechanism and therefore, attributing a dispersion coefficient, either in vertical or lateral direction, to the movement of solids in the bed (e.g., May, 1959). The second type model divides the solids into upward moving and downward moving and assumes convective motion for both of the solid flows with mass transfer between them (e.g., van Deemter, 1967). It is possible to relate the

counterflow to the dispersion model where the interchange mass transfer coefficient of solids could be associated with an effective dispersion coefficient (Kunii and Levenspiel; 1991). Both types of the models assume a mechanism, either diffusive or convective, for the movement of solids in the dense bed. In practice, it is not possible to determine the mechanism of movement of the solids in the dense bed in a specific direction. In fact, if in order to study the upward movement of the solids in the dense bed, some labelled tracers are released, for example, at the bottom of the bed, there is no guarantee that the tracers keep their upward moving direction until they reach the top of the bed and even if they do, they have to return back to the bottom of the bed when they reach the top. However, since a typical RPT experiment is being done for a long time, all kind of solid movements can be recognized in such an experiment and it is possible to study these kind of motions from the RPT data.

1.2 Objectives

The main objective of the present study is to investigate the movement of solids and solid mixing in three different levels, i.e., movement of a single particle, local behavior of solids, and global behavior of solids in the fluidized bed. Specific objectives are as follows:

- To present the effective drag coefficient in the fluidized beds as a function of porosity of the bed, physical properties of the falling particle, and physical properties of the fluidized solids.

- To examine the validity of the two different approaches for calculation of the buoyancy force acting on a particle in a fluidized bed.
- To evaluate the local properties of the solids, such as diffusivity and restitution coefficient, in gas-solid fluidized beds and study the effect of different parameters on these quantities.
- To evaluate the global properties of the solids, such as dispersion coefficient and effective velocity of solids, in gas-solid fluidized beds and study the effect of operating parameters on these quantities.
- To investigate the mechanisms of solid movement in the axial direction in gas-solid fluidized beds.

1.3 Thesis Structure

This thesis is consisted of three papers. In addition to these three papers, in which the main work and findings of the present study are introduced, there are general introduction, conclusions, and recommendations. The content of each part is described below:

- Chapter 2 is the paper titled “Prediction of Effective Drag Coefficient in Fluidized Beds” published in *Chemical Engineering Science*, volume 54, pages 851-858, February 1999. In this paper, the movement of a single particle in a fluidized bed is studied. A new correlation for the effective drag coefficient of a particle in fluidized is developed and the performance of bulk density and fluid density models for prediction of the particle velocity in fluidized beds are examined.

- Chapter 3 consists of the manuscripts titled “Local Solid Mixing in Gas-Solid Fluidized Beds” submitted to Powder Technology on September 1999. In this paper the local movement of solids is studied and local properties of the bed such as radial and axial solid diffusivity and restitution coefficient are calculated. A linear relation between the solid diffusivity and the shear rate of solids was observed. The effect of gas superficial velocity on the calculated parameters was also investigated.
- Chapter 4 presents the article “On the Axial Movement of Solids in Gas-Solid Fluidized Beds” submitted to Chemical Engineering Research and Design on October 1999. In the article, the global movement of solids in fluidized bed is studied. The mechanisms of solid movement in axial direction were investigated and the global properties of the bed in the axial direction were measured.
- The overall conclusion of the present work is given in Conclusions.
- In the Recommendations section the future works that can be done according to the findings of this study are described.
- Details of the gas-solid fluidized bed apparatus employed in the experiments are given in appendix A. Also, two more papers in which the dynamic gas-solid distribution in gas-solid fluidized bed has been investigated appear as Appendixes B and C.

CHAPTER 2 : PREDICTION OF EFFECTIVE DRAG COEFFICIENT IN FLUIDIZED BEDS

Reference:

Navid Mostoufi and Jamal Chaouki: Prediction of Effective Drag Coefficient in Fluidized Beds, Chemical Engineering Science, vol. 54, 851-858, 1999.

Key Worde :

Drag coefficient, Drag force, Buoyancy force, Liquid-solid fluidization, Fluidized beds, Radioactive particle tracking

2.1 Abstract

A radioactive particle tracking technique is used to measure classification velocity of a radioactive tracer falling in a liquid-solid fluidized bed. The liquid passing through the fluidized bed is water and nine different types of particles are used as fluidized particles. A radioactive particle is dropped into the fluidized bed in order to measure its falling velocity. Emitted γ -rays from the radioactive tracer are detected by eight NaI scintillation detectors placed around the bed. The number of counts of γ -rays are then used to calculate the coordinates of the tracer from which the velocity of the tracer is calculated. The classification velocity is used to calculate the effective drag coefficient. The correction factor, f , which is defined as the ratio of effective drag coefficient over standard drag coefficient at the same slip velocity, is then evaluated. This factor is a strong function of the porosity and may be expressed as $f = \varepsilon^m$, in which ε is the porosity of the bed. The exponent m , is well known to be dependent on terminal Reynolds number of the falling particle. It is found from the present study that it is also a function of Archimedes number of the fluidized particles. The data from this work and some other data in the literature are used to develop a correlation for calculating the correction factor as a function of terminal Reynolds number of the falling particle, Archimedes number of the fluidized particles and a geometric parameter which is the ratio of diameters of the falling particle to the fluidized particles.

2.2 Introduction

When a particle moves with a constant velocity in a swarm of different particles, the forces acting on it have to be in dynamic equilibrium. These forces are gravitational, buoyancy, and fluid drag. To understand and predict fluidization phenomena, one has to have proper expressions for these governing forces. The gravitational force is well defined based on Newton's second law. However, the two other forces, i.e., buoyancy and fluid drag, are not being evaluated as precise as the gravitational force. In fact, the drag force can be evaluated if one knows how to define the buoyancy force properly.

Evaluation of the buoyancy force exerted on a particle in the fluidized beds has been a controversial subject in the recent years. Starting with Foscolo et al. (1983, 1984), some authors state that the buoyancy, which is due to the hydrostatic pressure, should be calculated based on the bulk density of the bed (e.g., Di Felice et al., 1989; Van der Wielen et al., 1996). Others reject this expression and believe that the buoyancy force should be based on the fluid density only (e.g., Clift et al., 1987; Fan et al., 1987; Jean and Fan, 1992). They argue that calculation of the buoyancy based on the bulk density should be restricted to the case when fluidized particles are much smaller than the immersed object itself (Roche and Chavarie, 1978; Nguyen and Grace, 1978; Grbavcic and Vukovic, 1992). In this paper, we refer to the correlations founded on these two expressions as the bulk density and the fluid density correlations, respectively.

There exist a number of definitions for the effective fluid drag force exerted on a particle in a fluidized media. However, reliable determination of effective drag force is still something to be investigated. Khan and Richardson (1990) have discussed different forms of drag relationships depending on how one considers buoyancy and relative velocity. Some correlations have been given for the drag coefficient itself (e.g., Dallavalle, 1948; Barnea and Mizrahi, 1973; Panigrahi and Murty, 1991). Other correlations have been given in terms of classification velocity of the particle as a function of the physical properties of both fluid and solid (e.g., Richardson and Zaki, 1954; Garside and Al-Dibouni, 1977; Foscolo et al, 1983; Van der Wielen et al., 1996). Classification velocity of a particle moving in a swarm of particles is the velocity of the particle, measured respect to a fixed system of coordinates, when it reaches a constant value. These two types of correlations, however, are easily interchangeable, i.e., effective drag coefficient can be calculated once the classification velocity is measured, and vice versa (Joshi, 1983).

The aim of the present work is, therefore, to study the effect of different parameters on the effective drag coefficient of a particle moving in a fluidized bed. For this purpose, a fluid density correlation is improved in this work. The correlation presented recently by Van der Wielen et al. (1996) is adopted as a sample of the bulk density correlations and comparison is made between the results of the fluid density and bulk density correlations with our own experimental data and other data from the literature. The new correlation is also compared with that of Grbavcic and Vukovic (1991) which is based on calculation of the buoyancy

force using fluid density.

2.3 Theory

There are three forces acting on a single particle falling freely in a swarm of other particles (Figure 2.1). They are gravitational force, buoyancy force, and fluid drag force. When the velocity of the particle reaches a constant value, these forces must be in dynamic equilibrium, i.e., its apparent weight must be equal to the fluid drag force:

$$\frac{\pi}{6} d_p^3 (\rho_p - \rho_f) g = \frac{1}{2} \rho_f V_{p,sl}^2 \cdot \frac{\pi}{4} d_p^2 \cdot C_D \quad (2.1)$$

where $V_{p,sl}$ is the relative velocity between fluid and the particle and in this particular case it is obtained from the following equation

$$V_{p,sl} = \frac{U_f}{\varepsilon_f} + V_p \quad (2.2)$$

The effective drag coefficient may be calculated from Eq. (2.1):

$$C_D = \frac{4 d_p (\rho_p - \rho_f) g}{3 \rho_f V_{p,sl}^2} \quad (2.3)$$

The value obtained for the effective drag coefficient from Eq. (2.3) is generally greater than that of the standard drag coefficient, $C_{D,0}$, which is the case if the same particle moves in an

infinite fluid in the absence of other solid particles. In the latter case, the slip velocity is called terminal velocity and single particle drag coefficient is calculated from Eq. (2.3) as

$$C_{D.o} = \frac{4d_p(\rho_p - \rho_f)g}{3\rho_f V_{p,t}^2} \quad (2.4)$$

There are numerous correlations for the standard drag coefficient with small numerical differences. For example, it may be calculated from the following correlation given by Turton and Levenspiel (1986):

$$C_{D.o} = \frac{24}{Re}(1 + 0.173 Re^{0.657}) + \frac{0.413}{1 + 16300 Re^{-1.09}} \quad (2.5)$$

It is common to relate these two drag coefficients by a correction factor:

$$C_D = f \cdot C_{D.o} \quad (2.6)$$

Wen and Yu (1966) showed that the correction factor, f , which they called the voidage function, is a strong function of porosity of the bed. Numerous functions have been presented for relating this correction factor to the concentration of particles (e.g., Dallavalle, 1948; Richardson and Zaki, 1954; Barnea and Mizrahi, 1973; Garside and Al-Dibouni, 1977; Foscolo et al, 1983; Panigrahi and Murty, 1991; Van der Wielen et al., 1996). In two different approaches, either drag coefficient of a single particle is modified to include the particle concentration, or equations for interphase drag in packed beds have been extended

to describe fluidized beds. Cox and Clark (1991) have briefly reviewed the effective particle drag relationships.

In this study, the following simple form is considered for the correction factor:

$$f = \varepsilon_f^{-m} \quad (2.7)$$

The exponent m in Eq. (2.7) is reported to be a constant or a function of falling particle properties, namely, $Re_{p,t}$ (e.g., Richardson and Zaki, 1954; Wen and Yu, 1966; Garside and Al-Dibouni, 1977).

The effective drag coefficient, C_D , in general, is a function of particle Reynolds number, porosity of the bed and physical properties of the falling particle and the fluidized particles. Dependence of the effective drag coefficient to Re is represented by $C_{D,o}$ in Eq. (2.6). Moreover, Eq. (2.7) indicates the effect of porosity of the bed on the effective drag coefficient. Therefore, the exponent m in Eq. (2.7) must be a function of physical properties of the falling particle and the fluidized particles. In this work, variation of number m with properties of the bed solids and the falling particle is investigated.

2.4 Experimental

To obtain the effective drag coefficient of a particle falling in a fluidized media of different

particles, classification velocity of a radioactive tracer in a liquid-solid fluidized bed is measured using a radioactive particle tracking technique. This advanced velocimetry technique allows us to determine the velocity of a particle falling through fluidized solids with a good precision. Since in this technique, it is not necessary to follow the particle visually, a wide range of solid particles, having different Archimedes numbers, may be used as the fluidized particles.

2.4.1 Experimental Set-up

The experiments are done in a liquid-solid fluidized bed. Figure 2.2 shows the experimental facilities used in this study. The column is made of a Plexiglas pipe with 100 mm internal diameter and 1500 mm height. Water at 25°C is introduced into the bed through a three stage distributor which ensures axisymmetrical flow of water in the fluidized bed. In the distributor, water passes a 150 mm high cone packed with 4 mm glass beads, a perforated plate and finally a 210 mm high bed packed with 2 mm glass beads. A fine mesh screen located at the top of the latter packed bed prevents mixing of the glass beads with the bed materials. Water flow rate is measured by a rotameter and overflows from the top of the column.

Nine different particles, with Archimedes number ranging from 7.92×10^2 to 2.72×10^5 , are used as fluidized particles. Specifications of these particles are shown in Table 2.1.

2.4.2 Radioactive Particle Tracking System

Two tracers, almost identical, were used in the experiments. Specifications of these two tracers is given in Table 2.2. The tracers are made of a mixture of soda lime powder and scandium oxide (10 - 12% Sc) melted at high temperature. The tracers are activated in the SLOWPOKE nuclear reactor of École Polytechnique. The produced isotope ^{46}Sc emits γ -rays which are monitored by eight cylindrical NaI(Tl) scintillation detectors on sliding rails. A typical arrangement of the scintillation detectors around the fluidized bed is shown in Figure 2.2. A personal computer simultaneously registers the number of γ -rays detected by each detector in every sampling period. These number of counts are used later to calculate the coordinates of the tracer. Details of the system calibration and the inverse reconstruction strategy for tracer position rendition are described by Larachi et al. (1994, 1995).

2.4.3 Experimental Procedure

The classification velocities of the radioactive tracer (V_p) in liquid fluidized beds of different particles are measured in the experimental set-up described above. Water flow rate and heights of the bed, both at rest and at fluidized state, are measured prior to the start of the particle tracking experiment. The tracer is then dropped into the bed from the top and almost at the centre of the column, while the detectors have already started counting the number of γ -rays.

A sample of primary data obtained in the particle tracking experiment is shown in Figure 2.3. This figure pictures trajectories of the tracer no. 1 which is dropped three times into a fluidized bed of 1 mm glass beads. It can be seen that shortly after entering the fluidized bed, the tracer reaches a constant falling velocity. The only falling section considered in the calculation of the classification velocity is the section between 500 mm and 100 mm above the top of the distributor. This precaution is applied to ensure that either the tracer has reached the constant velocity or probable end effect due to the distributor is not taken into account.

After each time that the tracer is dropped into the bed, the bed particles are taken out and the tracer is recovered from the bottom of the column. The falling velocity of the tracer for each operating condition, namely, fluidized particles and water flow rate, is measured three times as described above. Arithmetic average of these three velocities is considered to be the classification velocity of the tracer for that specified condition. Figure 2.3 illustrates that the experiment has a good reproducibility in the above mentioned section of the bed. The classification velocity of the tracer is measured for different fluidized particles and different water flow rates.

2.5 Results and Discussion

Results of the experiments are summarized in Table 2.3. Only the average classification

velocities are reported in this table. The following analysis is done based on the data reported in Table 2.3 and the data from literature.

2.5.1 Analysis of Experimental Data

Figure 2.4 shows the exponent m obtained from these data vs Ar_s . The line in this figure indicates an approximate trend of variation of m with Ar_s . Since the value of $Re_{p,t}$ for the tracers used in this study are very close, it can be concluded that the exponent m is also a function of Ar_s . In fact, most of the available correlations in the literature are given for the case of presence of just one type of particle in the bed. As a result, such data cannot be used to study the effect of both fluidized and falling particles. Therefore, it can be proposed that m is a function of the following combination of both $Re_{p,t}$ and Ar_s . A geometric factor, d_p/d_s , is also added deliberately.

$$m = a \cdot Ar_s^b \cdot Re_{p,t}^c \cdot \left(\frac{d_p}{d_s} \right)^d \quad (2.8)$$

Our experimental results (given in Table 2.3), as well as the data reported by Matin et al. (1981) and Van der Wielen et al. (1996) are used to estimate the four constants in Eq. (2.8). A least square technique is employed to evaluate a , b , c , and d simultaneously. The result of this evaluation relates m to physical and geometrical properties of the fluidized solids and falling particle by the following correlation

$$m = 3.02 Ar_s^{0.22} \cdot Re_{p,t}^{-0.33} \cdot \left(\frac{d_p}{d_s} \right)^{0.40} \quad (2.9)$$

Figure 2.5 shows the parity plot of the values of m calculated from Eq. (2.9) against value of m calculated from the experimental data reported in this work. The values of m calculated from the data reported by Martin et al. and Van der Wielen et al. are also shown in this figure.

2.5.2 Comparison of New Correlation with the Experimental Data

The experimental data employed to predict the parameters of the present model (i.e., the data obtained in this study, the data from Martin et al., 1981 and the data from Van der Wielen et al., 1996) are also used to test the performance of the new correlation. Two other correlations from the literature are also employed to compare their predictions with the new one. They are the correlation of Grbavcic and Vukovic (1991) which is a fluid density correlation and Van der Wielen et al.'s correlation which is a bulk density one. The correlations are compared based on their prediction of the slip velocity of the falling particle.

In order to calculate the slip velocity from our correlation and that of Grbavcic and Vukovic, where the drag coefficient is being calculated first, Eq. (2.1) is rearranged as following:

$$V_{p.sl} = \sqrt{\frac{4d_p(\rho_p - \rho_f)g}{3\rho_f C_D}} \quad (2.10)$$

The effective drag coefficient, C_D , can be calculated from Eqs. (2.4) and (2.6). Eq. (2.4) can be used to evaluate the standard drag coefficient of a particle only if its terminal velocity is known. If the terminal velocity of the falling particle is not measured experimentally, it may be calculated from the correlation of Turton and Levenspiel (1986) [Eq. (2.5)]. This is iterative procedure since the terminal velocity, which is required to calculate $Re_{p,t}$, is not known at the beginning.

Estimation of the correction factor in Eq. (2.6) by our correlation is possible through Eqs. (2.7) and (2.9). Grbavcic and Vukovic's correlation for f is also given as

$$f = e^{-1.5} \quad (2.11)$$

where

$$e = \frac{\varepsilon_f - \varepsilon_{f,mf}}{1 - \varepsilon_{f,mf}} \quad (2.12)$$

The slip velocity can be calculated directly using Van der Wielen et al.'s correlation:

$$V_{p.sl} = V_{p.t} \left(\frac{\rho_p - \rho_b}{\rho_p - \rho_f} \right)^{n_p/4.8} \varepsilon_f^{0.79n_p - 1} \quad (2.13)$$

All three correlations are compared to each other based on the mean relative error of the calculated value of slip velocity compared to its experimental value. This error is defined as

$$\delta = \frac{1}{k} \sum_{i=1}^k \frac{|V_{p.sl.i.exp} - V_{p.sl.i.cal}|}{V_{p.sl.i.exp}} \quad (2.14)$$

The parity plot of the predicted and experimental slip velocity data obtained in this work is shown in Figure 2.6. As it can be seen from the plot, the points which are obtained based on the new correlation [Eq. (2.9)] are evenly distributed around the unity line. The mean relative error for these points is 9.5%. Figure 2.6 also includes the predictions of Grbavcic and Vukovic's and Van der Wielen et al.'s correlations for these data. Grbavcic and Vukovic's correlation predicts our experimental data with relative error of 14.2%. The Van der Wielen et al.'s correlation over predicts the experimental data in most of the cases. The mean relative error for these points is 27.9%.

All three correlations approach to the unity line at higher velocities and shows almost the same behaviour. It should be noted that higher velocities correspond to voidages closer to unity where the bed density tends to the liquid density and the buoyancy force calculated based on the bulk density becomes closer to that of calculated based on the liquid density. Consequently, it may be concluded that when the bulk density becomes significantly higher than the fluid density, the bulk density correlation diverges from reality.

Figure 2.7 shows the parity plot of the experimental slip velocity data from Van der Wielen et al. (1996). This graph shows that both our correlation and Van der Wielen et al.'s correlation have almost the same behaviour in predicting the experimental data. Although Van der Wielen et al.'s correlation seems to predict these experimental data better, there is no significant difference between the two types of models. The mean relative errors for the correlation presented here and Van der Wielen et al.'s model are 12.1% and 10.6%, respectively. The deviation of the present correlation from the experimental value is greater in lower velocities. Grbavcic and Vukovic's correlation under predicts the data in almost all points with a mean relative error of 22.9%.

It should be noted that in the experiments of Van der Wielen et al. (1996), the fluidized solids density and the liquid density are very close to each other (1024 kg/m^3 and 1000 kg/m^3 respectively). Therefore, in their experiments, there is no significant difference between the liquid density and the bulk density. In fact, deviation of the bulk density from the liquid density in all the cases is less than 1.5%.

In Figure 2.8, the three correlations are compared in prediction of the data reported by Martin et al. (1981). The mean relative error for our correlation is 24.7%, while it is 28.5% for Van der Wielen et al.'s model. Grbavcic and Vukovic's correlation over predicts the data in almost all points with a mean relative error of 42.0%. Once again, all correlations shorten their distance and tend to the unity line at the higher slip velocities, where the voidage of the

bed approaches to one.

2.6 Statistical Analysis of the New Correlation¹

The correlation coefficient matrix for Eq. (2.9) was calculated to be

$$R = \begin{bmatrix} 1.0000 & -0.5513 & 0.1813 & 0.0304 \\ -0.5513 & 1.0000 & -0.9142 & 0.4685 \\ 0.1813 & -0.9142 & 1.0000 & -0.6195 \\ 0.0304 & 0.4685 & -0.6195 & 1.0000 \end{bmatrix} \quad (2.15)$$

Also, the 90% confidence intervals for the constants of Eq. (2.9) were calculated as

$$\begin{aligned} 2.66 &\leq a \leq 3.38 \\ 0.11 &\leq b \leq 0.32 \\ -0.48 &\leq c \leq -0.18 \\ 0.33 &\leq d \leq 0.47 \end{aligned} \quad (2.16)$$

2.7 Prediction of Slip Factor¹

As an independent test, the model which is presented in this article is used to predict the slip factor in the riser of a circulating fluidized bed which operates at fast fluidization condition.

¹ This section is not included in the original manuscript and only provides additional information regarding the new correlation.

Assuming a one-dimensional flow with pressure drop only in gas phase and also neglecting the wall shear, solid phase momentum balance equation in the riser may be written as

$$\varepsilon_s \rho_s V_s \frac{dV_s}{dz} = - \frac{3C_D \varepsilon_s \rho_g}{4d_p} |V_s - U_g / \varepsilon_g| (V_s - U_g / \varepsilon_g) - g(\rho_s - \rho_g) \quad (2.17)$$

Solid phase mass balance in the riser is

$$\varepsilon_s \rho_s V_s = G_s \quad (2.18)$$

In the fully developed section of the riser, the left-hand side of the Eq. (2.17) vanishes and Eqs. (2.17) and (2.18) can be solved simultaneously to calculate V_s and ε_s (note that $\varepsilon_s + \varepsilon_g = 1$). The slip velocity is then calculated from the following definition

$$\varphi = \frac{U_g}{\varepsilon_g V_s} \quad (2.19)$$

Figure 2.9 compares the calculated slip factor in the riser of a fast fluidized bed with the experimental findings of some previous workers. Black keys in Figure 2.9 are calculated based on Eqs. (2.17) and (2.18) as described above. Effective drag coefficient in Eq. (2.17) is evaluated from the correlation presented in this article. The model predicts the slip factor well around 2 which agrees with the value reported by Matsen (1976) for industrial risers. Figure 2.9 also includes slip factors calculated by the correlation of Patience et al. (1992) which are shown by white keys. It can be seen that in the most cases, the model presented

here and Patience et al.'s correlation are in a good agreement with each other and even in some cases our model predicts the experimental data better than Patience et al.'s correlation. It is important to note that Patience et al.'s model is valid only in the fully developed section of the riser while the models which use momentum balance in their formulation [such as Eq. (2.17)] can be used to predict solids axial hold-up for both acceleration zone and fully developed section.

2.8 Conclusions

A new correlation is developed for prediction of the effective drag experienced by a single particle falling in a fluidized bed of different particles. In order to take particle concentration into account, the correlation is in the form of the drag coefficient of a single particle, modified by a correction factor. The correction factor strongly depends on the voidage and is also a function of the falling particle properties as well as the fluidized particles properties.

In general, the correlation developed in this article is not valid for the beds with $\epsilon_r < 0.5$ where error of calculation is extremely high and estimating the particle velocity by this method is not reasonable. This is not surprising since the correlation converges to single particle motion at its limit ($\epsilon_r = 1$). In fact, this technique sees the problem as a single particle motion with a correction to it. As a result, better results are expected in more dilute beds (less solids hold-up).

There is no significant difference between the bulk density correlation and the fluid density correlation in dilute beds ($\epsilon_f > 0.8$). In such a condition, bulk density is very close to fluid density and both models give almost the same results.

2.9 References

Barnea, E. and Mizrahi, J., 1973, Generalized approach to the fluid dynamics of particulate systems. Part I. General correlation for fluidization and sedimentation in solid multi particle systems. *Chem. Engng. J.* **5**, 171-189.

Clift, R., Seville, J. P. K., Moore, S. C. and Chavarie, C., 1987, Comments on the buoyancy in fluidized beds. *Chem. Engng. Sci.* **42**, 191-194.

Contractor, R. M., Patience, G. S., Garnett, D. I., Horowitz, H. S., Sisler, G. M. and Bergna, H. E., 1994, A new process for n-butane oxidation to maleic anhydride using a circulating fluidized bed reactor, in *Circulating Fluidized Bed Technology*, A. A. Avidan (Ed.), pp. 387-392. AIChE, New York.

Cox, J. D. and Clark, N. N., 1991, The effect of particle drag relationship on prediction of kinematic wave in fluidized beds. *Powder Technol.* **66**, 177-189.

Dallavalle, J. M., 1948, *Micrometrics: The technology of Fine Particles*, 2nd Edition.

Pitman, London

Di Felice, R., Foscolo, P. U., Gibilaro, L. G. and Rapagna, S., 1991, The interaction of particles with a fluid-particle pseudo-fluid. *Chem. Engng. Sci.* **46**, 1873-1877.

Fan, L. S., Han, L. S. and Brodkey, R. S., 1987, Comments on the buoyancy force on a particle in fluidized suspension. *Chem. Engng. Sci.* **42**, 1269-1271.

Foscolo, P. U., Gibilaro, L. G. and Waldram, S. P., 1983, A unified model for particulate expansion of fluidised beds and flow in fixed porous media. *Chem. Engng. Sci.* **38**, 1251-1260.

Foscolo, P. U. and Gibilaro, L. G., 1984, A fully predictive criterion for the transition between particulate and aggregate fluidization. *Chem. Engng. Sci.* **39**, 1667-1675.

Garside, J. and Al-Dibouni, M. R., 1977, Velocity-voidage relationship for fluidization and sedimentation in solid-liquid systems. *Ind. Eng. Chem. Process Des. Dev.* **16**, 206-214.

Godfroy, L., Patience, G. S. and Chaouki, J., 1996, Radial hydrodynamics in risers. *Ind. Eng. Chem. Res.*, **38**, 81-89.

Grbavcic, Z. B. and Vukovic, D. V., 1991, Single-particle settling velocity through liquid fluidized beds. *Powder Technol.* **66**, 293-295.

Grbavcic, Z. B., Vukovic, D. V., Jovanovic, S. D. and Littman, H., 1992, The effective buoyancy and drag on spheres in a water fluidized bed. *Chem. Engng. Sci.* **47**, 2120-2124.

Jean, R. H. and Fan, L. S., 1992, On the model equations of Gibilaro and Foscolo with corrected buoyancy force. *Powder Technol.*, **72**, 201-205.

Joshi, J. B., 1983, Solid-liquid fluidized beds: some design aspects. *Chem. Engng. Res. Des.* **61**, 143-161.

Khan, A. R. and Richardson, J. F., 1990, Pressure gradient and friction factor for sedimentation and fluidisation of uniform spheres in liquids. *Chem. Engng. Sci.* **45**, 255-265.

Larachi, F., Chaouki, J. and Kennedy, G., 1994, A γ -ray detection system for 3-D particle tracking in multiphase reactors. *Nucl. Instr. and Meth. A* **338** 568-576.

Larachi, F., Chaouki, J. and Kennedy, G., 1995, 3-D mapping of solids flow fields in multiphase reactor with RPT. *AIChE J.* **41**, 439-443.

Martin, B. L. A., Kolar, Z. and Wesselingh, J. A., 1981, The falling velocity of a sphere in a swarm of different spheres. *Trans. Instn. Chem. Engrs.* **58**, 100-104.

Matsen, J. M., 1976, Some characteristic of large solids circulation systems. *Fluidization Technology*, Keairns, D. L. (Ed.), 135-140, Hemisphere, New York.

Nguyen, T. H. and Grace, J. R., 1978, Forces on objects immersed in fluidized beds. *Powder Technol.* **19**, 255-264.

Panigrahi, M. R. and Murty, J. S., 1991. A generalized spherical multi-particle model for particulate systems: fixed and fluidized. *Chem. Engng. Sci.* **46**, 1863-1868.

Patience, G. S., 1990, *Circulating fluidized beds: Hydrodynamics and reactor modelling*, Ph. D. thesis, École Polytechnique de Montréal, Canada.

Patience, G. S., Chaouki, J., Berruti, F. and Wong, R., 1992, Scaling considerations for circulating fluidized bed riser. *Powder Technol.* **72**, 31-37.

Richardson, J. F. and Zaki, W. N., 1954, Sedimentation and fluidisation: Part I. *Trans. Instn. Chem. Engrs.* **32**, 35-53.

Roche, G. and Chavarie, C., 1978, Behaviour of shallow fluidized beds around immersed objects. *Can. J. Chem. Engng.* **56**, 281-285.

Turton, R. and Levenspiel, O., 1986, A short note on the drag correlation for spheres. *Powder Technol.* **47**, 83-86.

Van der Wielen, L. A. M., Van Dam, M. H. H. and Luyben, K. Ch. A. M., 1996, On the relative motion of a particle in a swarm of different particles. *Chem. Engng. Sci.* **51**, 995-1008.

Van Swaaij, W. P. M., Buurman, C. and Van Breugel, J. W., 1970, Sheer stress on the wall of a dense gas-solid riser. *Chem. Engng. Sci.* **25**, 1818-1820.

Wen, C. Y. and Yu, Y. H., 1966, Mechanics of fluidization. *Chem. Engng. Prog. Symp. Ser.* **62**, 100-111.

Table 2.1 Fluidized particles used throughout the experiments

Symbol	Material	Shape	$d_s \times 10^3$	ρ_s	$\epsilon_{f,mf}$	Ar_s
G ₁	Glass	Spherical	1.00	2500	0.42	1.85×10^4
G ₂	Glass	Spherical	0.35	2500	0.42	7.92×10^2
S ₁	Sand	Irregular	1.50	2650	0.45	6.86×10^4
S ₂	Sand	Irregular	1.14	2650	0.41	3.01×10^4
S ₃	Sand	Irregular	0.59	2650	0.44	4.17×10^3
PVC ₁	PVC	Cylindrical	3.81	1400	0.53	2.72×10^5
PVC ₂	PVC	Hexagonal	3.04	1400	0.49	1.39×10^5
PC	Polycarbonate	Cylindrical	2.67	1210	0.50	4.98×10^4
PS	Polystyrene	Cylindrical	2.85	1110	0.47	3.21×10^4

Table 2.2 Radioactive tracers used in the experiments

Number	$d_p \times 10^3$	ρ_p	$V_{p,t}$	$Re_{p,t}$
1	3.33	2170	0.349	1298
2	3.21	2370	0.331	1190

Table 2.3 Original experimental data obtained in this work

Fluidized Particle	Tracer No.	U_f	ε_f	V_p
G ₁	1	0.0302	0.5697	0.0469
	1	0.0440	0.6645	0.0757
	1	0.0577	0.7448	0.1070
	1	0.0714	0.8111	0.1304
G ₂	2	0.0165	0.6966	0.1640
	2	0.0302	0.8691	0.2318
	2	0.0405	0.9571	0.2714
S ₁	1	0.0371	0.5048	0.0091
	1	0.0440	0.5725	0.0096
	1	0.0577	0.6496	0.0139
	1	0.0714	0.7340	0.0389
S ₂	2	0.0302	0.5188	0.0339
	2	0.0371	0.5765	0.0285
	2	0.0488	0.6585	0.0704
	2	0.0618	0.7445	0.1026
	2	0.0714	0.7918	0.1208
S ₃	2	0.0199	0.6233	0.1436
	2	0.0302	0.7814	0.1732
	2	0.0440	0.8949	0.2421
	2	0.0577	0.9036	0.2702
	2	0.0714	0.9463	0.2439
PVC ₁	2	0.0440	0.6423	0.0643
	2	0.0508	0.6912	0.0660
	2	0.0577	0.7264	0.0979
	2	0.0646	0.7633	0.1030
PVC ₂	1	0.0336	0.5768	0.0209
	1	0.0385	0.5980	0.0627
	1	0.0474	0.6481	0.0797
	1	0.0522	0.6696	0.1041
	1	0.0577	0.7052	0.0987
	1	0.0666	0.7419	0.1450
	1	0.0714	0.7789	0.1776
PC	2	0.0233	0.6000	0.0934
	2	0.0302	0.7023	0.1120
	2	0.0440	0.8223	0.1579
	2	0.0577	0.8940	0.1778
	2	0.0714	0.9366	0.2271
PS	2	0.0165	0.7022	0.1593
	2	0.0233	0.8252	0.2265
	2	0.0302	0.9197	0.2604
	2	0.0371	0.9633	0.2744

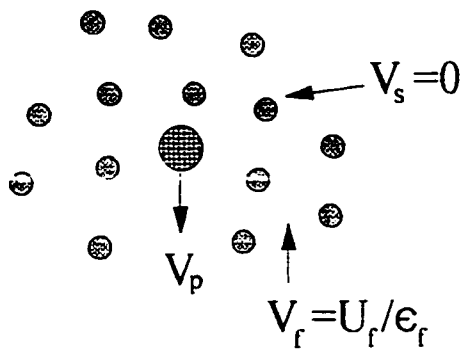


Figure 2.1 Velocities of different components in a system of a particle falling in a fluidized bed.

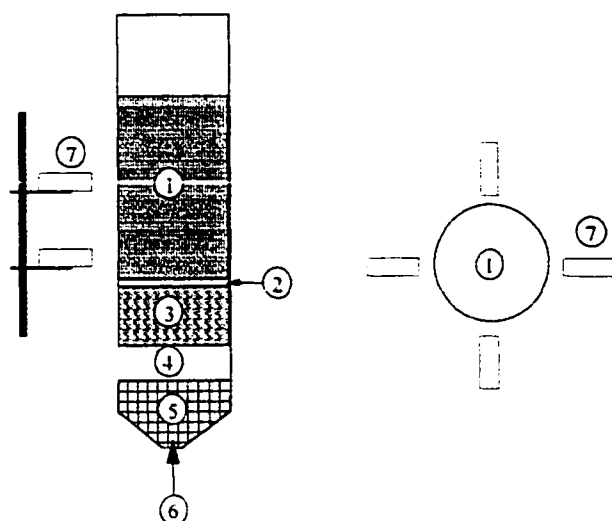


Figure 2.2 Schematic of the experimental set-up.
1- Fluidized bed, 2- Stainless steel screen, 3- 2 mm glass beads, 4- Perforated plate, 5- 4 mm glass beads, 6- Water inlet, 7- Detector.

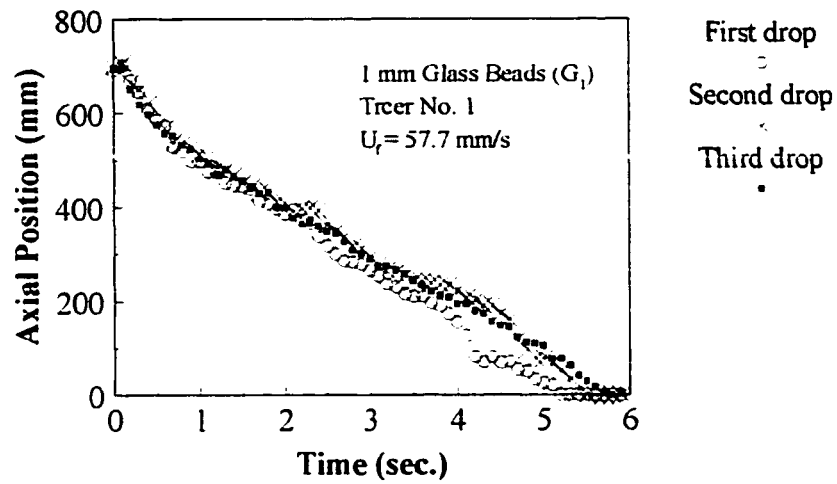


Figure 2.3 Axial coordinate of the tracer falling in a fluidized bed of glass beads, calculated based on the count rate of the detectors at every 20 ms. Only one out of five points is shown in this figure.

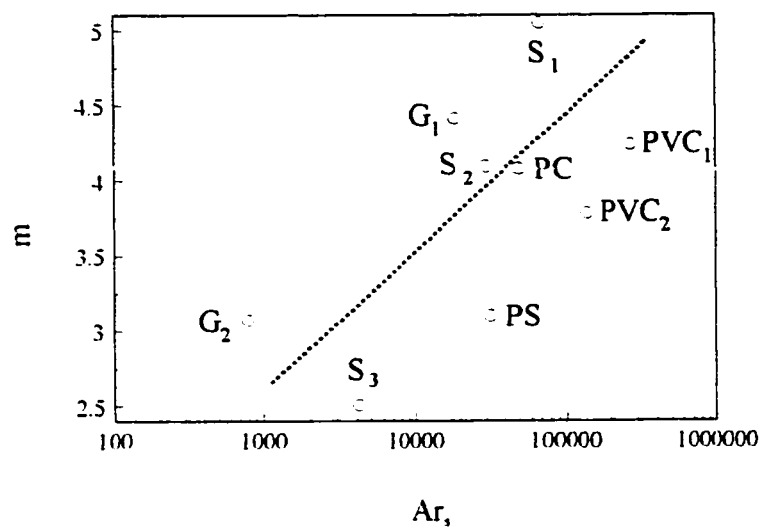


Figure 2.4 Experimental m vs Ar_s , based on the data presented in Table 2.3.

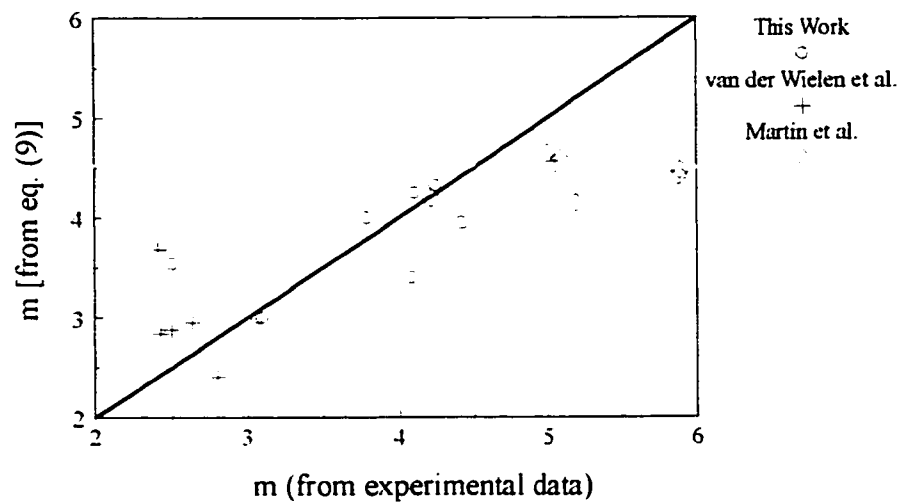


Figure 2.5 Parity plot of calculated m against experimental m .

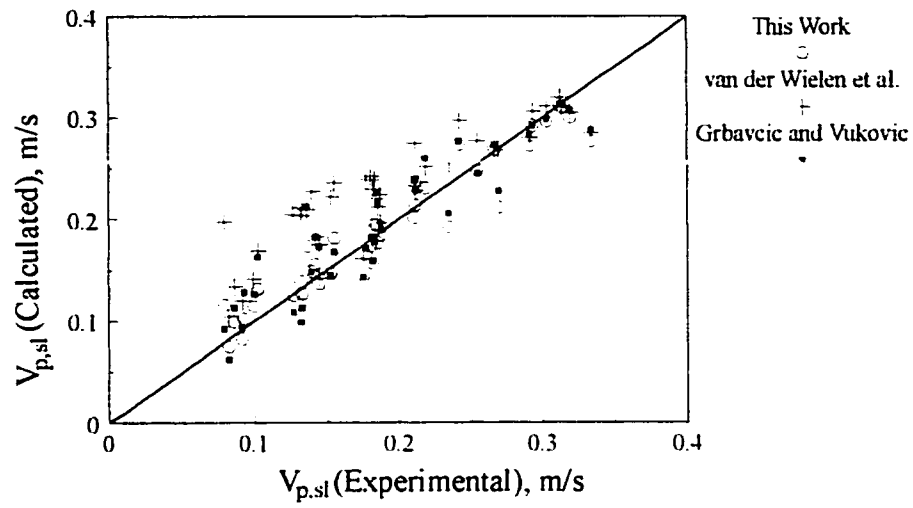


Figure 2.6 Comparison between experimental slip velocity and calculated slip velocity (Data from Table 2.3).

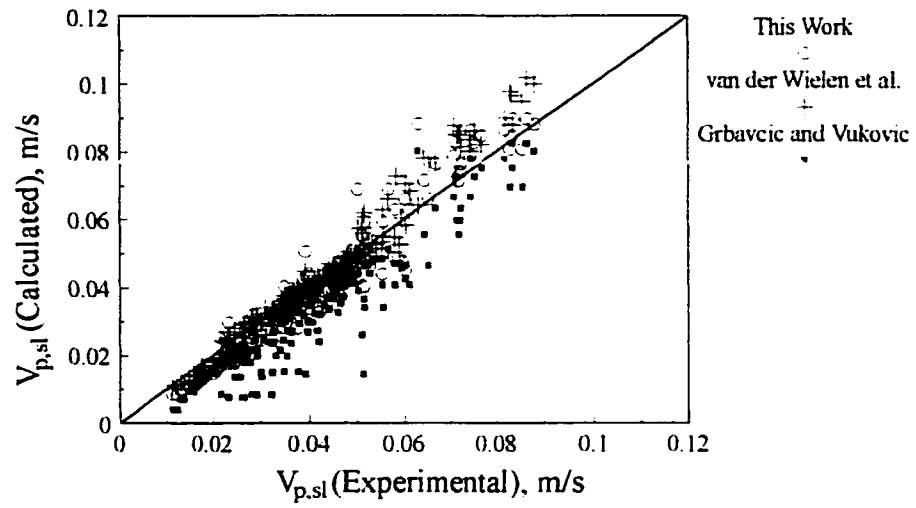


Figure 2.7 Comparison between experimental slip velocity and calculated slip velocity (Data from Van der Wielen et al., 1996).

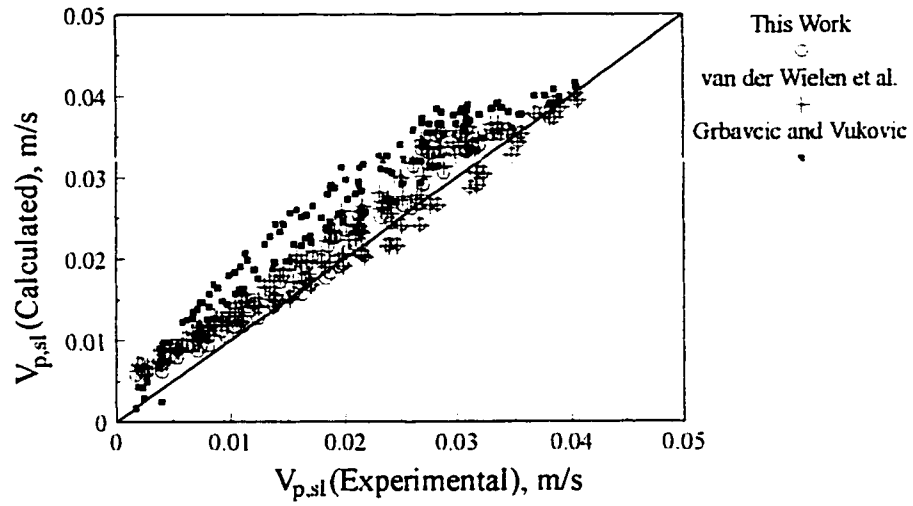


Figure 2.8 Comparison between experimental slip velocity and calculated slip velocity (Data from Martin et al., 1981).

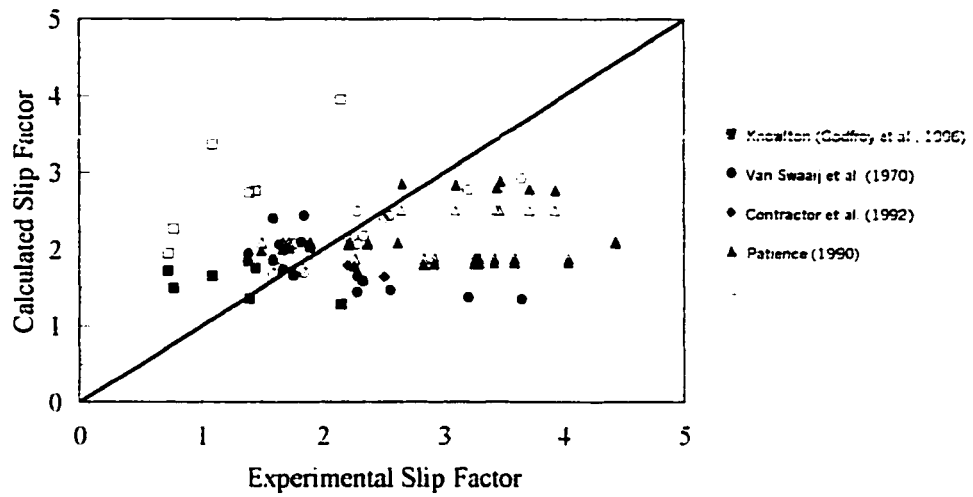


Figure 2.9 Comparison between experimental and calculated slip factor. Calculated based on this work: black keys; Calculated from the correlation presented in Patience et al. (1992): white keys.

CHAPTER 3 : LOCAL SOLID MIXING IN GAS-SOLID FLUIDIZED BEDS

Reference:

Navid Mostoufi and Jamal Chaouki: Local Solid Mixing in Gas-Solid Fluidized Beds, Submitted to Powder Technology (September 1999).

Key Words :

Solid diffusivity, Solid mixing, Gas-solid fluidization, Fluidized beds, Radioactive particle tracking

3.1 Context¹

In Chapter 2 the motion of a single particle in the fluidized beds was examined. The effective drag force exerted on the particle was obtained in and the two existing points of view on how to calculate the buoyancy force were surveyed. The experiments of Chapter 2 were done in liquid-solid beds because liquid fluidized beds provide almost uniform porosity through the bed. Since the porosity has a major effect on the drag coefficient, it was necessary to obtain the data in a bed of constant voidage. The gas-solid fluidized bed is able to supply constant porosity for only a limited range of operation and beyond these limits the particle would be exposed to two different phases, bubble and emulsion, with two extreme porosities. This fact makes it difficult to study the effect of porosity on the drag coefficient. In this chapter we advance the investigations into a higher scale which is the local behavior of solids in fluidized beds. The experiments of this section of work were carried out in gas-solid fluidized beds.

Most flows occurring in nature and in engineering applications are turbulent and fluidization is no exception. In this chapter, we deal with mechanisms which are associated with turbulence and hence, a brief description of the turbulence in gas-solid flow is given here. For single-phase flow applications, turbulence is associated with the chaotic time-dependent

¹ This section is not included in the original manuscript and only serves as a transition between the papers for the thesis.

multi-scale vortices occurring for flows with Reynolds numbers above a certain limit. The meaning of turbulence, however, is less established for gas-solid flows. The turbulence in the gas phase is similar to that of single-phase flows, although the generation and dissipation mechanisms may differ, as these are influenced by the presence of particles. Turbulence in the particulate phase can physically be understood as the particle velocity fluctuations caused by collisions between particles and interactions with the gas phase.

3.2 Abstract

Diffusivity of the solid particles in a 152 mm ID gas-solid fluidized bed was determined at different regimes of fluidization. The gas was air at room temperature and atmospheric pressure and the solids were 385 μm sand or 70 μm FCC particles. The experiments were done at gas superficial velocities from 0.5 to 2.8 m/s for sand and 0.44 to 0.9 m/s for FCC (in both bubbling and turbulent regimes). Movement of a tracer was monitored by Radioactive Particle Tracking (RPT) technique. Once the time-position data became available, local axial and radial diffusivity of solids were calculated from these data. Calculated diffusivities are in the range of 3.3×10^{-3} to 5.6×10^{-2} m^2/s for axial and 2.6×10^{-4} to 1.5×10^{-3} m^2/s for radial direction. The results show that the diffusivities, both axial and radial, increase with gas superficial velocity and are linearly correlated to the axial solid velocity gradient. Solid diffusivity in a bed of FCC was found to be higher than that of a bed of sand at the same excess gas superficial velocity.

3.3 Introduction

Mixing of solid particles is recognized as an important factor in the design of fluidized beds. This phenomenon affects heat and mass transfer rates in the bed and can influence the overall reaction rates in fluidized reactors. Mechanical design of fluidized bed accessories, such as position and number of solids feed and withdrawal points, can be improved by a better understanding of particle mixing in the bed.

Mixing of solids in a gas-solid fluidized bed is caused by different mechanisms. Global mixing of solids occurs by gross circulation of solids due to rising gas bubbles which is called bubble-induced mixing. In this mechanism, the solids are carried up to the surface, as bubble wakes and clouds, where they are dispersed by bursting bubbles and then descend to the bottom of the bed through the emulsion. In addition to this global mixing of particles, local mixing of solids happens, while the bubbles rise, within the bubble wakes and between the wakes and the emulsion. While the first mechanism (global) is characterized by the movement of the bubbles, the second one (local) can be attributed to the random movement of the solid particles. Both these mechanisms can be described by the Fick's law of diffusion with different diffusion coefficients which are called *dispersion coefficient* for the former and *particle diffusivity* for the latter.

Particle diffusivity arises from Brownian motion, wall interaction, and perturbation of the

flow by the particles and can be evaluated by the random walk theory using the Lagrangian coordinates of a set of labelled particles [1]. Corrsin [2] studied the effect of a constant velocity gradient on turbulent diffusion in a single phase pipe flow with zero Lagrangian velocity correlation. Later, Lee and Dukler [3] modified Corrsin's work to account for the cross-correlation terms. Eckstein et al. [4] made a dimensional analysis on the solid diffusivity and concluded that it depends on the local shear rate and the solid concentration of the mixture.

Most of the studies on the solid diffusivity in the literature are focussed on the particulate dispersion in the atmosphere (e.g., [5-7]). Recently, more attention is paid to evaluation of diffusivity in multiphase reactors. Kiared et al. [8] determined the solid diffusivity in a liquid fluidized bed and Degaleesan et al. [9] calculated the eddy diffusivity of liquid in a slurry bubble column reactor.

Local mixing of solids in a fluidized bed acts as an important parameter in the case of very rapid reactions where the reactants convert to products before the bubble reaches the surface or interacts with the other bubbles in the bed. A poor mixing may result in creating hot spots in the bed and/or low conversion at the outlet. In the present work, we intend to study the local mixing of solids by determining the solid diffusivity in a gas-solid fluidized bed in bubbling and turbulent regimes of fluidization. Most of the data reported in the literature are related to the global mixing of the solids resulting in calculation of the dispersion coefficient

(e.g., [10-12]). However, by using a radioactive particle tracking technique, we were able to measure instantaneous location of a tracer for a long time and evaluate the diffusivity of this tracer according to the random walk theory.

3.4 Theory

In the process of fluidization, a solid particle spend its time in different media: emulsion, bubble wakes, bubble clouds, and individual particles inside the bubble. The flow pattern of the particles (i.e, velocity, velocity fluctuation, ...) differ from one of these media to another. Therefore, it is evident that the behaviour of the particles and their interactions with the fluid and the other particles depends in which environment they are. While we acknowledge this difference in the particle motion in a fluidized bed, in the following it is assumed that all the solid particles behave in the same manner which is the average behaviour of the solids in the fluidized bed. This assumption can be justified by the fact that a large number of particles are employed in the calculation of the solid diffusivity, as described below.

Solid diffusivity, can be evaluated from the particle trajectory in the Lagrangian coordinates. If at the time $t = 0$, N particles are released from the point (r_0, z_0) which is located inside the bed, instantaneous excess axial displacement of each of the released tracer can be defined as

$$Z = z(t) - z_0 \quad (3.1)$$

The averaged displacement at the time t can be calculated from

$$\bar{Z} = \frac{1}{N} \sum_{i=1}^N Z_i \quad (3.2)$$

and mean-square displacement is given by

$$\bar{Z}^2 = \frac{1}{N} \sum_{i=1}^N (Z_i - \bar{Z})^2 \quad (3.3)$$

from which the axial solid diffusivity can be obtained

$$D_s = \frac{1}{2} \frac{d\bar{Z}^2}{dt} \quad (3.4)$$

The diffusivity calculated from Eqs. (3.1) to (3.4) does not take experimental error into account. The actual position of the tracer can be considered to be located within the following interval:

$$z_{actual} = z_{calculated} \pm \sigma_z \quad (3.5)$$

The experimental error of RPT technique in terms of the standard deviation of the calculated position can be evaluated from [13]:

$$\frac{1}{\sigma_z^2} = \sum_{j=1}^{N_D} C_j \left(\frac{\partial \ln C_j}{\partial z} \right)^2 \quad (3.6)$$

The same relation can be derived for radial diffusivity by replacing z with r in Eqs. (3.1) to (3.6).

3.5 Experimental

The experiments were done in a gas-solid fluidized bed as shown in Figure 3.1. The column was made of a Plexiglas pipe with 152 mm internal diameter and 1500 mm height. Air at room temperature was introduced into the bed through a conical section, passing through a stainless steel porous plate and a nozzle type air distributor. The nozzle type distributor was designed according to recommendations of Wen et al. [14]. Air flow rate was measured by an orifice plate connected to a water manometer. A cyclone placed at the air outlet of the column returns the entrained solids back to the bed.

The solids used in the experiments were sand. Some experiments were also done using FCC powder as solids for comparison. Initial height of the bed was 0.22 m (1.5 times the column diameter). Properties of these particles are given in Table 3.1 and particle size distributions of the solids are shown in Figure 3.2.

The tracers were made of a mixture of gold powder and epoxy resin. The ratio of gold to epoxy resin in the mixture was chosen such that to obtain a density equal to that of the sand at the end. Small pieces of the desired sizes were then taken off the solid mixture. The tracers of the size 420 μm , 500 μm , and 600 μm were used in the experiments. They were being activated in the SLOWPOKE nuclear reactor of École Polytechnique prior to each experiment. The produced isotope ^{198}Au emits γ -rays which were counted by 16 cylindrical NaI(Tl) scintillation detectors on sliding rails. A typical arrangement of the detectors around the fluidized bed is shown in Figure 3.1. Two personal computers simultaneously registered the number of γ -rays detected by each detector in every sampling period of 20 ms. These number of counts were used later to calculate the coordinates of the tracer. Details of the system calibration and the inverse reconstruction strategy for tracer position rendition are described by Larachi et al. [13, 15].

In each experiment a single tracer was placed into the bed to move freely with the other particles inside the bed. Movement of the tracer was then monitored for about 5 hours during which the count rate of the tracer at some 820,000 points were acquired. The bed was then made empty and the tracer was recovered from the solids in order to be used in the next experiment. Operating conditions and size of the tracers used in each run are summarized in Table 3.2.

3.6 Results and Discussion

In order to obtain axial and radial diffusivity of the solids as a function of axial and radial positions, a large number of solid tracers should be injected in a small cell in the bed, first. However, there was only one tracer in the RPT experiments. Therefore, it is essential to benefit from the principle of ergodicity for processing the data obtained in our experiments, as described below.

For calculation of the solid diffusivity the bed is divided into several small imaginary compartments, $\Delta r \times \Delta z$. Using the time-position data obtained from the particle tracking experiments, simultaneous injection of a large number of tracers (e.g., $N = 1000$) into each compartment was simulated. This was done by following up the tracer until it enters the desired compartment. The tracer was then pursued for 50 succeeding positions, or 1 second of the experiment, and these paths were set aside. Figure 3.3 shows a 20 seconds sample trajectory of the tracer in experiment no. 4 (see Table 3.2). The solid lines in this figure show the path of the tracer after it entered the specified compartment ($150 \text{ mm} < z < 200 \text{ mm}$, $19.1 \text{ mm} < r < 28.6 \text{ mm}$). In this sample trajectory two such paths could be found which start the 1 second journey from the above mentioned cell. Note that although in Figure 3.3 the tracer enters more than twice into the region of $150 \text{ mm} < z < 200 \text{ mm}$, the radial position of the tracer is not located in the desired cell and they are not considered as the desired paths. This follow-up procedure was repeated until the tracer passes N times

from that specific cell. A sample reconstruction of self diffusion of 1000 solid particles vs time by this method is shown in Figure 3.4. The 1 second pursuit time is enough for all the tracers to be completely mixed up with the other bed particles, forming a uniform distribution of the tracers throughout the bed.

Having tracer positions for the reconstructed self diffusion, mean-square displacement of the particles, both in axial and radial direction, can be obtained from Eqs. (3.1) to (3.3). Mean-square axial and radial displacements of the points shown in Figure 3.4 are plotted in Figures 3.5 *a* and *b*, respectively. It can be seen from these figures that at the beginning the mean-square displacement increases constantly. This is because the tracers are moving apart of each other and dispersing progressively in the bed, as can be seen in Figure 3.4. However, after a long enough time, the tracers are completely mixed in the bed and form a uniform mixture resulting in a constant mean distance of the tracers from the injection cell. The tracers are in dynamic equilibrium at this time and no more diffusion takes place after that due to the fact that the concentration gradient has vanished. This phenomena can be seen in Figures 3.5 *a* and *b* where the mean-square displacement reaches a constant value. Therefore, diffusivity of the solids can be obtained according to Eq. (3.4) from the slope of the linear part of the plot of mean-square displacement vs time. This line is also shown in Figures 3.5 *a* and *b*. In order to evaluate upper and lower limits of the calculated diffusivity, the calculations were repeated once with considering the error term in Eq. (3.5) to appear with negative sign in all the experimental points and once again with positive sign.

It is interesting to note that in Figure 3.5 *a* the initial slope of the plot of the mean square axial displacement against time is slightly different from the line shown in that figure. In fact, it is possible to define both short-time diffusivity which measures the average instantaneous mobility of a particle, and long-time diffusivity which measures the ability of a particle to wander far from its starting point. Short-time diffusivity cannot be obtained with a good precision from the experiments of this work simply because there are not enough number of data points at the initial moments of particle diffusion. However, it can be concluded from Figures 3.5 *a* and *b* that the short-time diffusivity is not much different from the long-time diffusivity (represented by the solid line) at the operating conditions of the experiments of this work.

The above procedure was repeated for all the imaginary compartments inside the bed and the diffusivities were determined by this procedure as a function of radial and axial positions. The velocity profiles of the tracer was also been calculated by taking average of all velocities of the tracer (both in radial and axial directions) passed through each compartment.

The operating height of the bed in our experiments was not high enough to show the fully developed behaviour of solids and observe a definite trend in the variables with respect to the axial position. Therefore, in the following discussion we use the average of all the local quantities over axial direction and present the results as a function of radial position only. Of course, a layer of the bed close to the distributor and that of top of the bed were excluded

in averaging in order to avoid any end effect in the results. In the following, only the data from sand/420 μm tracer experiments are shown in the illustrations. However, it should be emphasised that the discussions of these sample experiments are valid for all other experiments because the same trend was observed in the rest of experiments.

Figures 3.6 *a* and *b* show axial and radial diffusivities as a function of radial position. The value of the diffusivity is lower near the column wall and increases by moving toward the column center. If this trend could have been explained by the wall effect, the diffusivity should have reached a constant, i.e., its maximum, at the centre of the column. However, this is not the case since the axial diffusivity reaches a maximum at its half way from the column centre and decreases near the center. The upper and lower expected values of the diffusivity at each point are also shown in Figures 3.6 *a* and *b* by error bars which confirm that decrease of the diffusivity close to the center cannot be justified by the calculation error. According to Eckstein et al. [4] diffusivity is a function of the shear rate in the suspension:

$$D_z = f(\epsilon) d_s^2 \dot{\gamma}_z \quad (3.7)$$

Since the velocity profile of solids is also available, it is possible to study the effect of velocity gradient on the diffusivity in the fluidized beds.

The calculated Eulerian solid velocity profile is shown in Figure 3.7. This figure shows that both active height of the bed and solid velocity increases with gas superficial velocity. Based

on the data presented in Figure 3.7, it is possible to evaluate the shear rate of the solids. Axial and radial velocity gradients are shown in Figure 3.8. The velocity gradient presented in Figure 3.8 are averaged over the bed height, with the exception of the layers at the top and the bottom, and are presented as a function of radial position. Obviously, the radial velocity gradient is negligible with respect to the axial velocity gradient. In fact, radial gradient is at least an order of magnitude smaller than axial gradient. Therefore, axial velocity gradient can be considered to be the only effective gradient field in the bed.

In order to study the relationship between the diffusivity and velocity gradient, the axial diffusivity is plotted against the axial velocity gradient in Figure 3.9. This figure indicates that axial solid diffusivity is highly correlated with the velocity gradient and is a linear function of the gradient:

$$D_z = a \dot{\gamma}_z + D_{z,0} \quad (3.8)$$

The y-intercept of the line, $D_{z,0}$, gives the diffusivity at the zero gradient condition (i.e., solid diffusivity in a constant velocity field). The slope of the line is a function of the porosity of the bed and the particles diameter (Eckstein et al. [4]):

$$a = d_s^2 f(\varepsilon) \quad (3.9)$$

The same calculations were done for all the experiments listed in Table 3.2. The calculated axial diffusivities at zero gradient are summarized in Figure 3.10 *a*. This figure clearly shows that the solid axial diffusivity is not affected by the size of the tracer and changes only with the gas superficial velocity. This result suggests that dispersion of solids in a fluidized bed is governed by the interaction between the ensembles of solids such as bubble wakes, clouds, and clusters rather than random movement of individual particles. The axial Peclet number for the data of sand is

$$Pe_{z,0} = \frac{(U_0 - U_{mf})d_s}{D_{z,0}} = 0.02 \quad (3.10)$$

The slope α of Eq. (3.8) is found to be almost constant for all the experiments with sand. Since the experiments were done in superficial velocities from 0.5 to 2.8 m/s which provides different porosities (both in bubbling and turbulent regimes of fluidization), it may be concluded that the value of α is either not a function or a very weak function of the solid concentration in a fluidized bed. Therefore, Eq. (3.8) may be rearranged as

$$\frac{D_{z,0} - D_z}{\dot{\gamma}_z d_s^2} = 2.2 \times 10^3 \quad (3.11)$$

The characteristic length in Eq. (3.11) is taken as the mean size of the particles in the bed. This is due to the fact that under the experimental conditions of this work the diffusivity is not related to the size of the individual tracer, as discussed earlier.

It should be noted that there are major differences in the relationship between the solid diffusivity and shear rate obtained in this work [Eq. (3.8)] and that of Eckstein et al. [Eq. (3.7)]. According to Eckstein et al. [4] the slope of the line D_z vs $\dot{\gamma}_z$ in Eq. (3.7) is a function of solid concentration, while the slope α in Eq. (3.8) is found to be almost constant for all our experiments with sand. In fact, Eckstein et al. [4] reported solid concentrations in their work lower than what is in our experiments. As a result, it can be concluded that although the diffusivity of solids depends on solid concentration, but it reaches a saturation value at high solid concentrations. Another important difference between the two correlations is that Eq. (3.7) predicts increasing of the diffusivity with the value of the shear rate. However, we found a negative slope in Eq. (3.8) from the experiments of this work. Although we do not have a phenomenological explanation of the differences between the two correlations yet, but suggest that the difference arises from the difference in the geometry of the two systems. Eckstein et al. [4] studied self diffusion of solids in an unbounded linear shear flow and, therefore, they provided the absolute value of the shear rate of the fluid in their results. However, we used the actual value of the solid shear rate in a nonuniform velocity field in our correlation. Eq. (3.7) also fails to predict the diffusivity at zero shear condition correctly, while Eq. (3.8) is capable of providing this value.

The phenomena observed for the axial diffusivity is found to be valid for the radial direction too. The calculated radial diffusivities at zero solid velocity gradient are summarized in

Figure 3.10 *b*. The same analysis of radial diffusivity data of sand experiments can be summarized in the following equations:

$$Pe_{r,0} = \frac{(U_0 - U_{mf})d_s}{D_{r,0}} = 0.7 \quad (3.12)$$

$$\frac{D_{r,0} - D_r}{\dot{\gamma}_z d_s^2} = 1.5 \times 10^2 \quad (3.13)$$

The solid diffusivities at zero shear for experiments with FCC (experiments no. 15 to 20 in Table 3.2) are also shown in Figures 3.10 *a* and *b*. It is worth mentioning that the plot of solid diffusivity vs shear rate was very scattered for experiments with FCC and, in contrary to what was shown for experiments with sand, no general conclusion could be drawn from such a plot. As a result, the values shown for FCC in Figures 3.10 *a* and *b* should be considered as estimates only. Figure 3.10 *a* illustrates that the axial diffusivity of FCC particles can be properly described by Eq. (3.10). However, from Figure 3.10 *b* it can be concluded that radial solid diffusivity of FCC particles (Geldart classification A) is higher than that of sand particles (Geldart classification B) at the same excess superficial velocity. This is in consistent with the data reported in Kunii and Levenspiel [16].

3.7 Conclusions

Solid diffusivity in a fluidized bed cannot be considered as a property of the single particle diffusing in the bed. Local diffusion of solids mainly happens through interaction between groups of solids such as bubble wakes, bubble clouds, and solid clusters. In fact, a group of solids, regardless of the sizes of the individual particles, join one of these aggregates and moves along until the aggregate breaks-up or joins another one (e.g., break-up and coalescence of bubbles and the solids associated with them). Therefore, the solid diffusivity is determined by the hydrodynamic conditions of the bed such as gas superficial velocity, mean particle size of the solids, and their size distribution.

The axial velocity gradient, dV/dz , has a significant effect on the solid diffusivity. These two quantity are linearly correlated as shown in Eqs. (3.11) and (3.13). The constants at the right hand side of Eqs. (3.11) and (3.13) should be used cautiously because they are calculated for only one type of solids and may be different for the others. The radial velocity gradient, dV/dr , is found to be at least an order of magnitude smaller than the axial velocity gradient and therefore, has no significant effect on the solid diffusivity.

The set of Eqs. (3.10) to (3.13) are capable of predicting the solid diffusivities in each point in the fluidized bed. However, it should be noticed that solid diffusivity changes more rapidly at the wall and less sever at the center of the column. The value of the shear rate also

approaches zero at the center of the column. Consequently, in the large units, where the wall effect is negligible, the value of the solid diffusivity at zero shear rate could be considered as a reasonable average value of this quantity.

Axial diffusivity of solids at zero shear rate in a bed of FCC particles was found to be the same as that of sand particles. However, radial diffusivity in a bed of FCC is higher than that of sand particles at a given excess gas superficial velocity. This is due to enhancement of radial solid mixing in a bed of finer and lighter particles. In the case of FCC powder the wake fraction is higher and the cloud is thicker compared to a bed of sand particles. This phenomenon makes the solids more mobile when the bed particles are finer and/or have less density which results in a higher solid diffusivity.

The experiments done in this work cover a wide enough range of gas superficial velocity which allows drawing a general conclusion about transition from bubbling to turbulent fluidization. All the quantities studied in this work were increasing constantly without a sharp change in their trend. Thus, one can conclude that since the trend of the studied parameters with gas superficial velocity remains the same when entering turbulent fluidization, transition from bubbling to turbulent fluidization happens smoothly rather than sharply. It may be proposed that there exist two different type of fluid-particle-particle interaction in fluidized beds at the same time: diffusion and convection. While the former is predominant at low gas velocities, the latter is more significant at higher velocities and a

fluidized bed is a weighted combination of these two phenomena. Although this approach justifies the smooth transition from bubbling to turbulent fluidization, however, the capability of this approach in quantifying solid motion in fluidized beds have to be studied thoroughly.

3.8 References

1. Monin, A. S. and Yaglom, A. M.: *Statistical Fluid Mechanics: Mechanics of Turbulence*, J. L. Lumley, Ed., MIT Press, Cambridge, MA, vol. 1, 1971.
2. Corrsin, S.: An account of some features of the phenomenon in fully turbulent regions, *Proc. of Iowa Thermodynamics Symp.*, 5-29, 1953.
3. Lee, N. and Duckler, A. E.: Lagrangian simulation of dispersion in turbulent shear flow with hybrid computer, *AIChE J.* vol. 22, 449-456, 1976.
4. Eckstein, E. C., Bailey, D. G., and Shapiro, A. H.: Self-diffusion of particles in shear flow of a suspension, *J. Fluid Mech.* vol. 79, part 1, 191-208, 1977.
5. Pismen, L. M. and Nir, A.: On the motion of suspended particles in stationary homogeneous turbulence, *J. Fluid. Mech.* vol. 84, 193-206, 1978.

6. Maxey, M. R. and Riley, J. J.: Equation of motion for small rigid sphere in a nonuniform flow, *Phys. Fluids* vol. 26, 883-889, 1983.
7. Mei, R., Adrian, R. J., and Hanratty, T. J.: Particle dispersion in isotropic turbulence under stokes drag and basset force with gravitational settling, *J. Fluid Mech.* vol. 225, 481-495, 1991.
8. Kiared, K., Larachi, F., Cassanello, M., and Chaouki, J.: Flow structure of the solids in a three-dimensional liquid fluidized bed, *Ind. Eng. Chem. Res.* vol. 36, 4695-4704, 1997.
9. Degaleesan, S., Dudukovic, M. P., Toseland, B. A., and Bhatt, B. L.: A two-compartment convective-diffusion model for slurry bubble column reactors, *Ind. Eng. Chem. Res.* vol. 36, 4670-4680, 1997.
10. Berruti, F., Scott, D. S., and Rhodes, E.: Measuring and modelling lateral solid mixing in a three-dimensional batch gas-solid fluidized bed reactor, *Can. J. Chem. Eng.* vol. 64, 48-55, 1986.
11. Lee, G. S. and Kim, S. D.: Axial mixing of solids in turbulent fluidized beds, *Chem. Eng. J.* vol. 44, 1-9, 1990.

12. Asif, M., Kalogerakis, N., and Behie, L. A.: On the constancy of axial dispersion coefficient in liquid fluidized beds, *Chem. Eng. J.* vol. 49, 17-26, 1992.
13. Larachi, F., Chaouki, J., and Kennedy, G.: 3-D mapping of solids flow fields in multiphase reactor with RPT, *AIChE J.* vol. 41, 439-443, 1995.
14. Wen, C. Y., Krishnan, R., and Kalyanaraman, R.: Particle mixing near the grid region of fluidized beds”, in “Fluidization, Grace, J. R. and Matsen, J. M., Eds., Plenum, New York, 405-412, 1980.
15. Larachi, F., Chaouki, J., and Kennedy, G.: A γ -ray detection system for 3-D particle tracking in multiphase reactors, *Nucl. Instr. and Meth. A* vol. 338, 568-576, 1994.
16. Kunii, D. and Levenspiel, O.: *Fluidization Engineering*, 2nd ed., Butterworth-Heinemann, Boston, M.A., 1991.

Table 3.1 Properties of the solids

Solid	ρ_s (kg/m ³)	d_s (μm)	U_c (m/s)	U_{mf} (m/s)
Sand	2650	385	1.5	0.24
FCC	1670	70	0.77	0.003

Table 3.2 Summary of experimental conditions

No.	Solids	U_0	d_T
		(m/s)	(μm)
1	Sand	0.5	500
2	Sand	0.9	420
3	Sand	0.9	500
4	Sand	1	420
5	Sand	1	500
6	Sand	1	600
7	Sand	1.5	420
8	Sand	1.5	500
9	Sand	1.5	600
10	Sand	2	420
11	Sand	2	500
12	Sand	2	600
13	Sand	2.4	500
14	Sand	2.8	500
15	FCC	0.44	420
16	FCC	0.44	500
17	FCC	0.75	420
18	FCC	0.75	500
19	FCC	0.9	420
20	FCC	0.9	500

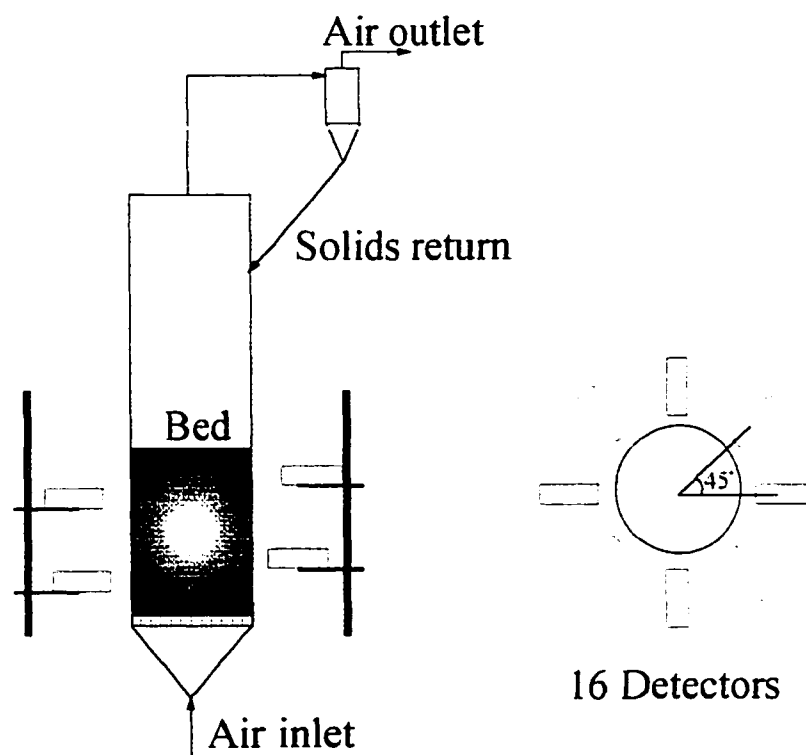


Figure 3.1 Experimental set-up and typical configuration of the detectors.

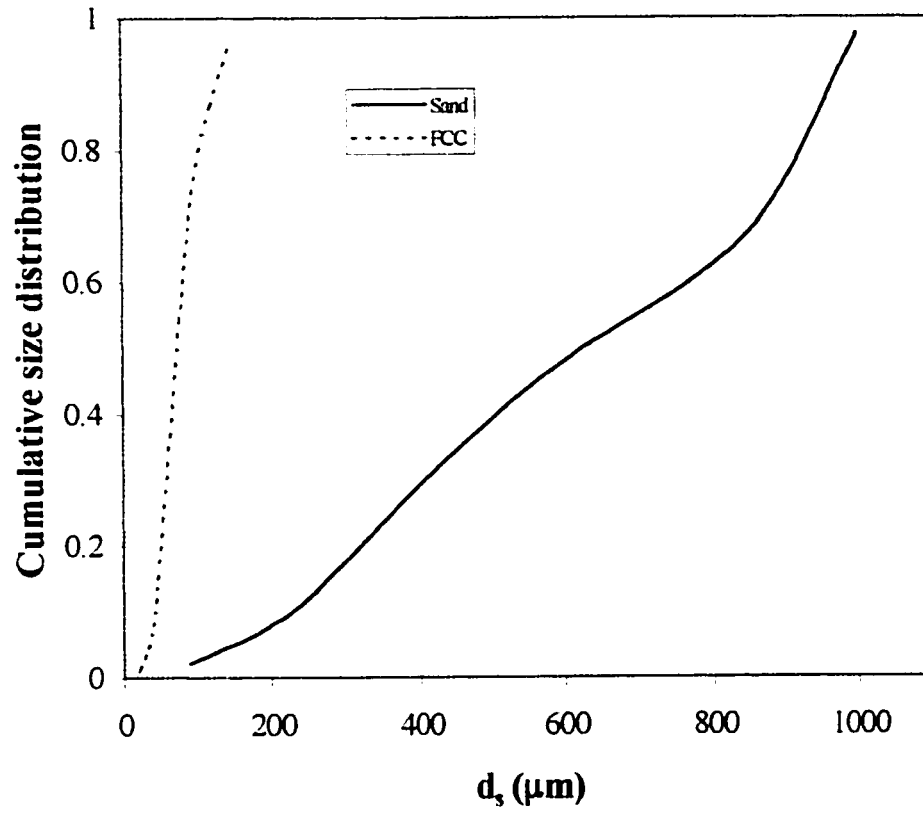


Figure 3.2 Particle size distribution of the solids employed in this work.

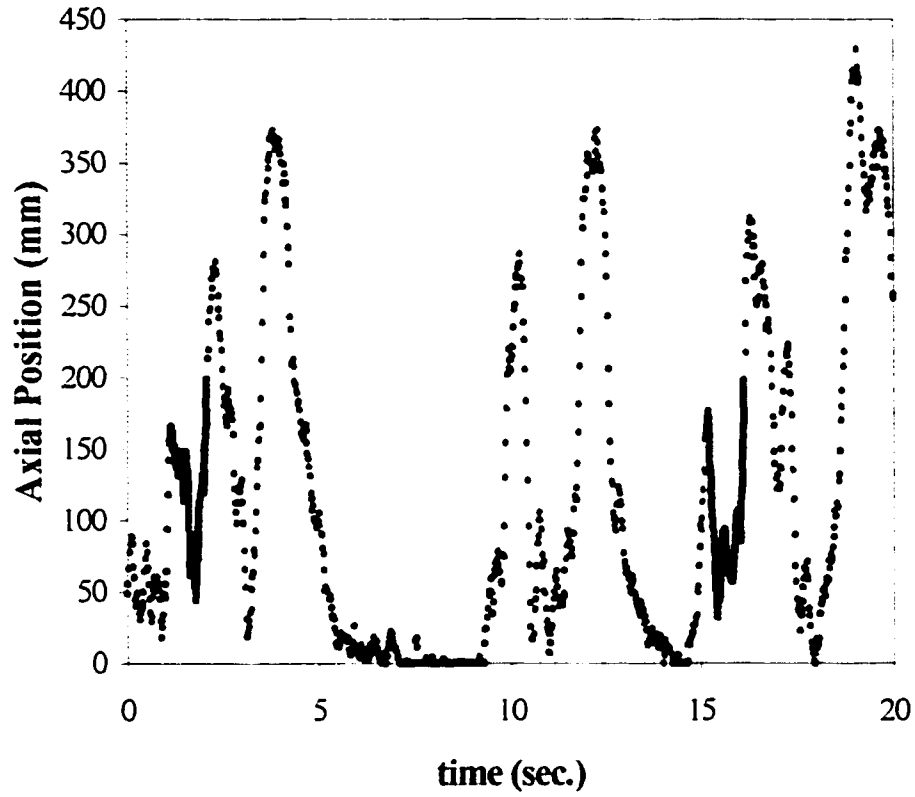


Figure 3.3 Sample trajectory of the tracer (Sand, $U_0 = 1$ m/s, $d_T = 420$ μ m). Solid lines are the parts that initiate their move from the cell: 150 mm $< z < 200$ mm, 19.1 mm $< r < 28.6$ mm.

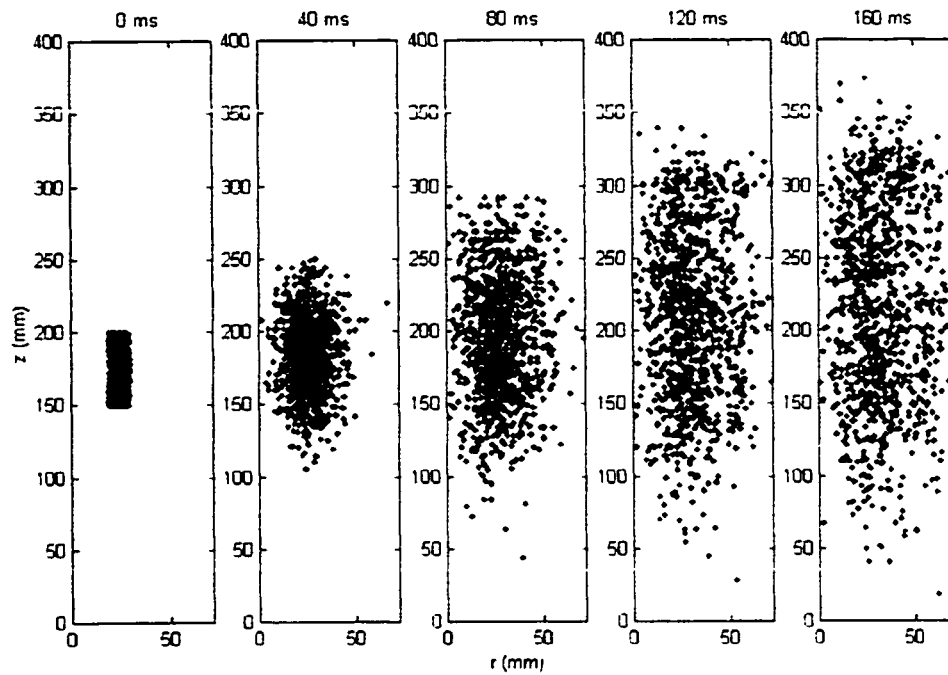


Figure 3.4 Self diffusion of 1000 tracers virtually injected in the imaginary compartment $150 \text{ mm} < z < 200 \text{ mm}$, $19.1 \text{ mm} < r < 28.6 \text{ mm}$ (Sand, $U_0 = 1 \text{ m/s}$, $d_T = 420 \text{ }\mu\text{m}$).

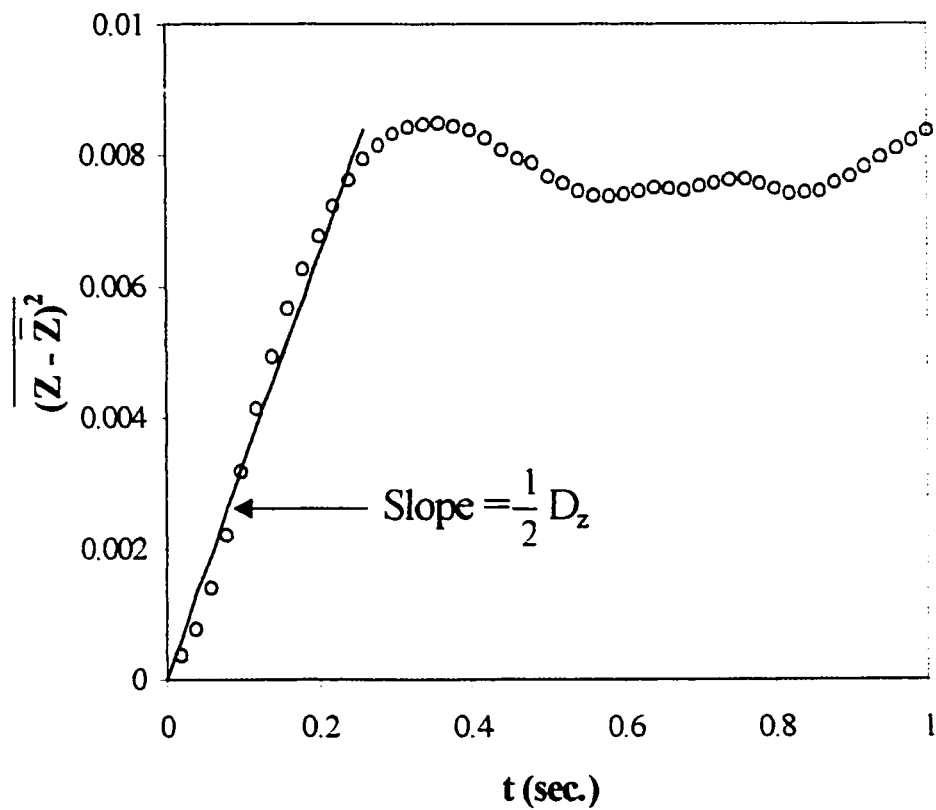


Figure 3.5 Mean square displacement of 1000 tracers virtually injected in the imaginary compartment $150 \text{ mm} < z < 200 \text{ mm}$, $19.1 \text{ mm} < r < 28.6 \text{ mm}$ (Sand, $U_0 = 1 \text{ m/s}$, $d_T = 420 \mu\text{m}$): (a) axial displacement.

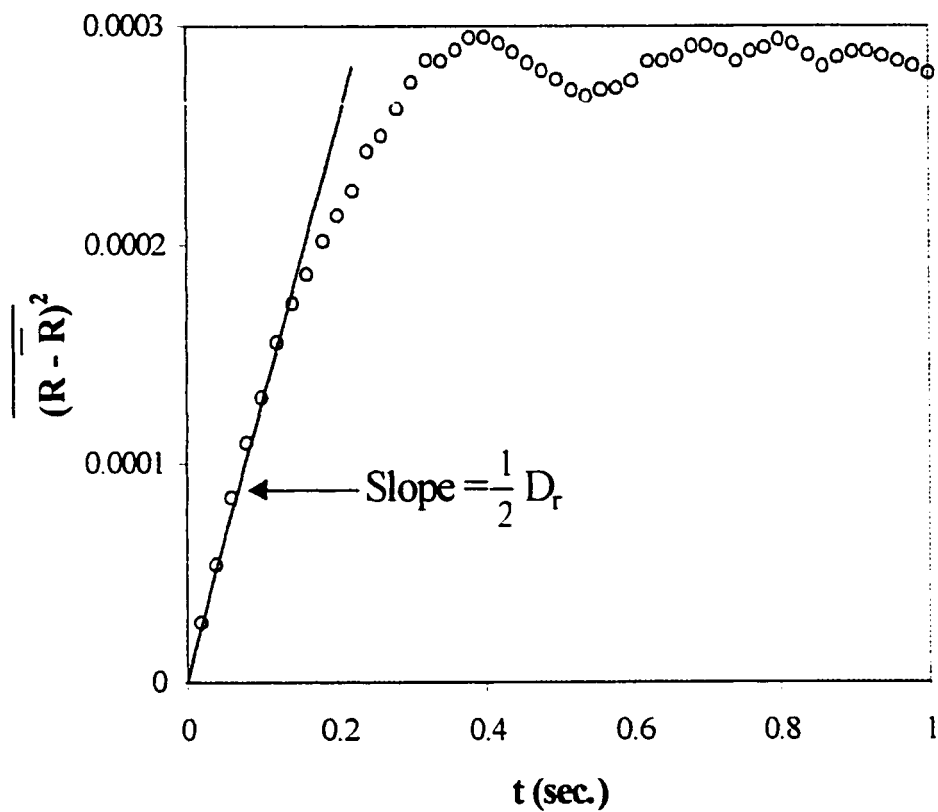


Figure 3.5 Mean square displacement of 1000 tracers virtually injected in the imaginary compartment $150 \text{ mm} < z < 200 \text{ mm}$, $19.1 \text{ mm} < r < 28.6 \text{ mm}$ (Sand, $U_0 = 1 \text{ m/s}$, $d_T = 420 \mu\text{m}$): (b) radial displacement.

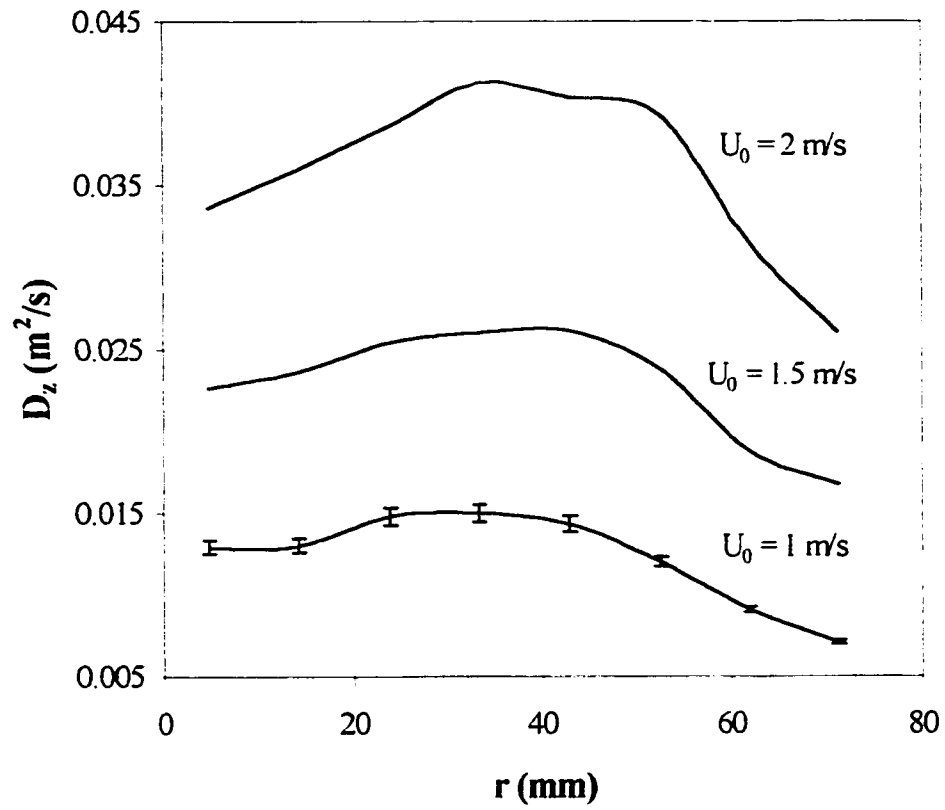


Figure 3.6 Solid diffusivity as a function of radial position (Sand, $d_T = 420 \mu\text{m}$): (a) axial solid diffusivity.

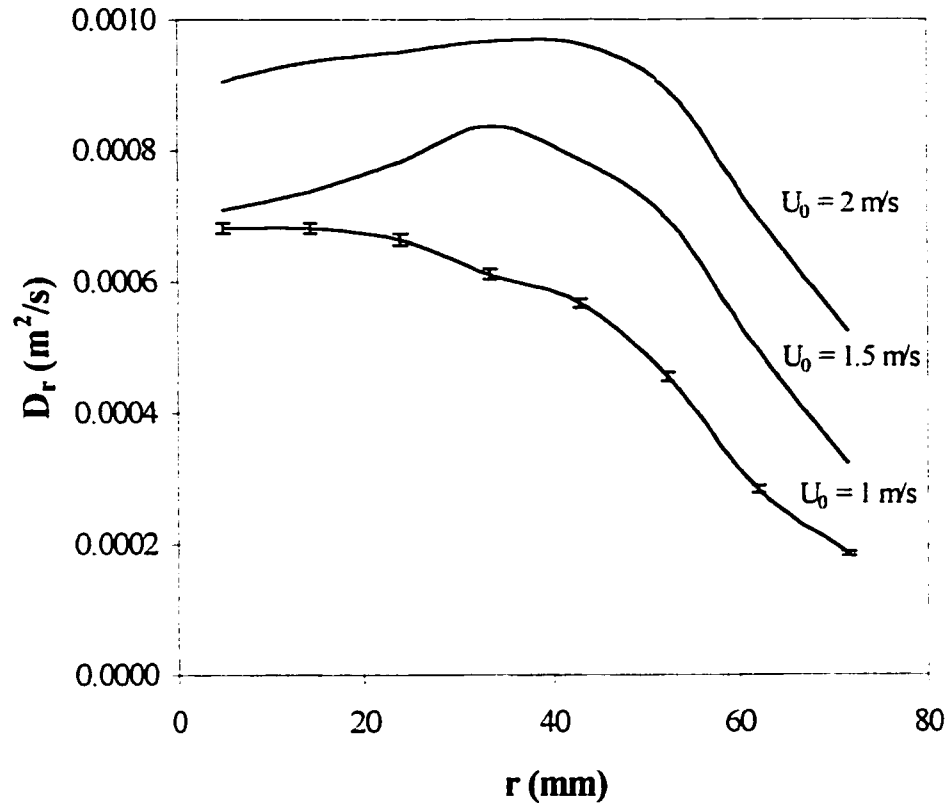


Figure 3.6 Solid diffusivity as a function of radial position (sand, $d_T = 420 \mu\text{m}$): (b) radial solid diffusivity.

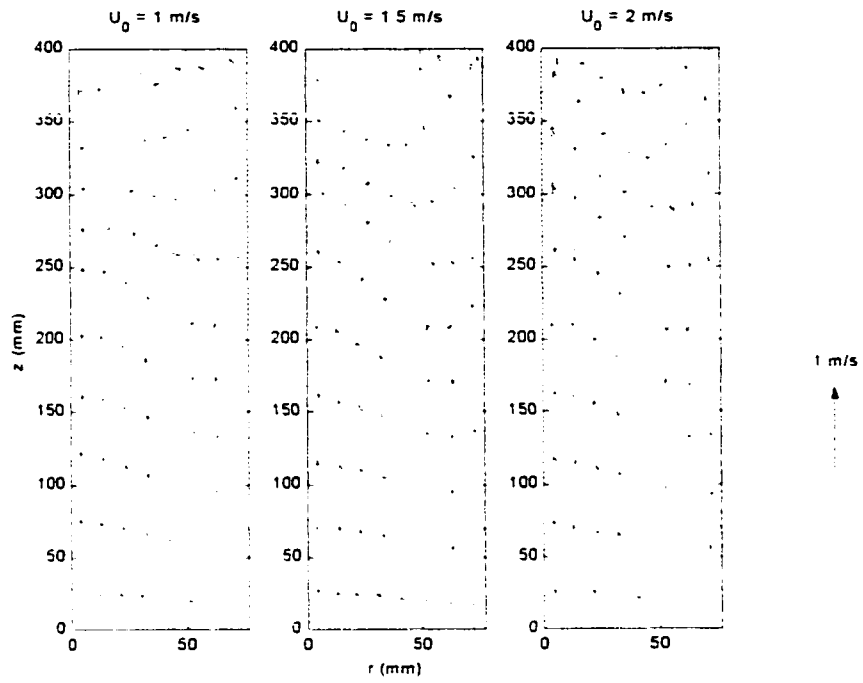


Figure 3.7 Eulerian velocity field of solids at different gas superficial velocities (sand, $d_T = 420 \mu\text{m}$).

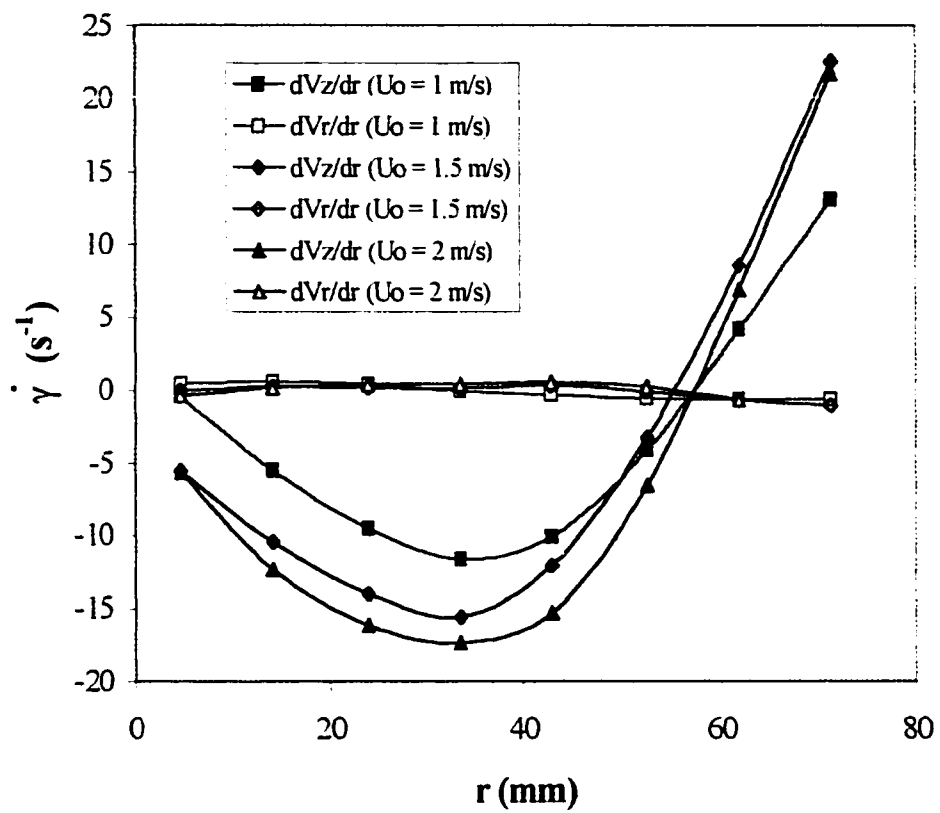


Figure 3.8 Axial and radial solid velocity gradient (Sand, $d_T = 420 \mu\text{m}$).

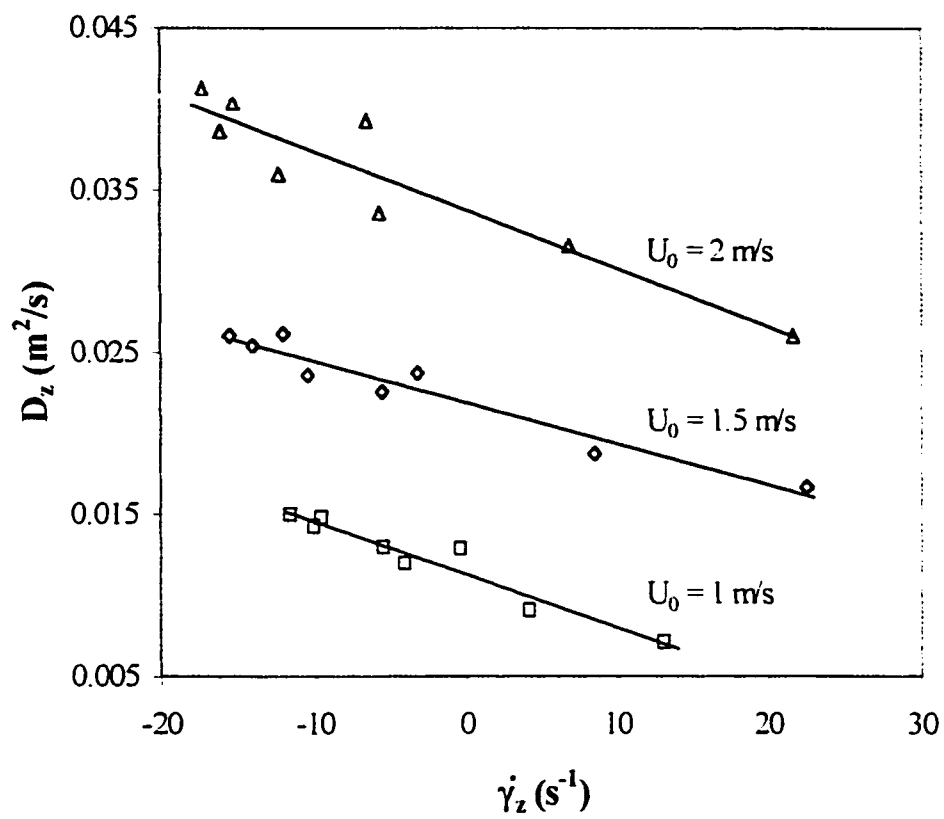


Figure 3.9 Axial solid diffusivity as a function of axial solid velocity gradient (Sand, $d_T = 420 \mu\text{m}$).

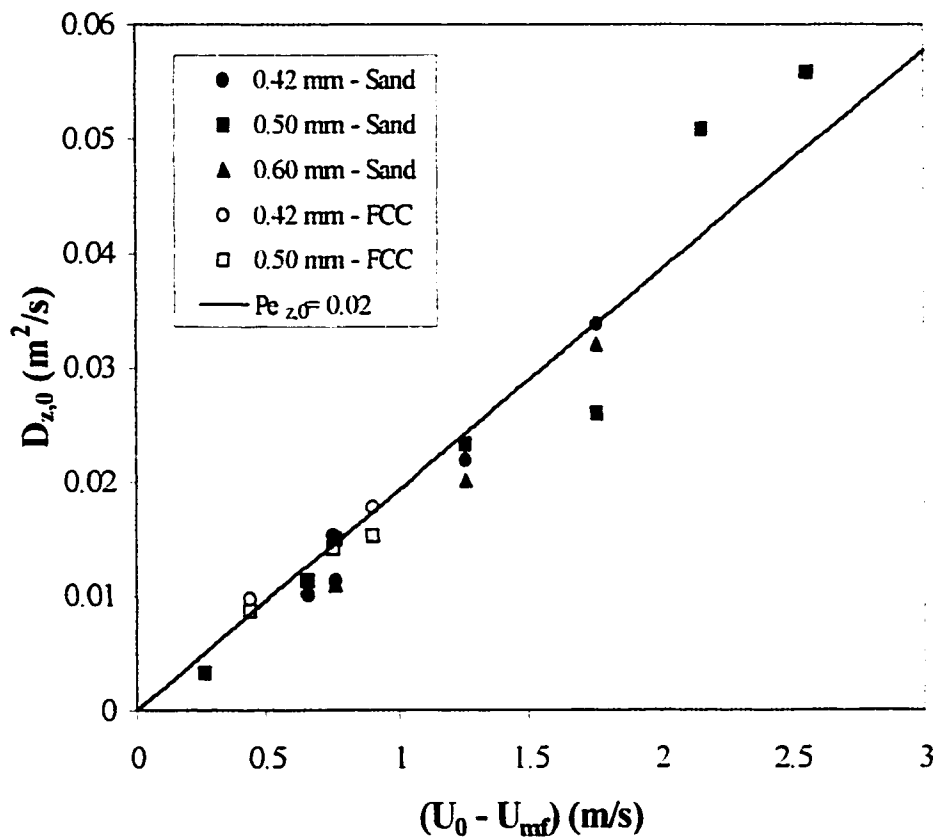


Figure 3.10 Solid diffusivity in the absence of velocity gradient: (a) axial solid diffusivity.

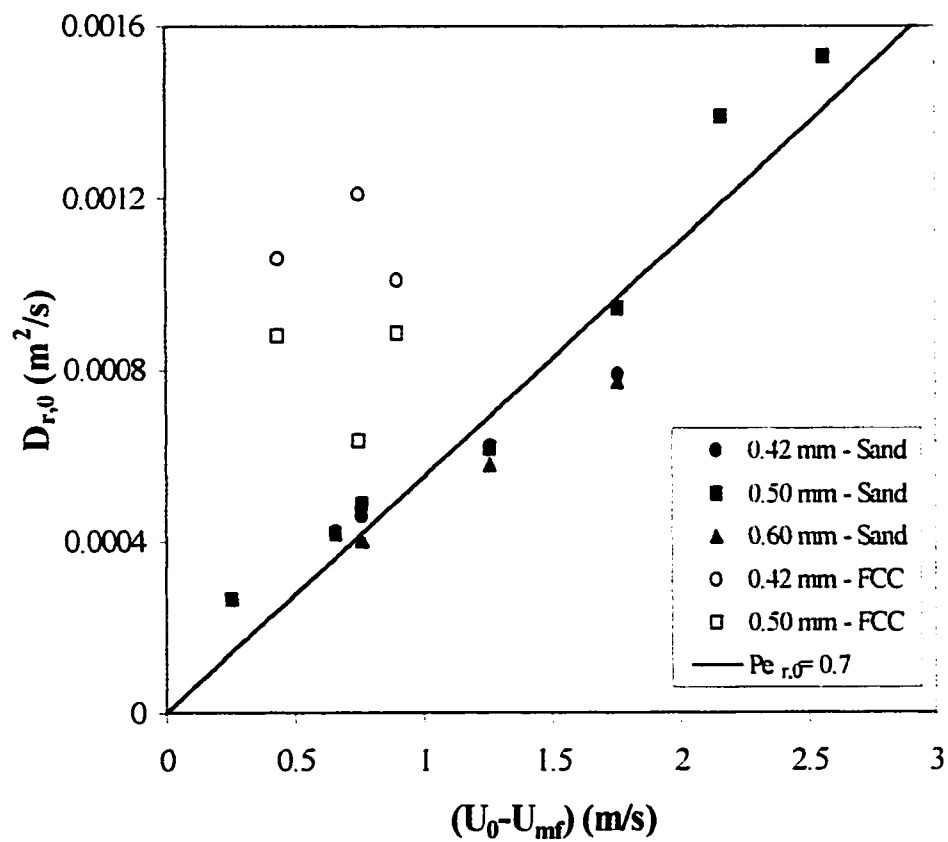


Figure 3.10 Solid diffusivity in the absence of velocity gradient: (b) radial solid diffusivity.

CHAPTER 4 : ON THE AXIAL MOVEMENT OF SOLIDS IN GAS-SOLID FLUIDIZED BEDS

Reference:

Navid Mostoufi and Jamal Chaouki: On the Axial Movement of Solids in Gas-Solid Fluidized Beds, Submitted to Chemical Engineering Research and Design (October 1999).

Key Words :

Solid mixing, Gas-solid fluidization, Fluidized beds, Radioactive particle tracking

4.1 Context¹

In Chapter 3 the local mixing of the solids in gas-solid fluidized beds was studied. The solids diffusivity, both in radial and axial directions, were determined from the RPT data. The same experimental data can be employed for investigating the global mixing of solids in the same operating conditions. Therefore, in this chapter we study the global movement of solids in higher scale, which is the movement of the particles in the axial direction. The same experimental data obtained in Chapter 2 in gas-solid fluidized beds will be used to investigate such a behaviour.

4.2 Abstract

Solids movement in a gas-solid fluidized bed was monitored by a Radioactive Particle Tracking (RPT) technique. The gas was air at room temperature and atmospheric pressure and the solid was sand or FCC powder. The experiments were done at gas superficial velocities from 0.5 to 2.8 m/s for sand and 0.44 to 0.9 m/s for FCC (both in bubbling and turbulent regimes). A variety of solids behaviours, including overall dispersion, restricted axial movement, and unrestricted axial movement of solids, were studied by processing the data in an appropriate manner. The value of dispersion coefficient of solids was evaluated

¹ This section is not included in the original manuscript and only serves as a transition between the papers for the thesis.

from the overall dispersion of solids and was found to be constant ($\sim 0.04 \text{ m}^2/\text{s}$) under the experimental conditions of this work. The variance test was performed on the Retention Time Distribution (RTD) of solids in the restricted upward and downward movement. The results of the test clearly showed that upward movement of solids could be explained by a diffusive mechanism while the mechanism of downward movement of solids should be considered as convective. The variance test for unrestricted axial movement of solids showed that this type of movement cannot be explained by either of the two above mentioned mechanisms. In order to model the axial movement of the solids, it was assumed that solids move according to the two diffusive and convective mechanisms. By comparing the RTD of unrestricted movement of solids with the unsteady state formulation of the solid movement it was found that the solid velocity in the convective term of the model have to be less than the velocity of a single particle moving in a fluidized bed at the same condition. This fact suggests that the solid particles do not move separately in the fluidized bed, but move as a part of a solid aggregate, or clusters, which exercises a drag force greater than that of a single particle and, therefore, move at a lower velocity.

4.3 Introduction

Solid mixing is a fundamental subject in the design of many physical and chemical processes involving fluidized beds. The movement of solids in a fluidized bed has a crucial effect on the rate of mass and heat transfer and is able to control the final conversion of the chemical

reaction carried out in the bed. Consequently, reliable knowledge of the mechanism of solid mixing and solid movement in the fluid beds will help in designing a more efficient unit. Solids mixing has been reviewed by Fan et al.¹ and Kunii and Levenspiel².

It is often assumed that the solid mixing in a fluidized bed occurs based on a diffusion-type mechanism and therefore, attributing a dispersion coefficient, either in vertical or lateral direction, to the movement of solids in the bed. May³ was among the first researchers who measured the axial dispersion coefficient of solids in the fluidized bed. However, he reported that the experimental data do not fit the equation of diffusion satisfactorily in large units. Avidan and Yerushalmi⁴ found that the dispersion model represented the mixing data appropriately in the turbulent regime of fluidization where the bed is close to homogeneous, but fitted the data poorly in the bubbling regime. In general, the one-dimensional diffusion model is considered to be inadequate in describing axial mixing of solids, especially for large particle systems⁵.

Another category of models for characterization of the solid mixing in fluidized beds is the counterflow solid circulation, the simplest version of which is developed by van Deemter⁶ and later generalized by Gwyn et al.⁷. In this model, the solids are divided into upward moving and downward moving streams with their own velocities and volume fractions. The set of partial differential equations describing this model consists of two convective-type equations, one for each flow direction, with interchange mass transfer between upflow and

downflow streams. It is possible to relate the counterflow to the dispersion model where the interchange mass transfer coefficient of solids could be associated with an effective dispersion coefficient². Although the counterflow solid circulation model describes the solid mixing in bubbling fluidized beds better than the diffusion model, the key limitation of this method is the lack of reliable solids exchange coefficients⁸ which prevents using it with higher certainty.

In the present study, we have employed the radioactive particle tracking (RPT) technique to study the movement of solids in a gas-solid fluidized bed for various gas superficial velocities, both in bubbling and turbulent regimes of fluidization. This non-intrusive measurement technique allows us to visualize mixing of the solids and thoroughly investigate the mechanisms of the movement of solids in the fluidized bed.

4.4 Experimental

The experiments were done in a gas-solid fluidized bed as shown in Figure 4.1. The column was made of a Plexiglas pipe with 152 mm internal diameter and 1500 mm height. Air at room temperature was introduced into the bed through a conical section, passing through a stainless steel porous plate and a nozzle type air distributor. The nozzle type distributor was designed according to recommendations of Wen et al.⁹. Air flow rate was measured by

an orifice plate connected to a water manometer. A cyclone placed at the air outlet of the column returns the entrained solids back to the bed.

The solids used in the experiments were sand or FCC powder. Initial height of the bed was 0.22 m (1.5 times the column diameter). Properties of these particles are given in Table 4.1. The reported values of U_c were obtained by analyzing the pressure fluctuations of the bed measured by an absolute pressure transducer.

The tracers were made of a mixture of gold powder and epoxy resin. The ratio of gold to epoxy resin in the mixture was chosen such that to obtain a density equal to that of the sand at the end. Small pieces of the desired sizes were then taken off the solid mixture. The tracers of the size 420 μm , 500 μm , and 600 μm were used in the experiments. They were being activated in the SLOWPOKE nuclear reactor of École Polytechnique prior to each experiment. The produced isotope ^{198}Au emits γ -rays which were counted by 16 cylindrical NaI(Tl) scintillation detectors on sliding rails. A typical arrangement of the detectors around the fluidized bed is shown in Figure 4.1. Two personal computers simultaneously registered the number of γ -rays detected by each detector in every sampling period of 20 ms. These number of counts were used later to calculate the coordinates of the tracer. Details of the system calibration and the inverse reconstruction strategy for tracer position rendition are described by Larachi et al.^{10, 11}.

In each experiment a single tracer was placed into the bed to move freely with the other particles inside the bed. Movement of the tracer was then monitored for about 5 hours during which the count rate of the tracer at some 820,000 points were acquired. The bed was then made empty and the tracer was recovered from the solids in order to be used in the next experiment. Operating conditions and size of the tracers used in each run are summarized in Table 4.2.

4.5 Treatment of Data

The particle tracking technique enables us to study a variety of solids behaviours by processing the experimental data in an appropriate manner. Some of these behaviours are impossible to study with other experimental methods. In the following data processing we use the concept of ergodicity¹² from which it can be simply concluded that if a particle passes several times from a specific location, it can be considered equivalent to a process that several particles start their movement simultaneously from that location in the same operating condition.

4.5.1 Overall Dispersion of Solids

In order to evaluate the axial dispersion coefficient of solids in a fluidized bed, it is common to inject a certain amount of solids at the top of the bed and monitor the tracers until they

completely disperse in the bed. Assuming that axial mixing of the solids in the fluidized bed is solely due to dispersion of solid particles (no convection), the axial dispersion coefficient of solids, D_{sz} , can be evaluated by fitting the data obtained in evolution of the tracer concentration across the bed height to the one-dimensional unsteady state equation of dispersion:

$$\frac{\partial C}{\partial t} = D_{sz} \frac{\partial^2 C}{\partial z^2} \quad (4.1)$$

Having the time-position data obtained in particle tracking experiments, it is possible to virtually inject a large amount of tracers into top or bottom part of the fluidized bed in each experiment and follow the tracers until they completely disperse and form a uniform distribution across the bed. In order to do so, the tracer was followed until it would reach the top (or bottom) of the bed. The position of the tracer was then set aside for the next one second of the experiment to be used later. This procedure was continued until the tracer would pass 1000 times from the top (or bottom) section of the bed. In the next step, based on the concept of ergodicity, it was assumed that all these trajectories obtained according to the above procedure have initiated their journey at the same time, that is, 1000 tracers were injected at $t = 0$ into the top (or bottom) of the bed. Therefore, the tracer concentration as a function of time and axial position was available at the end of this step. A sample reconstruction of the solids diffusion by this method is shown in Figure 4.2.

The experimental tracer concentration data obtained above as a function of time and axial position were fitted to Eq. (4.1) by the least square technique using the Marquardt method and the value of the solid dispersion coefficient is determined. Since there is no withdrawal or consumption of solids in the bed, Eq. (4.1) should be solved subject to the following boundary conditions:

$$\frac{\partial C}{\partial z} = 0 \quad \text{at } z = 0 \quad \text{and } z = H$$

Initial condition for injection at the top:

$$t = 0, \quad H - \delta < z \leq H, \quad C = C_0$$

Initial condition for injection at the bottom:

$$t = 0, \quad 0 \leq z \leq \delta, \quad C = C_0$$

It is worth mentioning that the dispersion model [Eq. (4.1)] does not fit the experimental data satisfactorily. For instance, the correlation coefficient for different operating conditions of the present work was generally below 0.7. However, this problem has been commonly reported by previous workers^{3,4}.

The dispersion coefficients obtained by this method are shown in Figure 4.3. This figure demonstrates that the dispersion coefficient is not affected by the size of the tracer used in the experiment. Based on this result it can be concluded that solid dispersion in fluidized beds happens due to the movement of solid aggregates rather than diffusion of individual particles. This behaviour has been also reported by other researchers who have studied the clusters in high velocity fluidized beds. For instance, Horio et al.¹³ reported that decreasing the gas superficial velocity, from fast to turbulent fluidization, causes the formation of the larger clusters. Zou et al.¹⁴ also confirmed this trend and presented a statistical model for prediction of the cluster size as a function of the solids concentration in the bed. Therefore, it is reasonable to assume that the solids in the dense bed spend most of their time in the solid aggregates and the mixing of solids arises from the movement of these aggregates, leaving the individual particles with little effect on the overall mixing of the bed materials.

Predicted value of dispersion coefficient of solids by Lee and Kim¹⁵ for both FCC (Geldart A particles) and sand (Geldart B particles) are also shown in Figure 4.3. Although the dispersion coefficients calculated in the present study have the same order of magnitude of Lee and Kim's prediction, their correlations underpredict our data for sand and overpredict our data for FCC. Moreover, the correlation of Lee and Kim¹⁵ predicts an increase in the solid dispersion coefficient with increasing the gas superficial velocity. However, the calculated dispersion coefficients are essentially constant over the range of the excess gas superficial velocities ($U_0 - U_{mf}$) of this study. This difference in the trend and values between

our data and those predicted by Lee and Kim¹⁵ could be due to the difference in the range of the excess gas superficial velocities and the column diameter of this work and those considered by Lee and Kim. The experimental data adopted by Lee and Kim for deriving their correlation for Geldart B particles are mostly in lower excess gas superficial velocities and smaller column diameters which result in lower values of dispersion coefficient than this work. Wei and Zhu¹⁶ have also reported that at high gas superficial velocities the gas velocity has little influence on the dispersion of the solids. No definite conclusion can be drawn from the comparison of the dispersion coefficient of FCC powder obtained in this work and the correlation of Lee and Kim¹⁵ for Geldart A particles since the radioactive tracer in our FCC experiments cannot be considered to represent the typical FCC particle in the bed.

4.5.2 Restricted Axial Movement of Solids

As mentioned in the above section, the dispersion model does not fit the experimental data satisfactorily. This lack of fit could be because the mechanism of the mixing of solids in fluidized beds cannot be described by dispersion of solid particles. The results shown so far in the present study confirm that the movement of individual particles does not play an important role in the process of solid mixing which explains the shortcoming of the one-dimensional single parameter dispersion model in quantifying the solid mixing in fluidized beds. In fact, the assumption of diffusion of single particles is an over-simplification of the

solid mixing mechanism in the fluidized beds and it is necessary to investigate the behaviour of the solids in the dense fluidized bed more thoroughly. Hence, in the next stage of the study, the upward and downward movement of solids were surveyed.

Analysis of the Retention Time Distribution (RTD) of solids in axial direction can help to obtain a better understanding of the movement of solids in this direction. Although measurement of RTD in the riser of a circulating fluidized bed can be done easily by injecting some labelled solid particles at the bottom and monitoring them as they pass through the riser (e.g., Patience et al.¹⁷, Wei and Zhu¹⁶), it is not practically possible to perform the same test in the dense bed. This difficulty is because the injected tracers do not exit from the other end of the dense bed, but they re-enter the bed and re-circulate in there until a uniform mixture is achieved (like what is obtained in the previous section). Therefore, in the case of the dense bed we deal with a close system which its RTD is impossible to obtain. However, the radioactive particle tracking technique enables us to overcome this difficulty and study the open circuit of solid movement in the dense bed.

In order to obtain and analyse the RTD of axial movement of solids, we first studied the *restricted axial movement* of solids in the fluidized bed. By the term “restricted axial movement” we mean those movements of solids which start from one end of the bed (top or bottom), terminate at the other end of the bed (bottom or top), and no (or negligible) change in the axial direction of the move occurs in the midway. The experimental data

obtained in this work were used to explore this type of solid movement. This time, the tracer was again followed until it would reach the top (or bottom) part of the bed. The tracer was then pursued and its position was set aside until it would reach the bottom (or top) of the bed. If in the midway the tracer would change its direction, the whole trajectory would be rejected and search for finding another proper trajectory was continued. However, small deviation (less than 20 mm) from the main direction of the movement of the tracer in the midway was tolerated. This procedure was continued until all the “restricted” trajectories were found. Examples of such trajectories are shown in Figures 4.4 *a* for restricted upward and 4 *b* for restricted downward movement of solids. Also a sample of evolution of restricted upward movement of solids is shown in Figure 4.5.

At this stage, the RTD of solids in their upward or downward movement can be achieved inside the dense bed. The most important information that could be sought from the RTD is to verify whether the mechanism of the axial movement of solids is diffusive or not. Levenspiel and Fitzgerald¹⁸ proposed a simple test for discriminating between the dispersion model and the convective model. According to Levenspiel and Fitzgerald¹⁸ the variance of the RTD curve in the dispersion model is

$$\sigma_t^2 = \left(\frac{2D_{sz}}{V_s^3} \right) L \quad (4.2)$$

while in the convective model the variance is

$$\sigma_t^2 = \left(\frac{\sigma_\theta}{V_s} \right)^2 L^2 \quad (4.3)$$

where σ_θ is a constant. Plotting the variance of the RTD curve vs length of the reactor in full logarithmic scale would result in a line with a slope of 1 for the diffusion model [Eq. (4.2)] while the slope would be 2 for the convective model [Eq. (4.3)]. The treatment of the RPT data for observing the restricted axial movement of solids, as described above, allows us to extract the RTD of solids at several axial positions in the dense bed. Therefore, by performing the variance test it is possible to determine the mechanisms of the axial movement of solids in the experiments of the present work.

Figure 4.6 illustrates the variance test for experiment no. 5 (see Table 4.2). The slope of the variance of RTD curve vs height of the bed is very close to 1 for upward movement and very close to 2 in the case of downward movement of solids. This trend was observed in all the experiments of the present study. Therefore, it can be clearly concluded that the solids move upward according to the diffusive mechanism while the mechanism of downward movement of solids is convective. This result demonstrates that the solids do not rise from bottom to the top of the dense bed, as bubble wakes and clouds, by convective motion of bubbles and also their return back to the distributor level through emulsion phase does not occur by the diffusion of single particles. These phenomena can be explained by the movement of solids as aggregates. The variance test shows that in fact, the solids do rise attached to the bubbles

and clusters in a convective manner, but at the same time there is a high rate of redistribution of accompanying solids due to break up and coalescence of the bubbles and clusters which makes the upward movement of solids diffusive. The solids released from the bubble wakes and clouds at the top of the bed form clusters of different sizes. These clusters return the bottom of the bed with no or little exchange between the solids in them which make downward movement of solids convective.

The solids flow pattern described above can be also detected in the fast fluidization regime and works of other researchers confirm such pattern. Horio and Kuroki¹⁹ observed the clusters in the freeboard of the bubbling and in the circulating fluidized beds and found upward moving, stagnant, and even downward moving clusters. Tuzla et al.²⁰ further indicated that particles clusters exist in the downflow of the solids in the downer. Moreover, Horio et al.¹³ demonstrated that the clusters are not completely suspended by the gas in the turbulent regime, but they are suspended in the fast fluidization regime. As a result, since the experiments of this work have been carried out in the bubbling and turbulent fluidization regimes (lower gas velocities than that of fast fluidization), it is reasonable to expect the existent of larger clusters, swinging up and down in the dense bed.

The difference in the flow mechanisms between upflow and downflow of the solids was likewise suggested by Wei and Zhu¹⁶. They found that the existent of particle aggregates leads to large solids dispersion in the riser of the fast fluidized bed and that the solid mixing

is small in the downflow of solids, resulting in a flow pattern close to that of the plug flow in the downer. Based on the careful examination of the RTD curves, Wei and Zhu¹⁶ proposed that most particles flow in the form of individual particles or small particle clusters in their downward movement. Since the experiments of this work were carried out in lower gas superficial velocities than that of Wei and Zhu¹⁶, the effect of single particle movement is negligible in our results, nevertheless, the tendency of downward moving clusters to remain as individual aggregates is proved by the variance test.

It is possible to evaluate the upward dispersion coefficient of solids based on Eq. (4.2). The velocity of a single particle moving upward (V_p) was assumed to be the same as the effective velocity of the upward-moving solids ($V_p = V_s$). The upward dispersion coefficient of solids was then extracted, according to Eq. (4.2), from the slope of the line obtained from plotting the variance of the RTD curve against the height of the bed. The strictly upward dispersion coefficients obtained by this method are shown in Figure 4.7. Comparison between Figures 4.3 and 4.7 reveals that for sand the strictly upward dispersion coefficient of solids (D_{up}) is an order of magnitude greater than that previously obtained from the overall dispersion of solids (D_{s2}). The existence of this difference in the order of magnitude has two reasons. First, the overall movement of solids, from which the dispersion coefficients in Figure 4.3 was obtained, includes both upflow and downflow of solids while in the restricted movement, only upward movement was considered for calculation of the dispersion coefficients shown in Figure 4.7. The portion of the solids moving in the opposite direction diminishes the

overall mass transfer in the upward direction which in turn results in a lower value of the dispersion coefficient. The second factor is the assumption that the average velocity of the upward-moving solids can be estimated from the upward movement of a single particle. As it was discussed earlier (and again can be confirmed in Figure 4.7), the solid particles do not move freely in the bed, but they move as a part of a solid aggregate which can be several times bigger than the particle itself. Consequently, the effective velocity of the solids in the bed is lower than that of the single particle ($V_s < V_p$) and the dispersion coefficients reported in Figure 4.7 are over estimated. However, at this stage we are not able to have a better estimation for the effective velocity of the solids in their axial movement and will accomplish this task in the next section.

In the case of experiments with FCC powder, the estimated strictly upward dispersion coefficients of solids have the same order of magnitude as those obtained by overall dispersion of solids in the previous section. However, the estimated dispersion coefficient of the upward movement of solids in this case are also larger than that of overall dispersion of solids and show reasonable agreement with the prediction of the correlation of Lee and Kim¹⁵ for Geldart A particles.

4.5.3 Unrestricted Axial Movement of Solids

The restricted axial movement of the solids in fluidized beds cannot represent the solids movement in this direction. The solids may change their directions many times during a sample trajectory. In fact, the restricted trajectories constitute up to about 30% of all trajectories, generally about 3000 to 4000. Consequently, although studying the restricted axial movement of solids was advantageous in understanding the mechanisms of the movement of solids in axial direction, the results obtained so far based on such a movement cannot be applied to modeling the global movement of solids in fluidized beds. Therefore, in the next step of this study, the unrestricted movement of the solids has been investigated.

In unrestricted axial movement of solids, they start their journey from one end of the bed (top or bottom), terminate at the other end of the bed (bottom or top), and the solid particles move in their natural manner, i.e., they may change their axial direction as many times and by any extent as possible in the midway. The RTD of the solids can be obtained in the same way that was described in the previous section. Examples of such trajectories are shown in Figures 4.8 *a* for upward and 4.8 *b* for downward movement of solids.

Figure 4.9 illustrates the plot of the variances of RTD curves vs height of the bed for both unrestricted upward and downward movement of solids in experiment no. 5 (see Table 4.2). It can be clearly observed in this figure that the calculated variances against height of the bed

in a full logarithmic scale are not linear and furthermore, the slopes calculated by the least squares technique are far from 1 (diffusion model) or 2 (convective model). The same trend was observed for all the experiments of this work. As a result, the solids movement in fluidized beds cannot be described neither by the diffusive nor by the convective model. However, it is known from the analysis of the restricted movement of solids that the overall movement of solids is in fact a combination of diffusive and convective mechanisms. Thus, it is appropriate to assume that the actual movement of solids in the dense bed can be described by the interpolation between the two extreme mechanisms.

In order to describe the unrestricted movement of solids in the dense bed it can be imagined that the movement of the solids is the superposition of the diffusive motion of the solids in the emulsion phase and their convective motion at the same time. The following assumptions were considered in developing a model for describing the unrestricted axial movement of solids:

- (a) The solids in the dense bed are consisted of two parts with extreme behaviours: emulsion and upward moving solids.
- (b) In the emulsion, the solids move according to diffusion of particles only with the solid diffusivity taken into account for describing the diffusive behaviour of solids. Moreover, it is assumed that no velocity gradient exists in the emulsion. As a result, the solid diffusivity at zero shear rate is employed in the model. The axial solid diffusivity at zero shear rate is given by Mostoufi and Chaouki²¹:

$$Pe_{z,0} = \frac{(U_0 - U_{mf})d_s}{D_{z,0}} = 0.02 \quad (4.4)$$

The value of solid diffusivity obtained from Eq. (4.4) is in most cases an order of magnitude less than the dispersion coefficient of the solids due to the fact that the solid diffusivity is a local property of the bed and arises from the self diffusion of solids particles, while the dispersion coefficient represents a diffusion-like process superimposed on plug flow of solids and, therefore, is a global property of the flow of solids.

- (c) The solid velocity in the model is considered as the effective solid velocity. As discussed earlier, the particles do not move individually in the dense bed, therefore, the effective solid velocity is expected to be smaller than the single particle velocity. Since the effective solid velocity is not available at this stage, we employ the following relation for evaluating it:

$$V_s = \beta V_p \quad (4.5)$$

where $0 < \beta \leq 1$.

The governing equation for representing the RTD of solids based on these assumptions is:

$$\frac{\partial C}{\partial t} = D_{z,0} \frac{\partial^2 C}{\partial z^2} - \beta V_p \frac{\partial C}{\partial z} \quad (4.6)$$

The value of β was obtained by fitting the RTD of solids in their unrestricted movement to Eq. (4.6) by the least square technique. The initial and boundary conditions are:

Unrestricted upward movement of solids:

$$\begin{aligned} t = 0, \quad 0 \leq z \leq \delta, \quad C &= C_0 \\ z = 0, \quad \frac{\partial C}{\partial z} &= 0 \\ z = H, \quad C &= 0 \end{aligned}$$

Unrestricted downward movement of solids:

$$\begin{aligned} t = 0, \quad H - \delta \leq z \leq H, \quad C &= C_0 \\ z = H, \quad \frac{\partial C}{\partial z} &= 0 \\ z = 0, \quad C &= 0 \end{aligned}$$

The β values calculated by this method for the experiments with sand are shown in Figure 4.10. The estimated correlation coefficient for β at different operating conditions of the present work was about 0.8 which indicates that the convective-diffusive model [Eq. (4.6)] represents the movement of solids in the fluidized beds better than the diffusion model [Eq. (4.1)]. For both upward and downward movement of solids the following correlation can be applied

$$\beta = \frac{V_s}{V_p} = \exp\left[\frac{-A}{(U_0 - U_{mf})^p}\right] \quad (4.7)$$

where the constants A and p are given in Table 4.3. The correlation coefficient matrix for Eq. (4.7) was calculated to be

$$R_{up} = \begin{bmatrix} 1 & -0.1131 \\ -0.1131 & 1 \end{bmatrix} \quad R_{down} = \begin{bmatrix} 1 & 0.0854 \\ 0.0854 & 1 \end{bmatrix} \quad (4.8)$$

Also, the 95% confidence intervals for the constants of Eq. (4.7) were calculated as:

Upward:

$$\begin{aligned} 0.551 &\leq A \leq 0.610 \\ 0.631 &\leq p \leq 0.809 \end{aligned} \quad (4.9)$$

Downward:

$$\begin{aligned} 0.753 &\leq A \leq 0.887 \\ 0.384 &\leq p \leq 0.676 \end{aligned} \quad (4.10)$$

Figure 4.10 illustrates that the value of β is higher for upward movement than that of the downward movement of solids which simply indicates that the solids tend to be transported upward faster than downward. This difference is greater at high gas superficial velocities, where the convective mechanism becomes more important, and is lower at lower gas

superficial velocities, where diffusion is the predominant mechanism in transporting the solids in the fluidized bed. The increase in the value of β with the gas superficial velocity for both upward and downward movement of solids indicates that the solid aggregates are more likely to break-up and form smaller clusters at higher gas velocities. This result is consistent with the observations of Horio et al.¹³ and the cluster size distributions given in the literature (e.g., Zou et al.¹⁴). Wei and Zhu¹⁶ also concluded that increasing gas velocity tends to destroy the clusters and therefore, increases the presence of smaller clusters and dispersed particles.

At very high gas superficial velocity both β values for upward and downward movement reach unity, based on Eq. (4.7), which predicts that no solid aggregate exists at high enough gas velocity and the particles move independent of the other particles in the bed. Wei and Zhu¹⁶ evaluated fraction of dispersed particles and illustrated that this fraction increases with increasing superficial gas velocity, reaching unity at very high velocities. It should be emphasised that the experiments of Wei and Zhu¹⁶ were carried out in the freeboard of the fast fluidized bed whereas in this work the solids behaviour in the dense bed has been investigated. A comparison between their results and those reported in the present study suggests that the convective-diffusive model developed here [Eq. (4.6)] can be equally applied to the fast fluidization regime.

According to Eq. (4.7), at the gas superficial velocity close to the minimum fluidization both β values for upward and downward movement reach zero. This is the region that the solids

move mainly due to the diffusion mechanism and the convection term in Eq. (4.6) (the second term in the right hand side) vanishes.

It is possible to estimate the cluster diameter in the dense bed from the effective solid velocity achieved in this work. Assuming that the effective solid velocity is in fact the velocity of the clusters in the bed and that the voidage of the cluster is ε_{mf} , the equivalent spherical cluster diameter can be calculated by considering these clusters as individual species moving in the dense bed. Results of such calculations are shown in Figure 4.11. It can be seen from this figure that at low gas superficial velocity, the cluster size is almost equal to the average size of the particles in the bed ($d_c = d_s$) which suggests that the dense phase is mainly in the form of emulsion rather than freely moving clusters. However, by increasing the gas velocity the clusters start to form and grow bigger. The plot in Figure 4.11 is shown in an extended range of the excess gas superficial velocity to illustrate the slight decrease in the cluster size at high gas velocities for the upward curve. The same trend could be seen for the downward curve at higher velocities (not shown in Figure 4.11). This behaviour is consistent with fact that by increasing the gas superficial velocity in the bed, the clusters break into smaller clusters and at very high velocity the particles exist as individuals. At low to moderate gas superficial velocity (i.e., bubbling and turbulent regimes) this decrease in the cluster size may be neglected and the following correlation can be proposed for estimating the equivalent cluster diameter in the dense bed

$$\frac{d_c}{d_s} = a - b e^{-c(U_0 - U_{mf})} \quad (4.11)$$

where the constants a , b and c are given in Table 4.3. It is worth mentioning that the existent models for predicting the cluster size (e.g., Horio and Ito²², Xu and Li²³) give unacceptably high values of the cluster size due to the fact that these models have been developed for circulating fluidized beds where the voidage is considerably higher than that of the dense bed at bubbling and turbulent regimes.

For all of the experiments with FCC powder, it was found that the best model describing the unrestricted upward movement of solids is the dispersion model [i.e., $\beta = 0$ in Eq. (4.6)] and for the unrestricted downward movement of solids the effective velocity of solids is very close to the velocity of the single particle [i.e., $\beta = 1$ in Eq. (4.6)]. This outcome is different from that obtained in the case of sand particles where β found to be between zero and one, either for upward or downward movement of solids. However, it is not possible to draw a clear conclusion for FCC beds from the data of the present work because the size and the density of the tracers employed in FCC experiments were considerably different from those of the bed particles. The tracers used in the experiments with FCC cannot represent the individual particles in the bed. Nevertheless, if the tracers associates itself with the solid aggregates in the bed, its movement can be considered to represent the bulk movement of

the solids during the fluidization process. Yet, an estimation of the size of the solid clusters in the dense bed is needed in order to determine whether the tracer can join these clusters. If the solid clusters were larger than the size of the tracer, it can be concluded that the tracer is qualified for entering the solid aggregates and thus the tracer would represent the overall movement of the solids in the fluidized bed. It is also possible to consider a distribution of the clusters in the fluidized bed, only some of which are large enough to carry the tracer with themselves. The validity of these assumptions should be verified in the future works.

In order to test the performance of the dispersion model [Eq. (4.1)] and the new diffusive-convective model [Eq. (4.6)], the mean residence time of solids at 300 mm (equals to two times the bed diameter) above the injection point (in the case of injection at the bottom of the bed) or below the injection point (in the case of injection at the top of the bed) was calculated and compared to the corresponding experimental value. This comparison is presented in Figure 4.12 in which only the calculated residence times based on Eq. (4.6) are shown. The calculated residence time from Eq. (4.6) was obtained by evaluating β from Eq. (4.7) rather than what was obtained from the experimental data by the least squares technique. Although the parity plot in Figure 4.12 is scattered with a mean error of about 35%, it shows that Eq. (4.6) predicts the correct order of magnitude for the residence time of solids. However, this is not the case for Eq. (4.1) which predicts the residence time of solids to be an order of magnitude greater than the experimental. The dispersion model over-predicts the residence time with a mean error of about 240% and its predictions are not

shown in Figure 4.12 because they fall beyond the scale of the plot. This comparison illustrates the extent of improvement in modelling the movement of solids by adding the convective term to the dispersion model and employing the solid diffusivity instead of the dispersion coefficient.

Now that the estimate of the effective solid velocity is available it is possible to re-calculate the strictly upward dispersion coefficient of solids (D_{up}) for sand, which was evaluated with over estimation, in the previous section. By employing V_s^* instead of V_p in the slope of Eq. (4.2), the actual values of the strictly upward dispersion coefficient were calculated and are displayed in Figure 4.7 as black keys. The prediction of Lee and Kim¹⁵ is also repeated in this figure. As expected and discussed before, the actual upward dispersion coefficients are lower than that estimated by assuming that the effective solid velocity is equal to the single particle velocity. The actual upward dispersion coefficients show the same order of magnitude and the same trend as that given by Lee and Kim¹⁵. However, as explained earlier, the corrected upward dispersion coefficients obtained in this work, are still higher than the prediction of Lee and Kim¹⁵ due to the fact that their correlation considers unrestricted movement of solids. Since we were not able to estimate the effective solid velocity for experiments with FCC, it is not possible to correct the upward dispersion coefficient of solids for these experiments and are not shown in Figure 4.7.

As explained before, changes in the variance of the RTD curve is proportional to the vessel length or square of the vessel length in the case of the dispersive model or convective model, respectively. Levenspiel and Fitzgerald¹⁸ posed the question that in the case of the intermediate situation if we can develop a flow model in which

$$\sigma_r^2 \propto L^n \quad 1 \leq n \leq 2 \quad (4.12)$$

where n characterizes the location between extremes. It was indicated in the present study that the answer to this question is no. The data of the experiments of this work showed that for a diffusive-convective model, n is not between 1 and 2 but is much less than 1. The solution of Eq. (4.6) with the specified boundary conditions also confirms this fact.

4.6 Conclusions

Solids in a fluidized bed do not move independently but as aggregates such as bubble wake, bubble cloud, and clusters. All the quantities evaluated in the present study show that these parameters change only with gas superficial velocity and are independent of the size of the tracer. In other words, the solid particles do not move individually. Each single particle is attached to a solid aggregate in the dense bed and moves with it until it breaks-up. The particle then enters another solid ensemble and continues its move with the new ensemble. The clusters may also join each other and proceed as a single solid ensemble.

The dispersion coefficient of solids obtained from releasing the tracers at the top or bottom of the bed show a constant value of about $0.04 \text{ m}^2/\text{s}$ over the range of the gas superficial velocity employed in this work. However, the dispersion coefficient evaluated from overall dispersion of solids in the fluidized bed was based on the assumption that the mixing process in the dense bed is diffusive while the equation of diffusion fits poorly to the experimental data.

The restricted movement of the solids, in which the tracers move from one side of the bed (top or bottom) to another (bottom or top) without considerable change in the direction, has also been studied. It has been found by performing the variance test on the RTD curves that the upward movement of solids in the dense bed is diffusive while their downward movement is convective. This behaviour can be justified by the high frequency of bubble-bubble and/or cluster-cluster and/or bubble-cluster interactions while rising in the bed which makes the upward movement of solids diffusive rather than convective. On the other hand, the solid descend as clusters with no or very little interactions between themselves which makes the downward movement of solids convective.

Analyzing the RTD of solids in the unrestricted axial movement demonstrated that this kind of movement cannot be considered either convective or diffusive alone. A diffusive-convective model has been proposed to describe the axial movement of solids in which the particle velocity was replaced with the effective solids velocity. This model is capable of

predicting the behaviour of solids from low gas superficial velocities, where solid mixing takes place only based on diffusion, up to very high gas superficial velocities, where all the solid particles move independently. The effective solid velocity has been estimated to be equal to zero at gas superficial velocities close to the minimum fluidization and reaches the single particle velocity at very high gas superficial velocities. In the experiments with FCC, it was not possible to evaluate the effective solid velocity due to the fact that the employed tracer was much bigger than the average size of the FCC powder in the experiments.

The change in the value of the ratio of effective solid velocity to particle velocity with gas superficial velocity was indicated to be smooth and gradual which can be interpreted as incremental, rather than sudden, change in the state of fluidization with gas superficial velocity. In other words, transition between fluidized regimes, from minimum fluidization to pneumatic transport, is essentially gradual and the behaviour of the bed may be considered as an interpolation between the behaviour of the emulsion phase (roughly at minimum fluidization) and that of the pneumatic transport. This claim can be verified for transition from bubbling to turbulent fluidization from the experiments of this study since no sharp change in the trend of the studied parameters was observed with gas superficial velocity. The similarities between the bubbling and turbulent regimes and turbulent and fast fluidization has been also reported by other researchers²⁴. In fact, the change in the gas superficial velocity changes the size and the solid content of the clusters but not the two-phase structure of the bed. The dynamic two-phase flow structure of the gas-solid fluidized

beds has been studied by employing fiber optics and this behaviour of the bed has been observed directly²⁵.

4.7 Calculation of the Single Particle Velocity (V_p)

The particle velocity can be estimated from the force balance on the upward moving particle:

$$\frac{\pi}{6} d_s^3 (\rho_s - \rho_g) g = \frac{1}{2} \rho_g V_{sl}^2 \cdot \frac{\pi}{4} d_s^2 \cdot C_D \quad (4.10)$$

which can be rearranged to

$$V_{sl}^2 = \frac{4 d_p (\rho_s - \rho_g) g}{3 \rho_g C_D} \quad (4.11)$$

In the case of upward moving particle, the slip velocity is obtained from

$$V_{sl} = \frac{U_0}{\varepsilon} - V_p \quad (4.12)$$

The effective drag coefficient was calculated from

$$C_D = f \cdot C_{D,o} \quad (4.13)$$

where the standard drag coefficient was calculated from the following correlation given by²⁶:

$$C_{D.o} = \frac{24}{Re_t} (1 + 0.173 Re_t^{0.657}) + \frac{0.413}{1 + 16300 Re_t^{-1.09}} \quad (4.14)$$

and the correction factor was obtained from

$$f = \varepsilon^{-m} \quad (4.15)$$

in which the exponent m is given by Mostoufi and Chaouki²⁷:

$$m = 3.02 Ar^{0.22} \cdot Re_t^{-0.33} \cdot \left(\frac{d_p}{d_s} \right)^{0.40} \quad (4.16)$$

where, in the case of this study, $d_p = d_s$. The voidage of the dense bed was calculated from²⁸:

$$\frac{\varepsilon - \varepsilon_{mf}}{1 - \varepsilon_{mf}} = 0.14 Re_s^{0.4} Ar^{-0.13} \quad (4.17)$$

The velocity of an upward moving single particle (V_p) was calculated from Eqs. (4.10) to (4.17).

4.8 References

1. Fan, L. T., Chen, Y., and Lai, F. S., 1990, Recent Developments in Solids Mixing, *Powder Technol.*, 61: 255-287.

2. Kunii, D., and Levenspiel, O., 1991, Fluidization Engineering, 2nd ed., Butterworth-Heinemann, Boston, MA.
3. May, W. G., 1959, Fluidized-Bed Reactor Studies, *Chem Eng Prog*, 55: 49-56.
4. Avidan, A., and Yelushalmi, J., 1985, Solids Mixing in an Expanded Top Fluid Bed, *AIChE J*, 31: 835-841.
5. Lim., K. S., Zhu, J. X., Grace, J. R., 1995, Hydrodynamics of Gas-Solid Fluidization," *Int J Multiphase Flow*, 21(Suppl.): 141-193.
6. van Deemter, J. J., 1967, The Counter-Current Flow Model of a Gas-Solids Fluidized Bed, *Proc Int Symp On Fluidization*, Drinkenburg, A. A., ed., Netherlands Univ. Press, Eindhoven, 334-341.
7. Gwyn, J. E., Moser, J. H., and Parker, W. A., 1970, A Three-Phase Model for Gas-Fluidized Beds, *Chem Eng Prog Symp Ser*, 66: 19-27.
8. Lim, K. S., Gururajan, V. S., and Agarwal, P. K., 1993, Mixing of Homogeneous Solids in Bubbling Fluidized Beds: Theoretical Modeling and Experimental Investigation Using Digital Image Analysis, *Chem Eng Sci*, 48: 2251-2265.

9. Wen, C. Y., Krishnan, R., and Kalyanaraman, R., 1980, Particle Mixing Near the Grid region of Fluidized Beds, *Fluidization*, Grace, J. R., and Matsen, J. M., eds., Plenum, New York, 405-412.
10. Larachi, F., Chaouki, J., and Kennedy, G., 1994, A γ -Ray Detection System for 3-D Particle Tracking in Multiphase Reactors, *Nucl Instr and Meth A*, 338: 568-576.
11. Larachi, F., Chaouki, J., and Kennedy, G., 1995, 3-D Mapping of Solids Flow Fields in Multiphase Reactor with RPT, *AIChE J*, 41: 439-443.
12. Monin, A. S. and Yaglom, A. M., 1971, *Statistical Fluid Mechanics: Mechanics of Turbulence*, Lumley, J. L., ed., MIT Press, Cambridge, MA, vol. 1.
13. Horio, M., Ishii, H., and Nishimuro, M., 1992, On the Nature of Turbulent and Fast Fluidized Beds, *Powder Technol*, 70: 229-236.
14. Zou, B., Li, H., Xia, Y., and Ma, X., 1994, Cluster Structure in a Circulating Fluidized Bed, *Powder Technol*, 78: 173-178.
15. Lee, G. S., and Kim, S. D., 1990, Axial Mixing of Solids in Turbulent Fluidized Beds, *Chem Eng J*, 44, 1-9.

16. Wei, F. and Zhu, J. X., 1996, Effect of Flow Direction on Axial Solid Dispersion in Gas-Solids Cocurrent Upflow and Downflow Systems, *Chem Eng J*, 64: 345-352.
17. Patience, G., Chaouki, J., and Kennedy, G., 1990, Solids Residence Time Distribution in CFB Reactors, *Circulating Fluidized Bed Technology III*, Basu, P., Horio, M., and Hasatani, M., eds., Pergamon Press, Oxford, 599-604.
18. Levenspiel, O., and Fitzgerald, T. J., 1983, A Warning on the Misuse of the Dispersion Model, *Chem Eng Sci*, 38: 489-491.
19. Horio, M., and Kuroki, H., 1994, Three-Dimensional Flow Visualization of Dilutely Dispersed Solids in Bubbling and Circulating Fluidized Beds, *Chem Eng Sci*, 49: 2413-2421.
20. Tuzla, K., Sharma, A. K., Chen, J. C., Schiewe, T., Wirth, K. E., and Molerus, O., 1998, Transient Dynamics of Solid Concentration in Downer Fluidized Bed, *Powder Technol*, 100:166-172.
21. Mostoufi, N., and Chaouki, J., 1999, Local Solid Mixing in Gas-Solid Fluidized Beds, Submitted to *Powder Technol*.

22. Horio, M., and Ito, M., 1997, Prediction of Cluster Size in Circulating Fluidized Beds, *J Chem Eng Jpn*, 30: 691-697.
23. Xu, G., and Li, J., 1998, Analytical Solution of the Energy Minimization Multi-Scale model for Gas-Solid Two-Phase Flow, *Chem Eng Sci*, 53: 1349-1366.
24. Bai, D., Issangya, A. S., and Grace, J. R., 1999, Characteristics of Gas-Fluidized Beds in Different Flow Regimes, *Ind Eng Chem Res*, 38: 803-811.
25. Cui, H., Mostoufi, N., and Chaouki, J., 1999, Characterization of Dynamic Gas-Solid Distribution in Fluidized Beds, Submitted to *Chem Eng J*.
26. Turton, R., and Levenspiel, O., 1986, A Short Note on the Drag Correlation for Spheres, *Powder Technol*, 47, 83-86.
27. Mostoufi, N., and Chaouki, J., 1999, Prediction of Effective Drag Coefficient in Fluidized Beds, *Chem Eng Sci*, 54: 851-858.
28. Werther, J., and Wein, J., 1994, Expansion Behavior of Gas Fluidized Beds in the Turbulent Regime, *AIChE Symp Ser*, 90(301): 31-44.

Table 4.1 Properties of the solids

Solid	ρ_s (kg/m ³)	d_s (μm)	U_c (m/s)	U_{mf} (m/s)	ϵ_{mf}
Sand	2650	385	1.5	0.24	0.42
FCC	1670	70	0.77	0	0.45

Table 4.2 Summary of experimental conditions

No.	Solids	U_0	d_T
		(m/s)	(μm)
1	Sand	0.5	500
2	Sand	0.9	420
3	Sand	0.9	500
4	Sand	1	420
5	Sand	1	500
6	Sand	1	600
7	Sand	1.5	420
8	Sand	1.5	500
9	Sand	1.5	600
10	Sand	2	420
11	Sand	2	500
12	Sand	2	600
13	Sand	2.4	500
14	Sand	2.8	500
15	FCC	0.44	420
16	FCC	0.44	500
17	FCC	0.75	420
18	FCC	0.75	500
19	FCC	0.9	420
20	FCC	0.9	500

Table 4.3 The constants of Eqs. (4.7) and (4.11)

	Upflow	Downflow
<i>A</i>	0.58	0.82
<i>p</i>	0.72	0.53
<i>a</i>	3.30	6.29
<i>b</i>	3.78	5.78
<i>c</i>	2.36	0.58

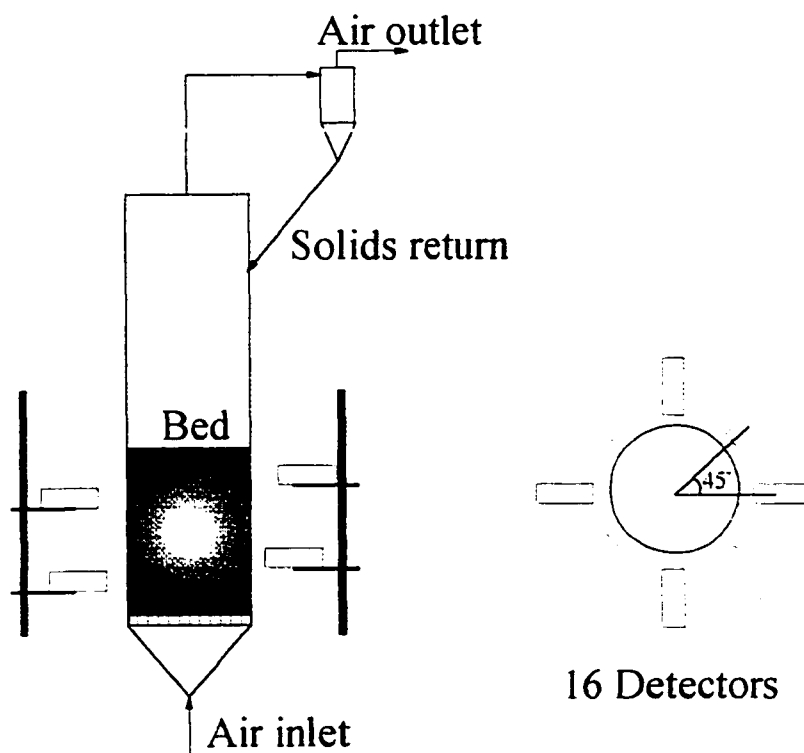


Figure 4.1 Experimental set-up and typical configuration of the detectors.

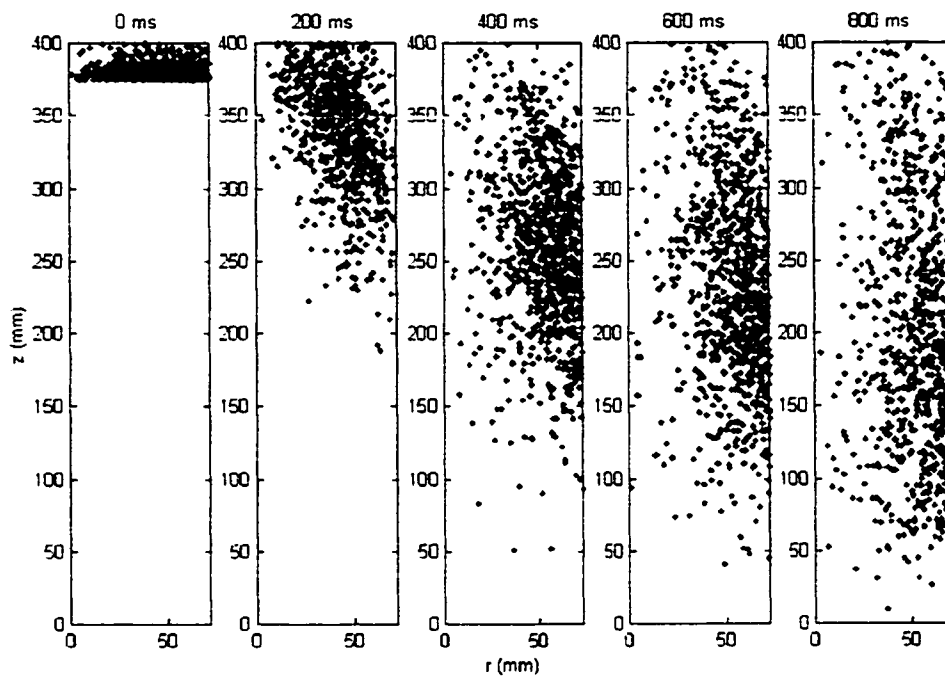


Figure 4.2 Overall diffusion of 1000 tracers injected to the top of the bed (sand, $U_0 = 1$ m/s, $d_T = 420\mu\text{m}$).

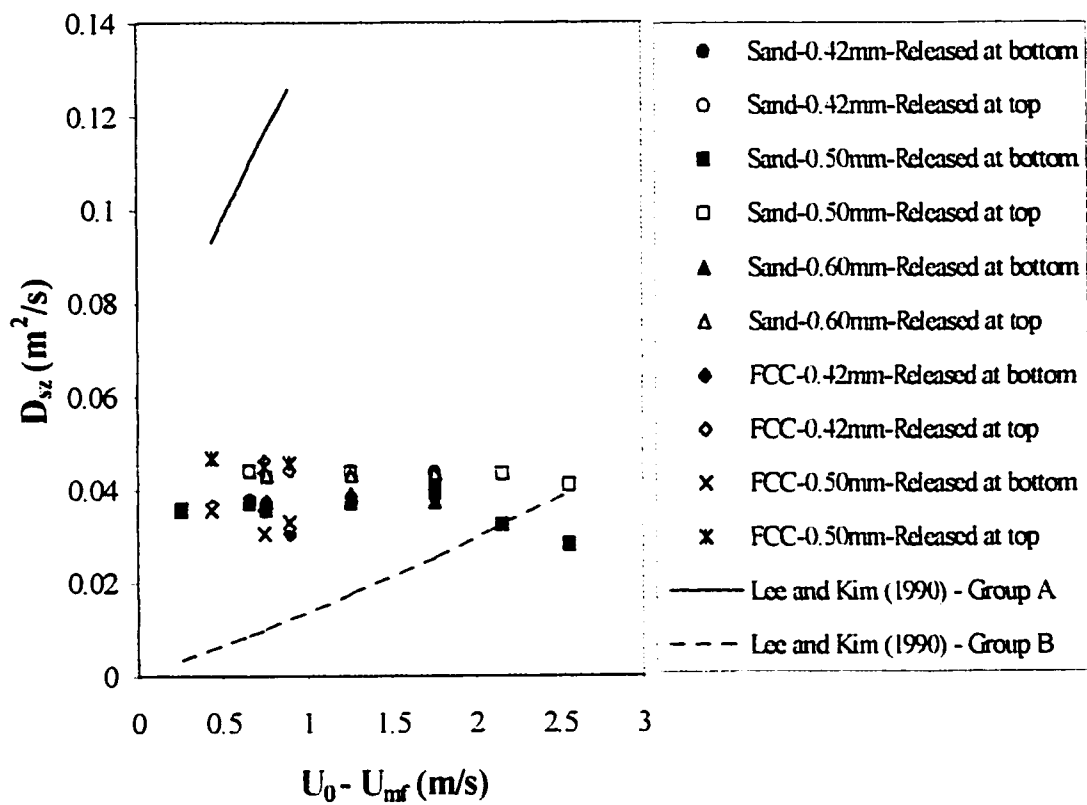


Figure 4.3 Calculated dispersion coefficient based on overall dispersion of solids.

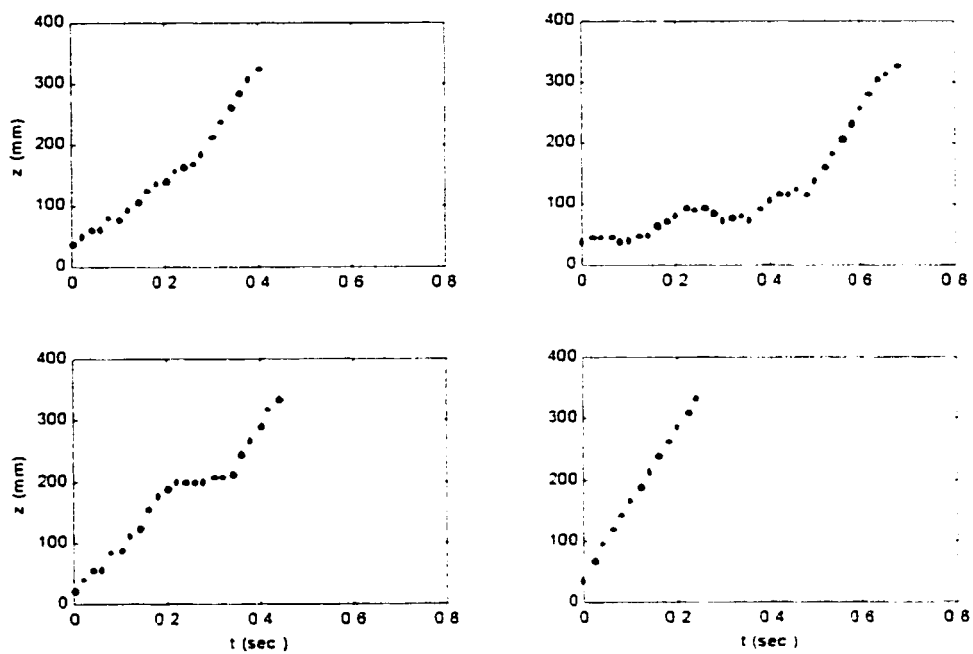


Figure 4.4 Restricted movement of solids (sand, $U_0 = 1$ m/s. $d_T = 420$ μ m): (a) Upward.

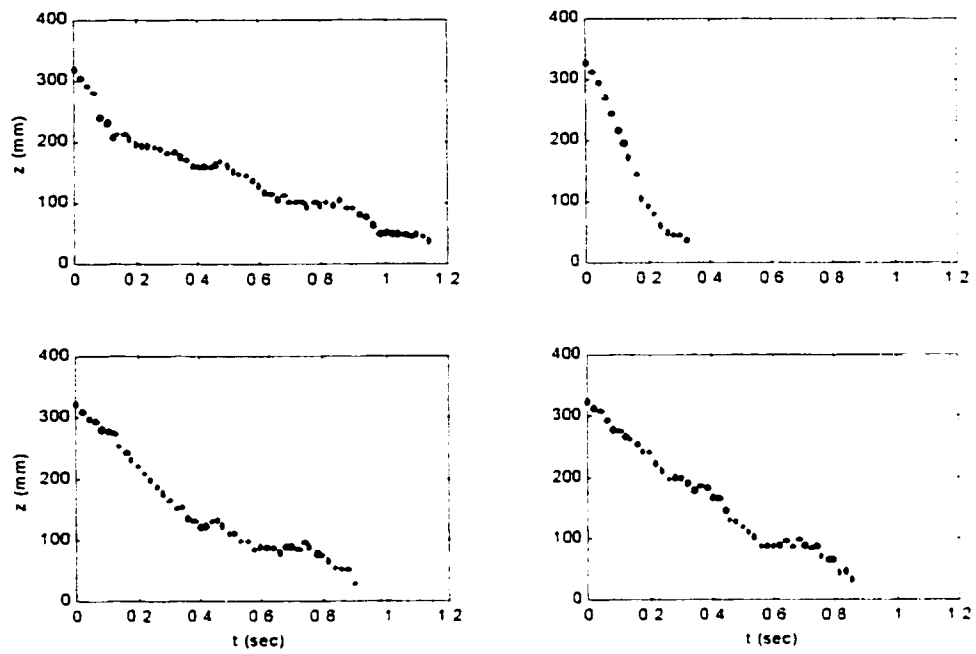


Figure 4.4 Restricted movement of solids (sand, $U_0 = 1$ m/s, $d_T = 420$ μm): (b) Downward.

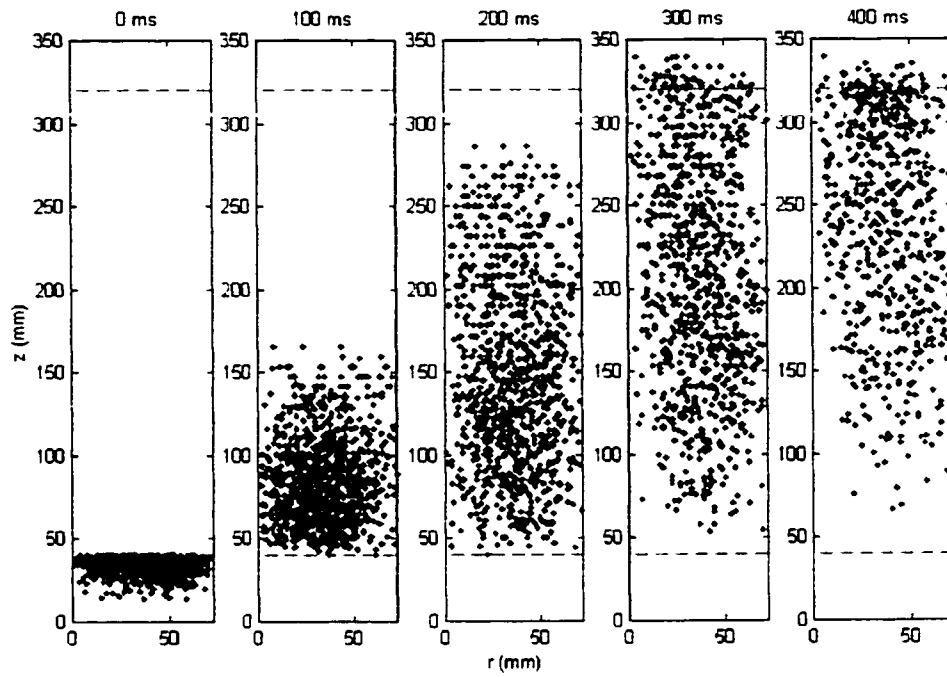


Figure 4.5 Evolution of restricted upward movement of solids (sand, $U_0 = 1$ m/s, $d_T = 420$ μ m). The RTD of solids was studied between the two dashed lines.

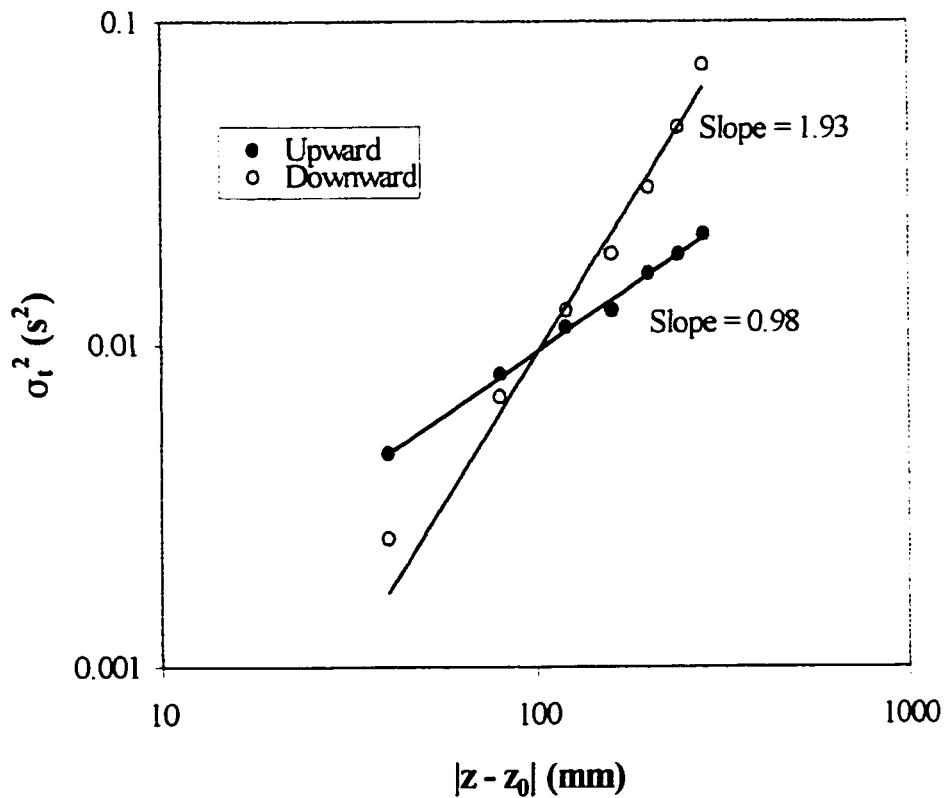


Figure 4.6 Performing the variance test on the RTD curve of restricted axial movement of solids in the dense bed (sand, $U_0 = 1$ m/s, $d_T = 420$ μ m).

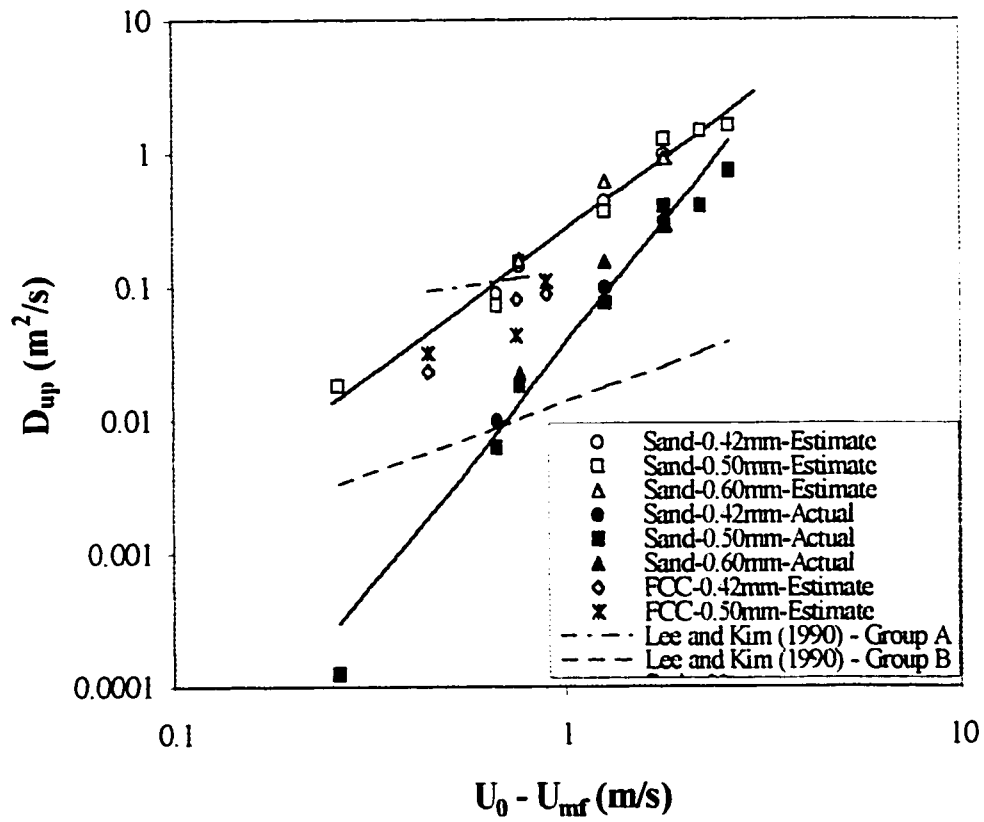


Figure 4.7 Dispersion coefficient of solids in strictly upward movement.

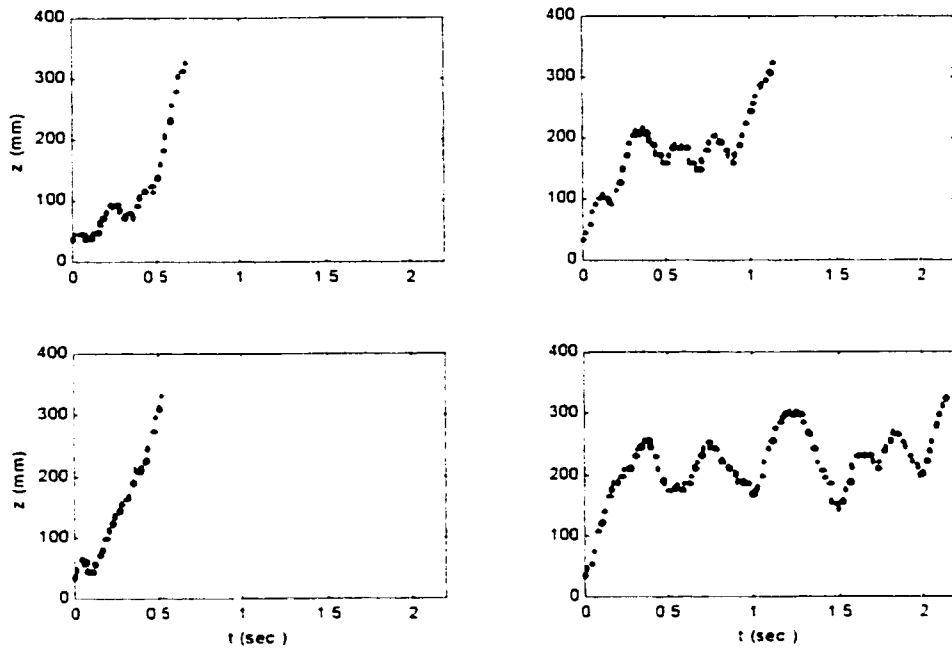


Figure 4.8 Unrestricted movement of solids (sand, $U_0 = 1$ m/s, $d_T = 420$ μ m): (a) Upward.

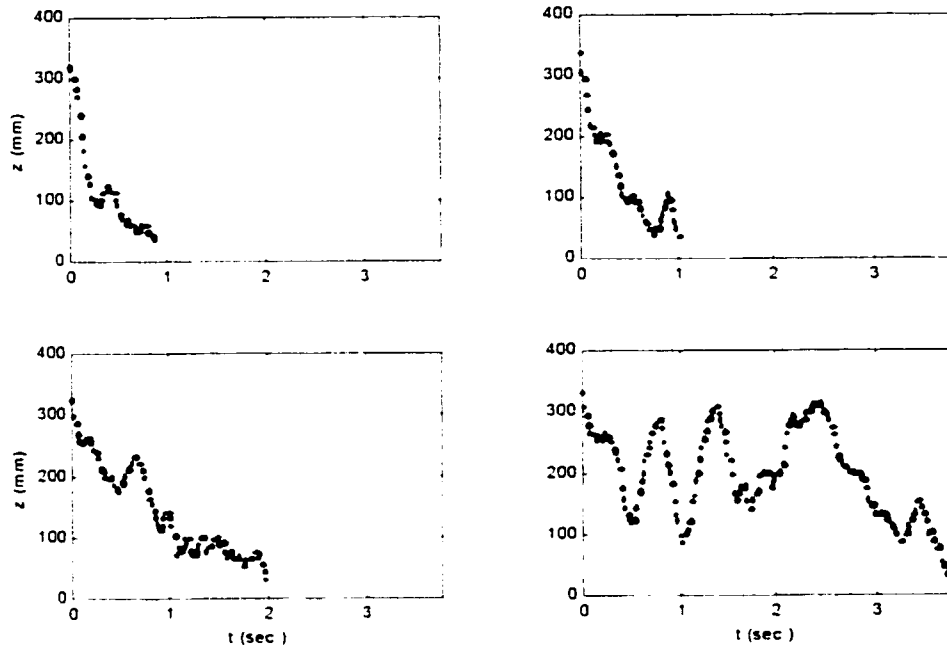


Figure 4.8 Unrestricted movement of solids (sand, $U_0 = 1$ m/s, $d_T = 420$ μ m): (b) Downward.

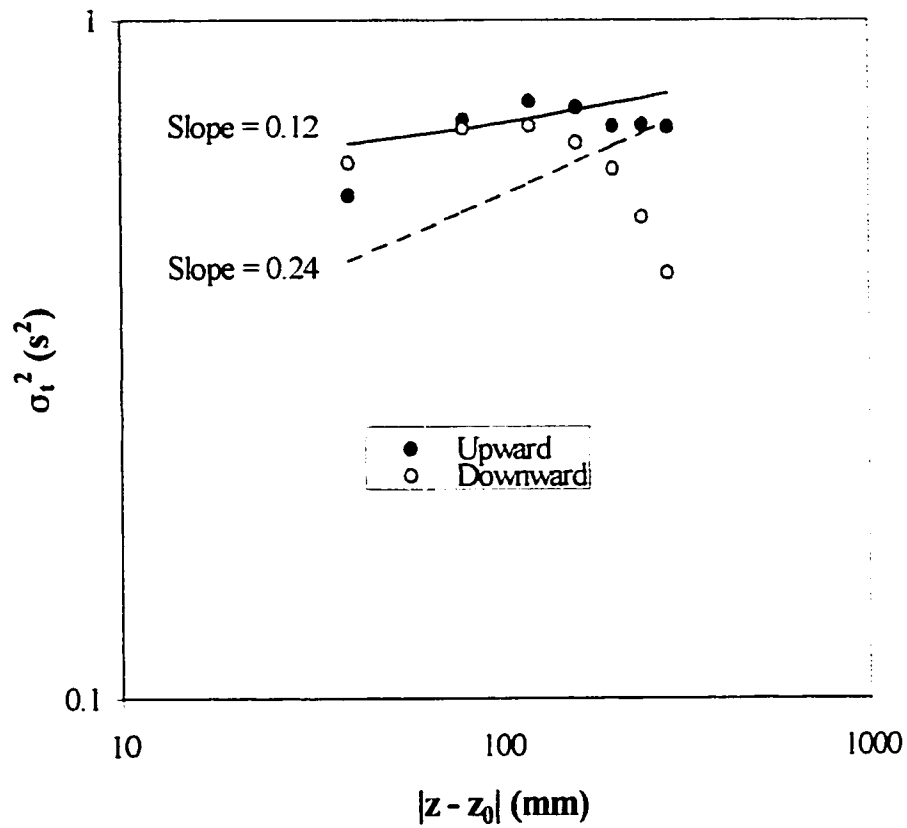


Figure 4.9 Performing the variance test on the RTD curve of unrestricted axial movement of solids in the dense bed (sand, $U_0 = 1$ m/s, $d_T = 420$ μ m).

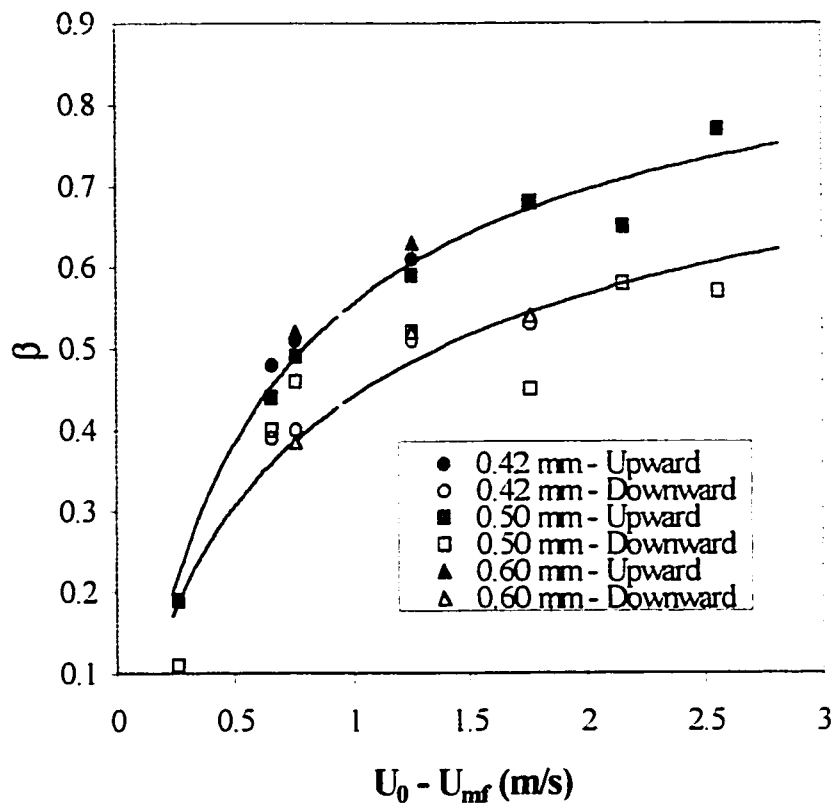


Figure 4.10 Ratio of effective solid velocity to single particle velocity as a function of excess gas superficial velocity for experiments with sand.

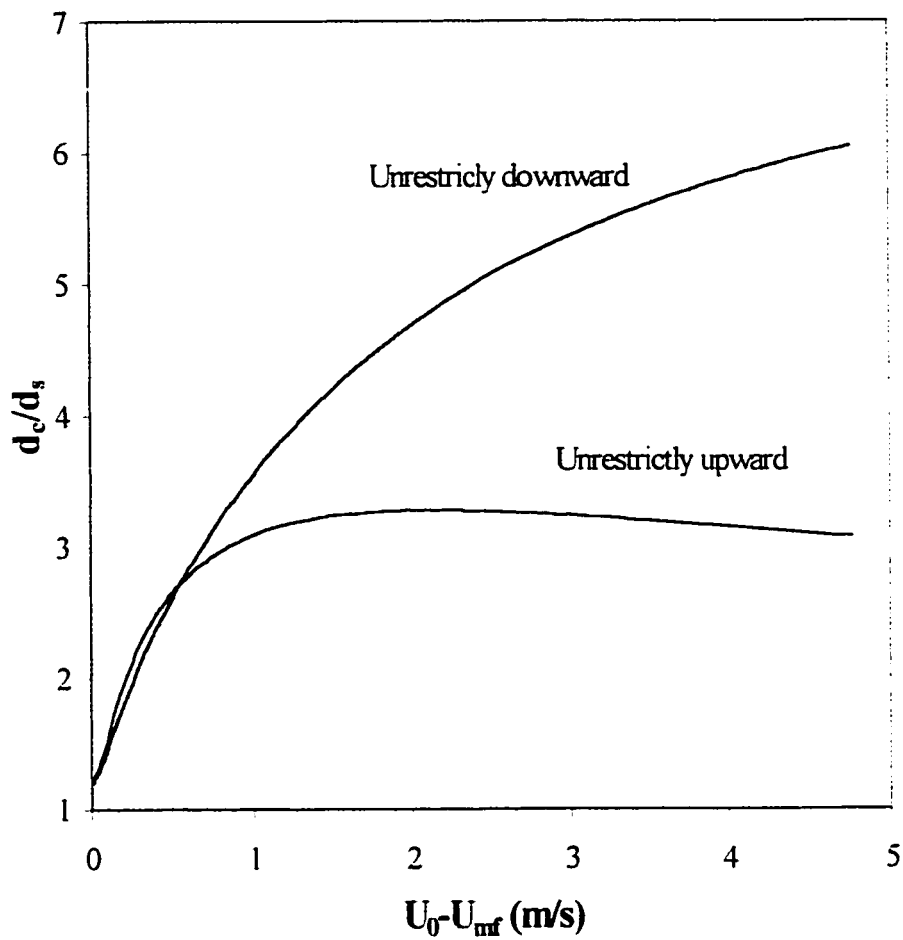


Figure 4.11 Relative cluster size in dense bed as a function of excess gas superficial velocity.

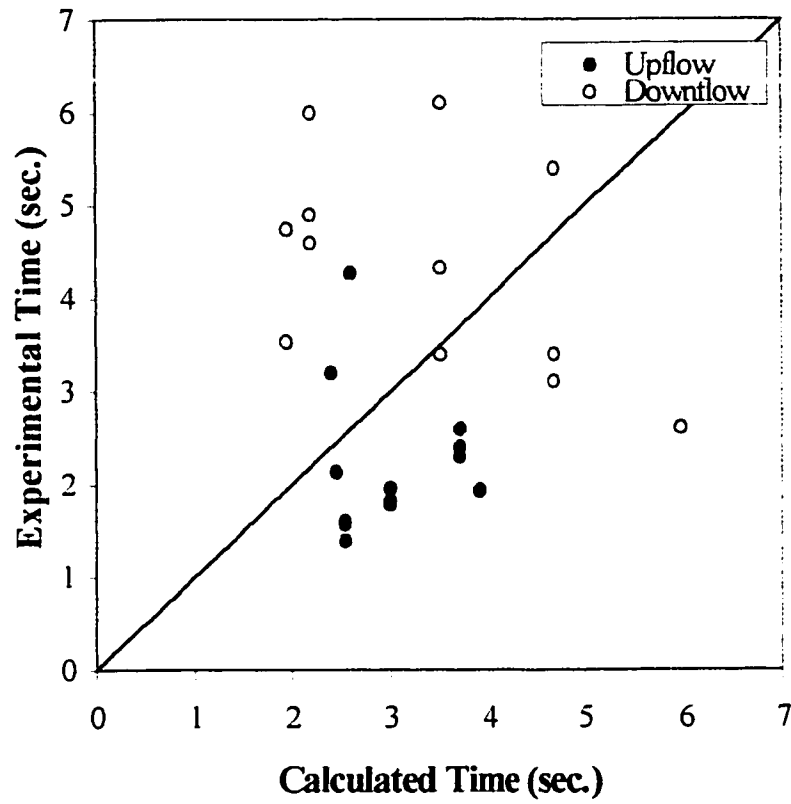


Figure 4.12 Comparison between calculated and experimental mean residence time of solids at 300 mm distance from the injection point.

CONCLUSIONS

A new correlation has been developed for prediction of the effective drag experienced by a single particle falling in a fluidized bed of different particles. The correction factor, i.e., the ratio of effective to standard drag coefficient, strongly depends on the voidage and is also a function of the falling particle properties as well as the fluidized particles properties. The correlation developed in this work is not valid for the beds with voidage less than 0.5 where error of calculation is extremely high and estimating the particle velocity by this method is not reasonable.

It has been found that the bulk density model (i.e., the model which calculates the buoyancy force acting on a single particle based on the average density of the bed) is not able to predict the velocity of the particles properly if the density of the bed is not close to the fluid density. The fluid density model (i.e., the model which calculates the buoyancy force acting on a single particle based on the density of the fluid) can predict the velocity of the particles better than the bulk density mode. However, there is no significant difference between the bulk density correlation and the fluid density correlation in dilute beds in which bulk density is very close to fluid density.

Solids in a fluidized bed do not move independently but as aggregates such as bubble wake, bubble cloud, and clusters. All the quantities evaluated in the present study show that these

parameters change only with gas superficial velocity and are independent of the size of the tracer, in the range of experimental conditions of this work. In other words, the solid particles do not move individually. Each single particle is attached to a solid aggregate in the dense bed and moves with it until it breaks-up. The particle then enters another solid ensemble and continues its move with the new ensemble.

The axial shear rate, dV_z/dr , has a significant effect on the solid diffusivity. The solid diffusivity is a linear function of the solids axial velocity gradient. The radial velocity gradient, dV_r/dr , is found to be at least an order of magnitude smaller than the axial velocity gradient and therefore, has no significant effect on the solid diffusivity. Two correlations have been developed in this study for prediction of axial and radial solid diffusivity at zero shear rate. It should be noticed that solid diffusivity changes more rapidly at the wall, where the shear rate is high, and less severe at the centre of the column, where the value of the shear rate approaches zero. Consequently, in the large units, where the wall effect is negligible, the value of the solid diffusivity at zero shear rate could be considered as a reasonable average value of this quantity.

In the experiments with FCC, the tracers are larger and denser than the bed particles. As a result, the tracer in these set experiments cannot be considered to represent the solids in the bed and the quantities calculated in FCC experiments may only be expected to show the trend rather than the actual value of the quantities. Axial diffusivity of solids at zero shear

rate in a bed of FCC particles was found to be the same as that of sand particles. However, radial diffusivity in a bed of FCC is higher than that of sand particles at a given excess gas superficial velocity. This is due to enhancement of radial solid mixing in a bed of finer and lighter particles. In the case of FCC powder the wake fraction is higher and the cloud is thicker compared to a bed of sand particles. This phenomenon makes the solids more mobile when the bed particles are finer and/or have less density which results in a higher solid diffusivity.

The dispersion coefficient of solids obtained from releasing the tracers at the top or bottom of the bed show a constant value of about $0.04 \text{ m}^2/\text{s}$ over the range of the gas superficial velocity employed in this work. The dispersion coefficient of the tracers released at the top of the bed are slightly higher than those released at the bottom and both are higher than the dispersion coefficient of solids predicted by the existing correlations in the literature. It has been proposed that the gravity helps dispersion of the solid aggregates to take place faster if released at the top, resulting in a higher dispersion coefficient. However, the dispersion coefficient evaluated from overall dispersion of solids in the fluidized bed was based on the assumption that the mixing process in the dense bed is diffusive while the equation of diffusion fits poorly to the experimental data.

The restricted movement of the solids, in which the tracers move from one side of the bed (top or bottom) to another (bottom or top) without considerable change in the direction, has

also been studied. It has been found by performing the variance test on the Residence Time Distribution (RTD) curves that the upward movement of solids in the dense bed is diffusive while their downward movement is convective. This behaviour can be justified by the high frequency of bubble-bubble interactions while rising in the bed which makes the upward movement of solids diffusive rather than convective. On the other hand, the solid descend as clusters with no or very little interactions between themselves.

Analyzing the RTD of solids in the unrestricted axial movement demonstrated that this kind of movement cannot be considered either convective or diffusive alone. A diffusive-convective model has been proposed to describe axial movement of solids in which the particle velocity was replaced with the effective solids velocity. This model is capable of predicting the behaviour of solids from low gas superficial velocities, where solid mixing takes place only based on diffusion, up to very high gas superficial velocities, where all the solid particles move independently. The effective solid velocity has been estimated to be equal to zero at gas superficial velocities close to the minimum fluidization and reaches the single particle velocity at very high gas superficial velocities. In the experiments with FCC, it was not been possible to evaluate the effective solid velocity due to the fact that the employed tracer was much bigger than the average size of the FCC powder in the experiments.

The experiments done in this work cover a wide enough range of gas superficial velocity

which allows drawing a general conclusion about transition from bubbling to turbulent fluidization. All the quantities studied in this work were either constant against gas superficial velocity or increasing constantly. Thus, one can conclude that since the trend of the studied parameters with gas superficial velocity remains the same when entering turbulent fluidization, transition from bubbling to turbulent fluidization happens smoothly rather than sharply. In other words, transition between fluidized regimes, from minimum fluidization to pneumatic transport, is essentially gradual and the behaviour of the bed may be considered as an interpolation between the behaviour of the emulsion phase (roughly at minimum fluidization) and that of the pneumatic transport. This claim can be verified at least for transition from bubbling to turbulent fluidization in the range which the experiments of this study have taken place since no sharp change in the trend of the studied parameters was observed with gas superficial velocity.

RECOMMENDATIONS

It has been found in this work that the solids do not move in fluidized beds as single particles, but as clusters and the average size of the clusters was estimated from the effective solid velocity in the present study. However, the average size and the size distribution of these solid clusters in the dense bed should be experimentally measured in the future works. It has also been proposed that the particles which are smaller than the solid clusters will join one of the clusters in the fluidized bed and larger particles may move independently. Therefore, it should be investigated in the future that what is the minimum size of a particle at which it starts to move independent of other particles in the bed.

It has been concluded from the results of this work that the transition between fluidization regimes is sooth rather than abrupt. This fact was shown for transition from bubbling to turbulent fluidization. This conclusion have to be examined experimentally also for transition between other fluidization regimes such as transition from turbulent to fast fluidization.

It was not possible in this work to employ the tracers smaller than 420 μm due to the fact that the radioactivity of a smaller tracer of the same mixture of this work would be very low such that the spacial resolution of the radioactive particle tracking technique would become very poor and the technique would loose its attractiveness. This problem resulted in unreliable experimental results for experiments with FCC powder. The possibility of

employing smaller tracers of different active materials have to be investigated.

This study has been focussing in most parts on axial movement of solids. The mechanism of radial movement of the solids in gas-solid fluidized beds can also be studied from the experimental data obtained in this work. It is also possible to analyze other solid flow modes (such as the counter-flow model) and evaluate more solid properties in the fluidized bed from these data. Especially based on the findings of this study, a counter-flow model in which the upflow of solids is considered as diffusive and their downflow as convective, can be developed.

GENERAL BIBLIOGRAPHY

ASIF, M., KALOGERAKIS, N., and BEHIE, L. A. (1992) On the constancy of axial dispersion coefficient in liquid fluidized beds. Chem. Eng. J., 49, 17-26.

AVIDAN, A., and YELUSHALMI, J. (1985) Solids mixing in an expanded top fluid bed. AIChE J., 31, 835-841.

BAI, D., ISSANGYA, A. S., and GRACE, J. R. (1999) Characteristics of gas-fluidized beds in different flow regimes, Ind. Eng. Chem. Res., 38, 803-811.

BARNEA, E. and MIZRAHI, J. (1973) Generalized approach to the fluid dynamics of particulate systems. Part I. General correlation for fluidization and sedimentation in solid multi particle systems. Chem. Eng. J., 5, 171-189.

BERRUTI, F., SCOTT, D. S., and RHODES, E. (1986) Measuring and modelling lateral solid mixing in a three-dimensional batch gas-solid fluidized bed reactor. Can. J. Chem. Eng., 64, 48-55.

CHAOUKI, J., LARACHI, F., DUDUKOVIC, M. P. (1997) Noninvasive tomographic and velocimetric monitoring of multiphase flows. Ind. Eng. Chem. Res., 33, 1889-1896.

CLIFT, R., SEVILLE, J. P. K., MOORE, S. C. and CHAVARIE, C. (1987) Comments on the buoyancy in fluidized beds. Chem. Eng. Sci., 42, 191-194.

CONTRACTOR, R. M., PATIENCE, G. S., GARNETT, D. I., HOROWITZ, H. S., SISLER, G. M. and BERGNA, H. E. (1994) A new process for n-butane oxidation to maleic anhydride using a circulating fluidized bed reactor. Circulating Fluidized Bed Technology. Avidan, A. A., Ed., AIChE, New York, 387-392.

CORRSIN, S. (1953) An account of some features of the phenomenon in fully turbulent regions. Proc. of Iowa Thermodynamics Symp., 5-29.

COX, J. D. and CLARK, N. N. (1991) The effect of particle drag relationship on prediction of kinematic wave in fluidized beds. Powder Technol., 66, 177-189.

DALLAVALLE, J. M. (1948) Micrometrics: The technology of Fine Particles, 2nd Edition. Pitman, London.

DEGALEESAN, S., DUDUKOVIC, M. P., TOSELAND, B. A., and BHATT, B. L. (1997) A two-compartment convective-diffusion model for slurry bubble column reactors. Ind. Eng. Chem. Res., 36, 4670-4680.

DI FELICE, R., FOSCOLO, P. U., GIBILARO, L. G. and RAPAGNA, S. (1991) The interaction of particles with a fluid-particle pseudo-fluid. Chem. Eng. Sci., 46, 1873-1877.

ECKSTEIN, E. C., BAILEY, D. G., and SHAPIRO, A. H. (1977) Self-diffusion of particles in shear flow of a suspension. J. Fluid Mech., 79, part 1, 191-208.

FAN, L. S., HAN, L. S. and BRODKEY, R. S. (1987) Comments on the buoyancy force on a particle in fluidized suspension. Chem. Eng. Sci., 42, 1269-1271.

FAN, L. T., CHEN, Y., and LAI, F. S. (1990) Recent developments in solids mixing, Powder Technol., 61, 255-287.

FOSCOLO, P. U., GIBILARO, L. G. and WALDRAM, S. P. (1983) A unified model for particulate expansion of fluidised beds and flow in fixed porous media. Chem. Eng. Sci. vol., 38, 1251-1260.

FOSCOLO, P. U. and GIBILARO, L. G. (1984) A fully predictive criterion for the transition between particulate and aggregate fluidization. Chem. Eng. Sci., 39, 1667-1675.

GARSDIE, J. and AL-DIBOUNI, M. R. (1977) Velocity-voidage relationship for fluidization and sedimentation in solid-liquid systems. Ind. Eng. Chem. Process Des. Dev.,

16, 206-214.

GODFROY, L., PATIENCE, G. S. and CHAOUKI, J. (1996) Radial hydrodynamics in risers. Ind. Eng. Chem. Res., **38**, 81-89.

GRBAVCIC, Z. B. and VUKOVIC, D. V. (1991) Single-particle settling velocity through liquid fluidized beds. Powder Technol., **66**, 293-295.

GRBAVCIC, Z. B., VUKOVIC, D. V., JOVANOVIC, S. D. and LITTMAN, H. (1992) The effective buoyancy and drag on spheres in a water fluidized bed. Chem. Eng. Sci., **47**, 2120-2124.

GWYN, J. E., MOSER, J. H., and PARKER, W. A. (1970) A three-phase model for gas-fluidized beds, Chem. Eng. Prog. Symp. Ser., **66**, 19-27.

HORIO, M., ISHII, H., and NISHIMURO, M. (1992) On the nature of turbulent and fast fluidized beds, Powder Technol., **70**, 229-236.

HORIO, M., and KUROKI, H. (1994) Three-dimensional flow visualization of dilutely dispersed solids in bubbling and circulating fluidized beds, Chem. Eng. Sci., **49**, 2413-2421.

HORIO, M., and ITO, M. (1997) Prediction of cluster size in circulating fluidized beds, J. Chem. Eng. Jpn., 30, 691-697.

JEAN, R. H. and FAN, L. S. (1992) On the model equations of Gibilaro and Foscolo with corrected buoyancy force. Powder Technol., 72, 201-205.

JOSHI, J. B. (1983) Solid-liquid fluidized beds: some design aspects. Chem. Eng. Res. Des., 61, 143-161.

KHAN, A. R. and RICHARDSON, J. F. (1990) Pressure gradient and friction factor for sedimentation and fluidisation of uniform spheres in liquids. Chem. Eng. Sci., 45, 255-265.

KIARED, K., LARACHI, F., CASSANELLO, M., and CHAOUKI, J. (1997) Flow structure of the solids in a three-dimensional liquid fluidized bed. Ind. Eng. Chem. Res., 36, 4695-4704.

KUNII, D., and LEVENSPIEL, O. (1991) Fluidization Engineering, 2nd ed., Butterworth-Heinemann, Boston, MA.

LARACHI, F., CHAOUKI, J. and KENNEDY, G. (1994) A γ -ray detection system for 3-D particle tracking in multiphase reactors. Nucl. Instr. and Meth. A, 338, 568-576.

LARACHI, F., CHAOUKI, J. and KENNEDY, G. (1995) 3-D mapping of solids flow fields in multiphase reactor with RPT. AICHE J., 41, 439-443.

LEE, N., and DUCKLER, A. E. (1976) Lagrangian simulation of dispersion in turbulent shear flow with hybrid computer. AICHE J., 22, 449-456.

LEE, G. S., and KIM, S. D. (1990) Axial mixing of solids in turbulent fluidized beds. Chem. Eng. J., 44, 1-9.

LEVENSPIEL, O., and FITZGERALD, T. J. (1983) A warning on the misuse of the dispersion model. Chem. Eng. Sci., 38, 489-491.

LIM, K. S., GURURAJAN, V. S., and AGARWAL, P. K. (1993) Mixing of homogeneous solids in bubbling fluidized beds: theoretical modeling and experimental investigation using digital image analysis. Chem. Eng. Sci., 48, 2251-2265.

LIM, K. S., ZHU, J. X., and GRACE, J. R. (1995) Hydrodynamics of gas-solid fluidization, Int. J. Multiphase Flow, 21(Suppl.), 141-193.

LOUGE, M. (1997) Experimental techniques, Circulating Fluidized Beds. Grace, J. R., Avidan, A. A., and Knowlton, T. M., Eds., Blackie Academic and Professional, London,

UK, 312-368.

MARTIN, B. L. A., KOLAR, Z. and WESSELINGH, J. A. (1981) The falling velocity of a sphere in a swarm of different spheres. Trans. Instn. Chem. Engrs., 58, 100-104.

MATSEN, J. M. (1976) Some characteristic of large solids circulation systems, Fluidization Technology, Keairns D. L., Ed., Hemisphere, New York, 135-140.

MAXEY, M. R., and RILEY, J. J. (1983) Equation of motion for small rigid sphere in a nonuniform flow. Phys. Fluids, 26, 883-889.

MAY, W. G. (1959) Fluidized-bed reactor studies. Chem. Eng. Prog., 55, 49-56.

MEI, R., ADRIAN, R. J., and HANRATTY, T. J. (1991) Particle dispersion in isotropic turbulence under stokes drag and basset force with gravitational settling. J. Fluid Mech., 225, 481-495.

MONIN, A. S. and YAGLOM, A. M.: (1971) Statistical Fluid Mechanics: Mechanics of Turbulence. LUMLEY, J. L., Ed. MIT Press, Cambridge, MA, 1.

NGUYEN, T. H. and GRACE, J. R. (1978) Forces on objects immersed in fluidized beds.

Powder Technol., 19, 255-264.

PANIGRAHI, M. R. and MURTY, J. S. (1991) A generalized spherical multi-particle model for particulate systems: fixed and fluidized. Chem. Eng. Sci., 46, 1863-1868.

PATIENCE, G. S. (1990) Circulating fluidized beds: Hydrodynamics and reactor modelling, Ph. D. thesis, École Polytechnique de Montréal, Canada.

PATIENCE, G., CHAOUKI, J., and KENNEDY, G. (1990) Solids residence time distribution in CFB reactors, Circulating Fluidized Bed Technology III, BASU, P., HORIO, M., and HASATANI, M., Eds., Pergamon Press, Oxford, 599-604.

PATIENCE, G. S., CHAOUKI, J., BERRUTI, F. and WONG, R. (1992) Scaling considerations for circulating fluidized bed riser, Powder Technol., 72, 31-37.

PISMEN, L. M., and NIR, A. (1978) On the motion of suspended particles in stationary homogeneous turbulence. J. Fluid. Mech., 84, 193-206.

RICHARDSON, J. F. and ZAKI, W. N. (1954) Sedimentation and fluidisation: Part I. Trans. Instn. Chem. Engrs., 32, 35-53.

ROCHE, G. and CHAVARIE, C. (1978) Behaviour of shallow fluidized beds around immersed objects. Can. J. Chem. Eng., 56, 281-285.

TURTON, R. and LEVENSPIEL, O. (1986) A short note on the drag correlation for spheres. Powder Technol., 47, 83-86.

TUZLA, K., SHARMA, A. K., CHEN, J. C., SCHIEWE, T., WIRTH, K. E., and MOLERUS, O. (1998) Transient dynamics of solid concentration in downer fluidized bed, Powder Technol., 100, 166-172.

VAN DEEMTER, J. J. (1967) The counter-current flow model of a gas-solids fluidized bed. Proc. Int. Symp. On Fluidization, A. A. DRINKENBURG, Ed., Netherlands Univ. Press, Eindhoven, 334-341.

VAN DER WIELEN, L. A. M., VAN DAM, M. H. H. and LUYBEN, K. CH. A. M. (1996) On the relative motion of a particle in a swarm of different particles. Chem. Eng. Sci., 51, 995-1008.

VAN SWAAIJ, W. P. M., BUURMAN, C. and VAN BREUGEL, J. W. (1970) Sheer stress on the wall of a dense gas-solid riser. Chem. Engng. Sci., 25, 1818-1820.

WEI, F. and ZHU, J. X. (1996) Effect of flow direction on axial solid dispersion in gas-solids cocurrent upflow and downflow systems, Chem. Eng. J., 64, 345-352.

WEN, C. Y., KRISHMAN, R., and KALYANARAMAN, R. (1980) Particle mixing near the grid region of fluidized beds. Fluidization, GRACE, J. R., MATSEN, J. M., Eds., Plenum, New York, 405-412.

WEN, C. Y. and YU, Y. H. (1966) Mechanics of fluidization. Chem. Eng. Prog. Symp. Ser., 62, 100-111.

WERTHER, J., and WEIN, J. (1994) Expansion behavior of gas fluidized beds in the turbulent regime. AIChE Symp. Ser., 90(301), 31-44.

XU, G., and LI, J. (1998) analytical solution of the energy minimization multi-scale model for gas-solid two-phase flow, Chem. Eng. Sci., 53, 1349-1366.

ZOU, B., LI, H., XIA, Y., and MA, X. (1994) Cluster structure in a circulating fluidized bed, Powder Technol., 78, 173-178.

APPENDIX A : DETAILS OF THE GAS-SOLID FLUIDIZED BED SET-UP

Details of the column, distributor, and cyclone used in the gas-solid experiments are shown in Figures A.1 to A.6. The data sheet of the orifice used for measuring the air flow rate is given in the next page. Based on the formula given by the manufacturer, the following relation is derived for obtaining the gas superficial velocity from the head of water column in the manometer:

$$U_0 = 0.0897122 \sqrt{\Delta h} \quad (\text{A.1})$$

where U_0 is the gas superficial velocity at 20°C and Δh is the differential head of water in the manometer.

OPERATING CONDITIONS :

UPSTREAM PIPE I.D. AT 20 DEG.C (MM)	26.645
DIFFERENTIAL PRESSURE AT MAX. FLOW (MM WATER)	1,250.000
MAXIMUM FLOW RATE (NCU-M/HR)	200.000
NORMAL PLOW RATE (NCU-M/HR)	140.000
BASE PRESSURE (KG/CM2)	1.033
BASE TEMPERATURE (DEC. C)	0.000
FLOWING PRESSURE (KG/CM2 GAUGE)	1.000
FLOWING TEMPERATURE (DEG. C)	25.000
BAROMETRIC PRESSURE (KG/CM2)	1.033
SPECIFIC GRAVITY (AIR = 1)	1.000
COMPRESSIBILITY AT BASE CONDITIONS	1.000
COMPRESSIBILITY AT FLOW CONDITIONS	1.000
RATIO OF SPECIFIC HEATS (ISENTROPIC EXPONENT)	1.400
VISCOSITY AT FLOW CONDITIONS (CENTIPOISES)	0.018
FLOWING FLUID	AIR
ORIFICE PLATE MATERIAL	304SS
UPSTREAM PIPE MATERIAL	CARBON STEEL
PRESSURE TAP LOCATIONS	FLANGE
STATIC PRESSURE TAP LOCATION	UPSTREAM

CALCULATION DETAILS :

$$Q_m = 0.00003512407 \times d \times d \times C \times F_a \times Y_1 \times \text{SQR} [H_w \times D_f / (1 - B^4)]$$

Q_m : MAXIMUM MASS FLOW RATE (KG/SEC) 0.0718

C : DISCHARGE COEFFICIENT 0.7650

F_a : THERMAL EXPANSION CORRECTION FACTOR 1.0002

Y_1 : EXPANSION FACTOR OF FLOWING FLUID 0.9889

H_w : MAXIMUM DIFFERENTIAL PRESSURE (KPa) 12.2371

D_f : DENSITY OF FLOWING FLUID (KG/CU-M) 2.3676

R_n : PIPE REYNOLDS NUMBER AT NORMAL FLOW 133.403

B : BETA RATIO (BORE / PIPE I.D.) 0.75975

d : ORIFICE BORE DIAMETER (MILLIMETERS) 20.2433

FLOW RATE (NCU-M/HR) = 5.6569 x SO. ROOT (DIFF. MM WATER)

DIFFERENTIAL PRESSURE AT NORMAL FLOW (MM WATER) 612.5000

PERMANENT PRESSURE LOSS AT MAXIMUM FLOW (KPa) 5.474

PERMANENT PRESSURE LOSS AT NORMAL FLOW (Kpa) 2.682

REFERENCE : FLOW MEASUREMENT ENGINEERING HANDBOOK, BY R.W.

MILLER ASME STANDARO MFC-3M-1989

UPSTREAM PIPE I.D. = 1.049 INCH. ORIFICE BORE DIA. = 0.7970 INCH.

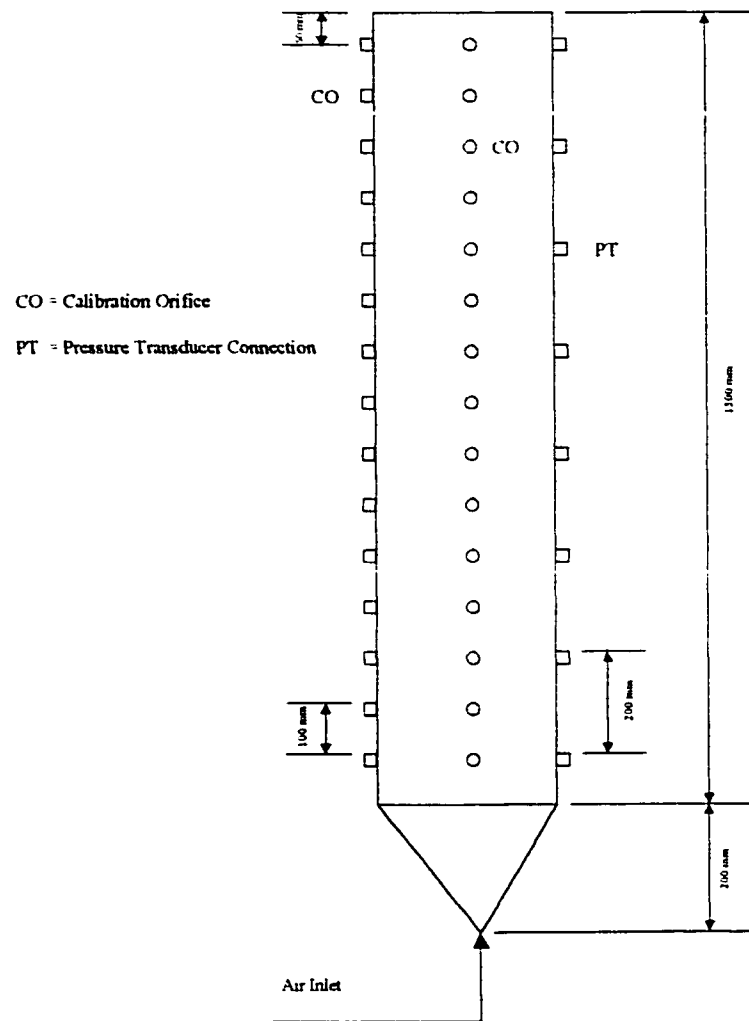


Figure A.1 The plexiglas column - Side view.

CO = Calibration Orifice

PT = Pressure Transducer Connection

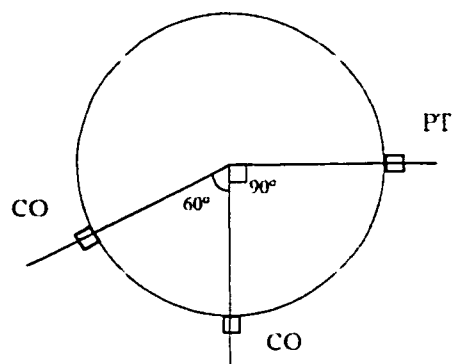


Figure A.2 The plixiglas column -
Top view.

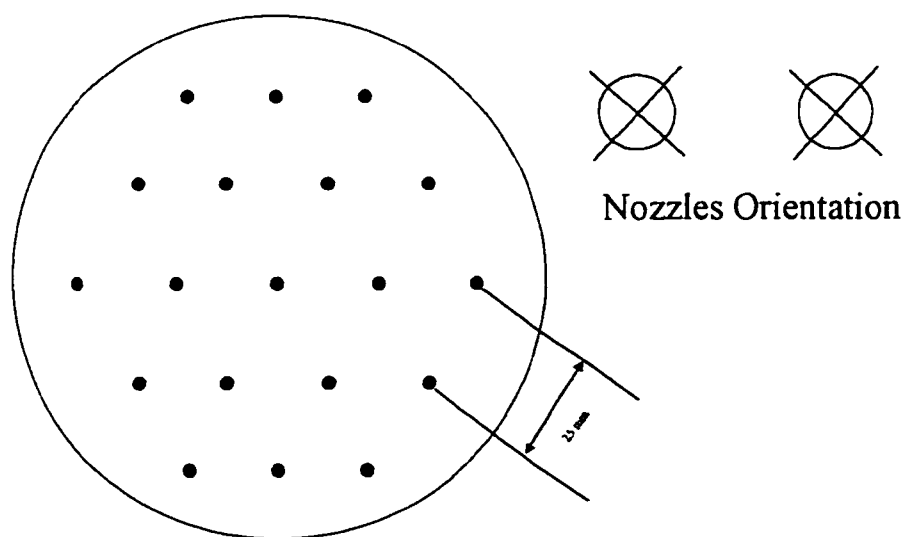


Figure A.3 The nozzle-type distributor.

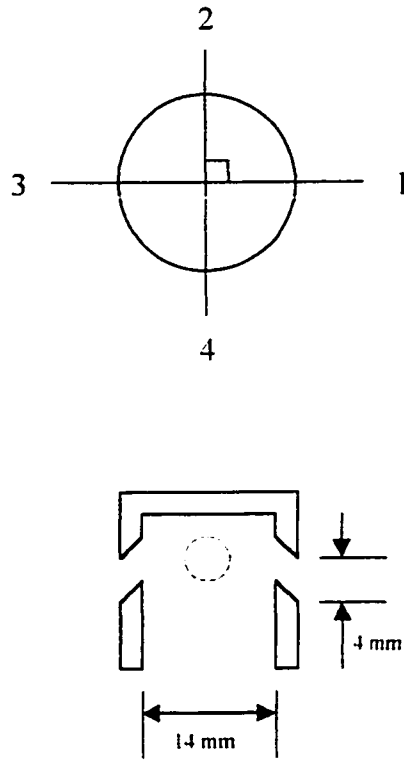


Figure A.4 The nozzles of the distributor.

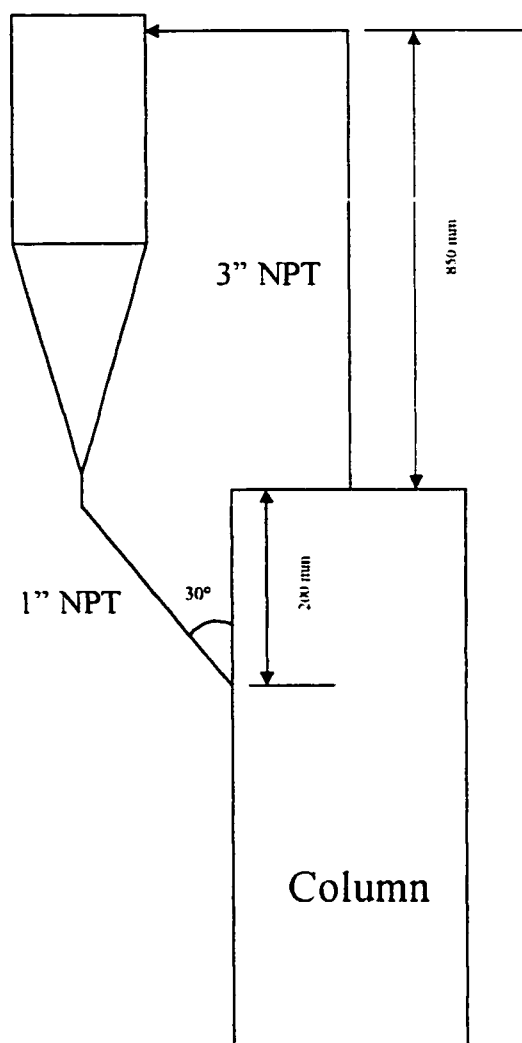


Figure A.5 Arrangement of the cyclone.

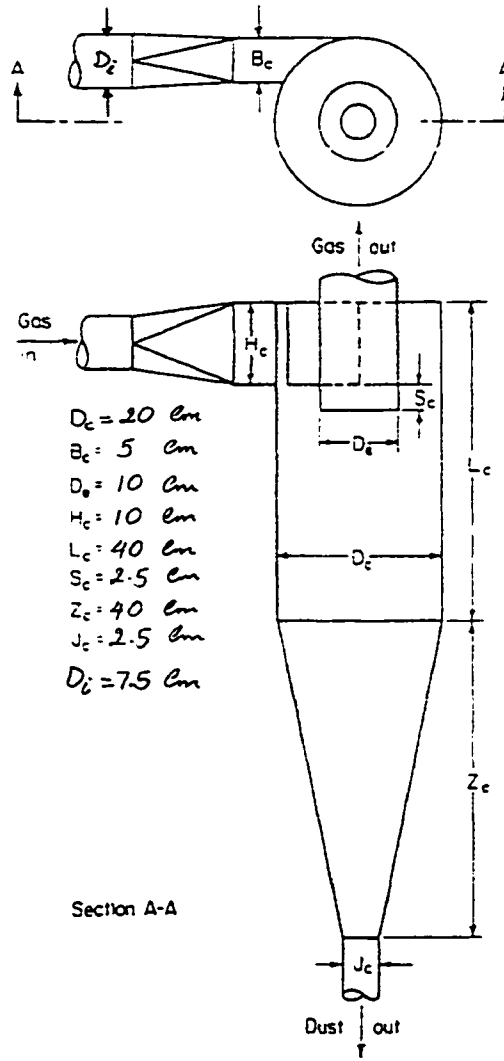


Figure A.6 The cyclone.

APPENDIX B : CHARACTERIZATION OF DYNAMIC GAS-SOLID DISTRIBUTION IN FLUIDIZED BEDS

Reference:

Heping Cui, Navid Mostoufi and Jamal Chaouki: Characterization of Dynamic Gas-Solid Distribution in Fluidized Beds, Submitted to The Chemical Engineering Journal (October 1999).

B.1 Abstract

A probability distribution model of the local voidage was proposed to describe and simulate dynamic gas-solid distribution in the bubbling and turbulent fluidized bed reactors. Experiments were carried out in an air-fluidized bed. The bed materials were FCC particles (Geldart A) and irregular sand particles (Geldart B). A cross-optical fiber probe was employed to measure dynamic voidage. The minimum probability method was introduced to identify the division between the emulsion phase and the bubble phase. The statistical analysis indicated that the two particle types employed have extremely different dynamic behaviors corresponding to different gas-solid distributions and the interaction between the bubble and emulsion phases. For the FCC particles, the voidage of the emulsion phase is very close to that of the minimum fluidization with little effect from the formation and motion of bubbles in bubbling regime, and deviate a little from ϵ_{mf} in turbulent regime. For

the sand particles, the voidage of the emulsion phase differs far from that of the minimum fluidization, and the bubble phase gradually become dilute from bubbling to turbulent regime. However, for both particles the dynamic voidage fluctuations in the emulsion phase and the bubble phase followed Beta distribution under various operating conditions. The probability density functions of the local voidage from ε_m to 1 showed the continuous double-peak phenomena, one peak for the emulsion phase and another for the bubble phase, and evolved with changing operating conditions and bed position. A particular distribution, called Coupled Beta distribution, was developed to describe and simulate such probability density function with double peaks and its complex evolution from bubbling to turbulent regime. The quantification of the probability density function then statistically introduced the spatiotemporal two-phase flow structure.

B.2 Introduction

Gas-solid fluidized bed reactors have found a wide range of industrial applications. However, the heat/mass transfer and reaction within such reactors are far from being well understood and effectively quantified due to the complexity of the gas-solid interactions. Many models with simple assumptions have been suggested to describe the behavior of the two phases. These models have been widely introduced in the literature [1-4]. They have explained and made sense of the main features of the bubble and emulsion phases in fluidized

beds and have been of great help in improving knowledge of the interaction between the two phases.

The traditional two-phase theory assumes existent of only two phases in the fluidized bed, i.e., solid-free bubbles ($\epsilon = 1$) and emulsion phase at minimum fluidization ($\epsilon = \epsilon_{mf}$). However, this assumption is over-simplification of what actually happens in the bed. The bubbles contain some solid particles[5-7]. The emulsion also does not stay at minimum fluidization state, but can contain more gas at higher gas velocities [8,9]. This phenomena results in a dynamic distribution of the two phases with the voidage. The dynamic gas-solid distribution can have a considerable effect on the apparent reaction and heat/mass transfer rate in the fluidized bed. The traditional two-phase theory is incapable of predicting these rates properly. Another shortcoming of the simplified two-phase theory is that it is mostly limited to explain the low-velocity bubbling fluidization and is not able to explain the evolution of the two phases by increasing the gas velocity. Increasing the gas superficial velocity in a fluidized bed causes a better mixing of the two phases which results in more solid particles entering the bubbles and more gas entering the emulsion phase. As a result, a wider dynamic distribution can be observed by increasing the gas velocity, while the simple two-phase models are unable to justify it.

In the recent years, more and more works have focused on the dynamic behavior of the two-phase flow structures in actual fluidized processes in order to improve the understanding of

the interaction between the two phases [10-13]. Some of these studies have demonstrated the complexity of the gas-solid distribution in the gas-solid fluidized beds [9, 14, 15]. A better understanding of how solids disperse in the bubbles and how gas enters the emulsion has an enormous impact on the practical use of the fluidized bed reactors [4], which is also highly valuable for improving the traditional two-phase models for industrial applications. Therefore, this paper focuses on quantitative description of the dynamic gas-solid distribution of the two phases in the bubbling and turbulent fluidization regimes by analyzing the probability distribution function of the local voidage from ε_{mf} to 1.

B.3 Probability Distribution Model

The simple two-phase model assumes the existence of two extreme phases, namely the solid-free bubble phase ($\varepsilon = 1$) and the emulsion phase at minimum fluidization ($\varepsilon = \varepsilon_{mf}$). Throughout this paper, we refer to the solid-free bubbles as pure bubble phase and the emulsion at minimum fluidization as saturated emulsion. In the simplified two-phase theory, the distribution of the voidage in the fluidized bed is assumed to be equal to either 1 or ε_{mf} , as illustrated by the dashed line in Fig. B.1. The corresponding cumulative probability distribution function could be expressed by a simplified two-phase model as follows:

$$Pr^0(\varepsilon) = Pr_e^0(\varepsilon) + Pr_b^0(\varepsilon) \quad (\text{B.1})$$

in which

$$Pr_e^0(\varepsilon) = f^0 \quad (\text{B.2})$$

$$Pr_b^0(\varepsilon) = \begin{cases} 0 & \varepsilon_{mf} \leq \varepsilon < 1 \\ 1 - f^0 & \varepsilon = 1 \end{cases} \quad (\text{B.3})$$

where $Pr^0(\varepsilon)$, $Pr_e^0(\varepsilon)$, and $Pr_b^0(\varepsilon)$ are the cumulative probability distribution functions of the local voidage for the overall, the saturated emulsion phase and the pure bubble phase, respectively, and f^0 is the emulsion phase fraction,

$$f^0 = \frac{1 - \varepsilon_r}{1 - \varepsilon_{mf}} \quad (\text{B.4})$$

where ε_r is the time-averaged voidage at an arbitrary local position.

The actual flow structure in the fluidized beds show highly complicated spatiotemporal dynamic behavior due to the nonlinearity of the gas-solid interaction. The emulsion and bubble phases, with various irregular structures at different time and position, exhibit not only extremum behavior with the voidages ε_{mf} or 1, but also dynamic behavior with a series of voidages in between [16], corresponding to dynamic gas-solid distribution, as shown in Fig.B.1. Therefore, we introduced a probability distribution model of the local voidage

varying from ε_{mf} to 1 in order to describe the cumulative probability distributions of the complex gas-solid distribution of the two-phase flow structure as following:

$$Pr(\varepsilon) = \frac{1}{1 - \varepsilon_{mf}} \int_{\varepsilon_{mf}}^{\varepsilon} pr(\varepsilon) d\varepsilon \quad (\text{B.5})$$

Eq. (B.5) can also be expressed as

$$Pr(\varepsilon) = Pr_e(\varepsilon) + Pr_b(\varepsilon) \quad (\text{B.6})$$

where

$$Pr_e(\varepsilon) = \frac{f}{1 - \varepsilon_{mf}} \int_{\varepsilon_{mf}}^{\varepsilon} pr_e(\varepsilon) d\varepsilon \quad (\text{B.7})$$

$$Pr_b(\varepsilon) = \frac{1-f}{1 - \varepsilon_{mf}} \int_{\varepsilon_{mf}}^{\varepsilon} pr_b(\varepsilon) d\varepsilon \quad (\text{B.8})$$

thus

$$\begin{aligned}
 Pr(\varepsilon) &= \frac{f}{1-\varepsilon_{mf}} \int_{\varepsilon_{mf}}^{\varepsilon} pr_e(\varepsilon) d\varepsilon + \frac{1-f}{1-\varepsilon_{mf}} \int_{\varepsilon_{mf}}^{\varepsilon} pr_b(\varepsilon) d\varepsilon \\
 &= \frac{1}{1-\varepsilon_{mf}} \int_{\varepsilon_{mf}}^{\varepsilon} (f pr_e(\varepsilon) + (1-f) pr_b(\varepsilon)) d\varepsilon
 \end{aligned}
 \tag{B.9}$$

$$pr(\varepsilon) = f pr_e(\varepsilon) + (1-f) pr_b(\varepsilon)
 \tag{B.10}$$

where $Pr(\varepsilon)$, $Pr_e(\varepsilon)$, and $Pr_b(\varepsilon)$ are the cumulative probability distribution functions of the local voidage of the overall, the emulsion phase and the bubble phase, respectively, while $pr(\varepsilon)$, $pr_e(\varepsilon)$, and $pr_b(\varepsilon)$ are the corresponding probability density functions, $\varepsilon_{mf} \leq \varepsilon \leq 1$;

and f is the dense phase fraction which determines the weight factors. All parameters and variables in the above model are functions of the operating conditions, bed position, and bed materials.

In order to further characterize the complex two-phase flow structure in time scale, we assumed that the maximum and minimum voidages exist on the ideal centre of the bubble phase and the ideal centre of the emulsion phase, respectively, and the voidage changes monotonously between the two centres. According to Eqs. (B.5) to (B.10), the gas-solid

distribution between an emulsion phase element and its neighbouring bubble phase element [15] at time scale, called the spatiotemporal gas-solid distribution for convenience, could then be statistically described by a series of local voidages from the ideal centre of the emulsion phase element to the ideal centre of its neighbouring bubble phase element at time scale. The method of equality of probability [17] was used to divide the probability function from ε_{mf} to 1 into n scopes of each probability equal to $1/n$, for which a distance of unit time between the two centres was assumed.

$$Pr(\varepsilon_{i+1}) - Pr(\varepsilon_i) = \frac{1}{1 - \varepsilon_{mf}} \int_{\varepsilon_i}^{\varepsilon_{i+1}} Pr(\varepsilon) d\varepsilon = 1/n \quad i=0, 1, \dots, n-1 \quad (\text{B.11})$$

where ε_i is the local voidage corresponding to the time coordinate i/n from the centre of the emulsion phase element to the centre of its neighbouring bubble and $Pr(\varepsilon)$ is the cumulative probability of the local voidages from ε_{mf} to ε_i . Eq. (B.11) gives the dependence of the local voidage (ε_i) with respect to the coordinate (i/n), which can be summarized into a two-dimensional vector $Y = \{(0, \varepsilon_0(\varepsilon_{mf})); (1/n, \varepsilon_1); \dots; (i/n, \varepsilon_i); \dots; (1, \varepsilon_n(1))\}$. The spatiotemporal gas-solid distribution shows how gas and solids interpenetrate the bubble and emulsion phases and statistically gives practical flow structure element (from the centre of an emulsion phase element to the centre of a bubble phase element) at time scale. This can help to understand quantitatively the gas-solid interactions in the fluidized bed.

In order to quantitatively characterize the gas-solid distribution and the influence of the operating conditions thereof, a large number of experiments were conducted using different bed materials. The resulting gas-solid distribution were then developed according to the probability model described above.

B.4 Experimental

Experiments were carried out in an air-fluidized bed of 152 mm in diameter and 1.5 m in height under ambient condition and different superficial gas velocities, covering the bubbling and turbulent fluidization regimes. Two kind of particles, i.e., FCC ($\rho_p = 1673 \text{ kg/m}^3$, $d_p = 70 \text{ }\mu\text{m}$) and irregular sand particles ($\rho_p = 2650 \text{ kg/m}^3$, $d_p = 385 \text{ }\mu\text{m}$) with a wide size distribution, as shown in Table B.1, were used as bed materials to understand and compare the gas-solid distribution of Geldart A and Geldart B particles. The transition superficial gas velocity from bubbling to turbulent fluidization, U_{tr} , was determined by the standard deviation analysis of absolute pressure fluctuations and found to be 0.77 m/s for the FCC particles and 1.50 m/s for the sand particles. A cross-optic fiber probe [18] with a measure volume defined by its two cross fiber bunches of 0.8 mm in diameter, was placed at an axial position of 150 mm above the distributor level and at different radial positions to measure instantaneous voidage. A PV-4A Particle Velocity Analyzer, made by the Institute of Chemical Metallurgy, Chinese Academy of Sciences, was employed to obtain time series of

dynamic voidages. For each run, more than 64,000 data, with a sampling frequency of 488 Hz, were acquired.

B.5 Results and Discussion

B.5.1 Minimum and Maximum Voidages

The minimum voidage (ε_{min}) and the maximum voidage (ε_{max}) of the two-phase flow structure were analyzed in order to verify whether or not the emulsion phase and the bubble phase actually show the extremum behavior. In this paper, the voidage corresponding to less than 1% cumulative probability distribution of the local voidage from ε_{mf} to 1 were defined as ε_{min} . The voidage corresponding to more than 99% cumulative probability distribution of the local voidage from ε_{mf} to 1 was defined as ε_{max} . The results indicated that, for the FCC particles, the formation and motion of the bubbles have less effect on the voidage of the emulsion phase, and the minimum voidage in the emulsion phase remains almost at that of the saturated emulsion, ε_{mf} , over a wide range of gas velocities. For the sand particles, however, more gas enters and dilutes the emulsion phase, and the minimum voidage increases from ε_{mf} almost linearly with increasing U_g , which indicates the increasing degree of dilution of the emulsion phase, as shown in Fig. B.2. On the other hand, the maximum voidage, ε_{max} , exhibits the similar trends for the FCC and sand particles, i.e., rising exponentially with

increasing gas velocity at the beginning and then remaining nearly constant at higher gas velocities, as illustrated in Fig. B.2. For the sand particles, bubbles seems to be very close to the pure bubbles at higher U_g , while for the FCC particles ϵ_{max} is lower than unity due to presence of more particles in the bubbles, as also shown in Fig. B.2. Such changes in ϵ_{min} and ϵ_{max} with U_g can be expressed as

$$\epsilon_{min} = \epsilon_{mf} + k_{min}(U_g - U_{mf}) \quad (\text{B.12})$$

$$\epsilon_{max} = k_{max(\infty)} - k_{max(1)} e^{-\frac{(U_g - U_{mf})}{k_{max(2)}}} \quad (\text{B.13})$$

where $(k_{min}, k_{max(\infty)}, k_{max(1)}, k_{max(2)}) = (0, 0.97, 0.189, 0.115)$ for the FCC particles, and

$(k_{min}, k_{max(\infty)}, k_{max(1)}, k_{max(2)}) = (0.034, 1, 0.045, 0.64)$ for the sand particles, at $r/R = 0$.

As shown in Fig. B.2, the experimental data indicate that the radial position influences the gas-solid distribution. At $r/R = 0$, the bubble phase showed the highest ϵ_{max} , and the emulsion phase was more diluted for the sand particles, while no significant change was observed for the FCC particles.

B.5.2 Probability Distribution Function

In order to study the gas-solid distribution of the bubble and emulsion phases, the probability distribution of the local voidage from ε_{mj} to 1 was cumulated according to the method described by Eqs. (B.5) to (B.8). It was found that the probability distribution of the local voidage shows nonlinearity, which indicates nonlinear gas-solid distribution in the fluidized beds. The results also show the complex evolution of the probability density function with increasing U_g for both FCC and sand particles. The same phenomena has been observed for MgO particles ($d_p = 120 \mu\text{m}$) [9]. Fig. B.3 gives such evolution of the probability distribution for the two types of particles at $r/R = 0$, that is, the cumulative probability distribution curves tend to the higher local voidage with increasing U_g as more gas goes into both the emulsion and bubble phases. It is worth mentioning that the probability distribution function changes gradually from bubbling to turbulent fluidization with no abrupt change at U_c .

Fig. B.3 also illustrates that the probability distribution of the local voidage for the FCC particles is different from that of the sand particles, even if they both have equal time-averaged voidages. The former has high probability at and nearby the saturation value ε_{mp} while the latter has very low probability in this region. The emulsion phase strongly shows to be close to the saturated emulsion for the FCC particles, while in the case of the sand particles, the emulsion is far from the saturated state due to the larger amount of the gas

entered this phase, as shown in Fig. B.3 a, b. Therefore, for different fluidized materials, the effect of the gas flow on the emulsion phase is different, their complex two-phase structure behave differently, with different dominant mechanisms for the gas-solid interaction.

The probability distribution of the local voidage and its evolution also depends on the radial position for both particles, as shown in Fig. B.4. The evolution of the probability distribution function happens to a greater extent on the bed core compared to that of the near the wall for the same gas velocity. Most runs show the highest cumulative probability near the wall and the lowest at $r/R = 0$, since more gas flows through the centre of the bed than close to the wall. The gas-solid distribution greatly depends on the gas velocity, the bed position and the particle properties, which indicates the complexity of quantifying the dynamic behavior of the gas and solids in fluidized bed.

B.5.3 Probability Density Function

The probability density function of the local voidage, $pr(\varepsilon)$, as expressed in Eqs. (B.5) to (B.10), was further analyzed to quantitatively explain the gas-solid distribution and its dependence on both the operating conditions and particle properties. This allowed for exploring the dynamic behavior of the bubble and emulsion phases. It was found that the local voidage from ε_m to 1 exhibits a double-peak probability density function for both particles tested, one peak for the emulsion phase and another peak for the bubble phase. The

double-peak probability density curve changes with increasing gas velocity, U_g . An increase in the gas velocity results in decreasing the probability density of the emulsion phase and increasing the probability density of the bubble phase. The average peak voidage of the emulsion phase is found to be equal or close to ε_{mj} for FCC particle and $\varepsilon \approx 0.55 (> \varepsilon_{mj})$ for the sand particles and the average peak voidage of the bubble phase was found to be $\varepsilon \approx 0.85$ for FCC particles and $\varepsilon \approx 0.95$ for the sand particles at $r/R = 0$, as shown in Fig. B.5 a, b.

Such a probability density function and its evolution also depends on the radial position for both particles tested, as shown in Figs. B.6 a1, a2 ($r/R = 0$ and $5/6$). The peak for the emulsion decreases gradually and the peak for the bubbles increases gradually from the wall to the core at the same gas velocity. Furthermore, the same observation still applies with the same time-averaged voidage in different positions as shown in Figs. B.6 b1, b2. In this case, the probability density for the bubbles is lower near the wall than in the core. As suggested by the data in Fig. B.6, the wall has a strong effect on the gas-solid distribution in the emulsion and bubble phases.

B.5.4 Quantification of the Probability Density Function

Although the gas-solid distribution showed the double-peak probability density function, the density function corresponding to the two phases are continuous for the both particles tested. In order to describe such a gas-solid distribution with the two-peak density function, the

minimum probability method was introduced to determine the division (ε_{div}) between the emulsion phase and the bubble phase, that is, to take the local voidage point with the minimum probability density between the two peaks as the division. The division, ε_{div} , was found to change with gas velocity and the bed position in both bubbling and turbulent regimes, which could be correlated as

$$\varepsilon_{div} = k_{div0} + k_{div1}(U_g - U_{mf}) \quad (\text{B.14})$$

where $(k_{div0}, k_{div1}) = (0.548, 0.027)$ for the FCC particles and $(k_{div0}, k_{div1}) = (0.815, 0.029)$ for the sand particles at $r/R = 0$. The division between two phases is different for different particles.

By using such a division, ε_{div} , for both FCC and sand particles the probability density function of the local voidage of the emulsion phase and that of the bubble phase could be found to satisfy the Beta distribution under various operating conditions. The complex double-peak probability density of the local voidage from ε_{mf} to 1 and its change could be quantified by the density function of a particular distribution, called the Coupled Beta distribution. This density function can be obtained by coupling two Beta probability density functions, one for the emulsion phase and another for the bubble phase, that is, in Eq. (B.10), taking

$$pr_b(\varepsilon) = \frac{\varepsilon^{\alpha_b-1}(1-\varepsilon)^{\beta_b-1}}{B(\alpha_b, \beta_b)} \quad (\text{Beta probability density function}) \quad (\text{B.15})$$

$$pr_e(\varepsilon) = \frac{\varepsilon^{\alpha_e-1}(1-\varepsilon)^{\beta_e-1}}{B(\alpha_e, \beta_e)} \quad (\text{Beta probability density function}) \quad (\text{B.16})$$

Thus

$$pr(\varepsilon) = f \frac{\varepsilon^{\alpha_e-1}(1-\varepsilon)^{\beta_e-1}}{B(\alpha_e, \beta_e)} + (1-f) \frac{\varepsilon^{\alpha_b-1}(1-\varepsilon)^{\beta_b-1}}{B(\alpha_b, \beta_b)} \quad \varepsilon_{mf} \leq \varepsilon \leq 1$$

(Coupled Beta probability density function) (B.17)

where

$$B(\alpha_k, \beta_k) = \frac{\Gamma(\alpha_k)\Gamma(\beta_k)}{\Gamma(\alpha_k + \beta_k)} \quad (k = e, b) \quad (\text{Beta function}) \quad (\text{B.18})$$

$$\Gamma(t) = \int_0^{\infty} x^{t-1} e^{-x} dx \quad t > 0 \quad (\text{Gamma function}) \quad (\text{B.19})$$

$$f = \frac{\varepsilon_b - \varepsilon_r}{\varepsilon_b - \varepsilon_e} \quad (\text{Emulsion phase fraction}) \quad (\text{B.20})$$

$$\alpha_e = \varepsilon_e \left[\frac{\varepsilon_e(1-\varepsilon_e)}{\sigma_e^2} - 1 \right] \quad (\text{B.21})$$

$$\beta_e = (1 - \varepsilon_e) \left[\frac{\varepsilon_e(1 - \varepsilon_e)}{\sigma_e^2} - 1 \right] \quad (\text{B.22})$$

$$\alpha_b = \varepsilon_b \left[\frac{\varepsilon_b(1 - \varepsilon_b)}{\sigma_b^2} - 1 \right] \quad (\text{B.23})$$

$$\beta_b = (1 - \varepsilon_b) \left[\frac{\varepsilon_b(1 - \varepsilon_b)}{\sigma_b^2} - 1 \right] \quad (\text{B.24})$$

Here ε_e and σ_e are the mean and variance of the Beta distribution for the voidage fluctuation in the emulsion phase and ε_b and σ_b are the mean and variance of the Beta distribution of the voidage fluctuations in the bubble phase, estimates of which may be given as

$$\hat{\varepsilon}_e = \frac{1}{m_1} \sum_{i=1}^{m_1} \varepsilon_{e(i)} \quad \text{and} \quad \hat{\varepsilon}_b = \frac{1}{m_2} \sum_{j=1}^{m_2} \varepsilon_{b(j)} \quad (\text{B.25})$$

$$\hat{\sigma}_e = \sqrt{\frac{1}{m_1 - 1} \sum_{i=1}^{m_1} (\varepsilon_{e(i)} - \hat{\varepsilon}_e)^2} \quad \text{and} \quad \hat{\sigma}_b = \sqrt{\frac{1}{m_2 - 1} \sum_{j=1}^{m_2} (\varepsilon_{b(j)} - \hat{\varepsilon}_b)^2} \quad (\text{B.26})$$

Figs. B.7 and B.8 show part of the experimental results achieved with two different particles. The voidage fluctuations, both in the emulsion phase and in the bubble phase, change with operating conditions. By increasing U_g in a moderate range, gradual increase is observed in the bubble phase fraction $(1 - f)$, the time-averaged voidage ε_r , the mean voidage of each phase ($\varepsilon_e, \varepsilon_b$), the mean variance σ , the variance for emulsion phase σ_e , and the variance for bubble phase σ_b , due to the stronger action of the gas. At higher gas velocities, though, these variables remain constant in the bed core, as shown in Fig. B.7. It can be seen from Figs. B.7 and B.8 that the two types of the particles provide different voidage fluctuations in the two phases. All these phenomena can be correlated with the operating conditions as follows.

$$f = A_{f(1)} + A_{f(2)} e^{\frac{(U_g - U_{mf})}{A_{f(3)}}} \quad (\text{B.27})$$

$$\varepsilon_b = A_{\text{void-b}(1)} + A_{\text{void-b}(2)} e^{\frac{(U_g - U_{mf})}{A_{\text{void-b}(3)}}} \quad (\text{B.28})$$

$$\varepsilon_e = A_{\text{void-e}(1)} + A_{\text{void-e}(2)} e^{\frac{(U_g - U_{mf})}{A_{\text{void-e}(3)}}} \quad (\text{B.29})$$

$$\sigma_b = A_{\text{var-b}(1)} + A_{\text{var-b}(2)} e^{\frac{(U_g - U_{mf})}{A_{\text{var-b}(3)}}} \quad (\text{B.30})$$

$$\sigma_e = A_{\text{var-}e(1)} + A_{\text{var-}e(2)} e^{\frac{(U_g - U_{mf})}{A_{\text{var-}e(3)}}} \quad (\text{B.31})$$

Table B.2 shows the values of the parameters in the above correlation at $r/R = 0$. The relation of the dense phase fraction and that of the saturated emulsion, described by Eq. (B.4), was found as

$$f = (A_{f\alpha(1)} + A_{f\alpha(2)}(U_g - U_{mf}))f^0 \quad (\text{B.32})$$

where at $r/R = 0$, for the FCC particles $(A_{f\alpha(1)}, A_{f\alpha(2)}) = (0.95, 1.17)$, and for the sand particles $(A_{f\alpha(1)}, A_{f\alpha(2)}) = (1.29, 0)$. Since $A_{f\alpha(2)} = 0$ for sand, the dense phase fraction is proportional to the assumed saturated emulsion fraction.

By using estimated values of f , α_e , β_e , α_b , and β_b obtained from Eqs. (B.20) to (B.24) and the corresponding correlations of the mean voidage and the variance in the two phases, the probability density of the local voidage was simulated with the density function described by Eq. (B.17). Fig. B.9 gives the comparison between the simulated results with the corresponding experimental data. The chi-square (χ^2) statistical test [19] shows a good agreement between the simulated and the experimental data. Therefore, the probability density of the local voidage from ε_{mf} to 1 for both the FCC and sand particles and its changes with operating conditions can be described and simulated effectively by the density function of the so-called Coupled Beta distribution.

B.5.5 Transition from bubbling to turbulent regime

Fig. B.10 shows the simulated evolution of the probability density function of the local voidage at $r/R = 0$, as described by Eq. (B.17). It can be seen from Fig. B.10 that the probability density of the bubble phase becomes higher and that of the dense phase becomes lower with increasing U_g . It can also be concluded from this figure that the gas-solid distribution evolves gradually from bubbling to turbulent regime. Nevertheless, two different state of gas-solid distribution can be observed in these regimes and this difference is distinct for each particle type.

In the case of FCC particles (Fig. B.10 a), the fraction of the emulsion phase reduces with increasing the gas velocity. However, in the bubbling regime the maximum density appears at ϵ_{mf} , while in the turbulent regime an apparent change in the shape of the probability density function can be observed and the maximum density gradually departs from ϵ_{mf} and the saturated emulsion tends to disappear due to more intensive action of gas. Moreover, the probability density of the bubble phase in fluidized FCC particles does not exhibit considerable difference in the turbulent regime which suggests that beyond U_c the excess gas enters and dilutes the emulsion rather than forming more bubbles and increasing the bubble phase fraction.

In the case of sand particles (Fig. B.10 b), increasing the gas superficial velocity results in decreasing the solid content of the bubbles and the bubble phase becomes more dilute. Upon approaching U_c the bubble phase displays noticeable change in its probability density. With increasing the gas velocity beyond U_c , the probability density of the pure bubble ($\epsilon = 1$) gradually rises and the voidage of the maximum probability density of the bubble phase approaches unity. Furthermore, the probability density of the emulsion phase does not show significant difference in the turbulent regime which suggests that at gas superficial velocities higher than U_c the excess gas enters the bubble phase and increases the bubble phase fraction rather than entering and diluting the emulsion.

The change in the state of the emulsion and bubble phases are more explicitly shown in Figs. B.11 a and B.11 b for FCC and sand particles, respectively. Fig. B.11 a demonstrates the change in the probability of the local voidage $\epsilon = \epsilon_{mf}$ for FCC particles and shows that the probability of the emulsion being at its saturation state ($\epsilon = \epsilon_{mf}$) is very high at low gas velocity and constantly decreases with increasing the gas velocity. At gas superficial velocity near U_c , this probability is very close to zero which indicates that the saturation emulsion almost diminishes at the transition from bubbling to turbulent. Fig. B.11 b shows the change in the probability of the local voidage $\epsilon = 1$ for sand particles and indicates that pure bubbles ($\epsilon = 1$) do not exist at low gas velocities. However, at gas superficial velocity near U_c , pure bubble phase begins to form and its probability increases with increasing the gas velocity.

B.5.6 Spatiotemporal Gas-Solid Distribution

According to Eqs. (B.11) and (B.17), the spatiotemporal gas-solid distribution between the two phases was statistically described and simulated by the dependence of the local voidage on the coordinate from the ideal centre of the emulsion phase element to the ideal centre of its neighbouring bubble, that is, in the vector $Y = \{(0, \varepsilon_{min}), (1/n, \varepsilon_1), \dots, (i/n, \varepsilon_i), \dots, (1, \varepsilon_{max})\}$, $(\varepsilon_{min}, 1)$ should be replaced with $(\varepsilon_{min}, \varepsilon_{max})$. Fig. B.10 shows the dependence of the local voidage ε , on the time coordinates i/n and the influence of the gas velocity at $r/R = 0$ for FCC and sand particles. It also indicates a considerable difference in the gas-solid distribution and two-phase flow structures, suggesting different dominant mechanisms influencing the gas-solid interactions for different particles.

The above description of the probability distribution of the local voidage and the spatiotemporal gas-solid distribution can contribute to further quantitative characterization of the gas-solid interaction, mass transfer and reaction rates in fluidized beds.

B.6 Conclusion

A probability distribution model of the local voidage was developed to describe and simulate the gas-solid distribution in the fluidized bed reactors. The two different particles tested

(FCC and sand) exhibited considerably different dynamic gas-solid distributions and two-phase flow structures, implying different dominant mechanisms ruling their gas-solid interactions. For FCC particles, the voidage of the emulsion phase with the highest probability is close to ϵ_{mj} in bubbling regime, increasing gradually in the turbulent regime due to more intensive action of gas. However, for the sand particles this voidage of the emulsion phase differs greatly from ϵ_{mj} . The bubble phase becomes dilute at higher U_g , and the amount of the pure bubbles increase gradually in turbulent regime.

The probability distribution function showed gradual evolution with gas superficial velocity, suggesting that there is no abrupt change in the two-phase flow structure in transition from bubbling to turbulent fluidization. However, in the case of FCC particles, the gas mostly enters and dilutes the emulsion phase constantly at velocities higher than U_c . For the sand particles, increasing the gas velocity beyond U_c results in forming more pure bubbles. The probability distribution function also showed a strong dependency on the radial position and particle type. By using the minimum probability method to identify the division between the emulsion and bubble phases, the voidage fluctuations of the two phases were found to follow Beta distribution, and the probability density function of the local voidage from ϵ_{mj} to 1 and its complex evolution from bubbling to turbulent fluidization regime could be effectively described and simulated by the Coupled Beta distribution. Such quantification further introduced statistically the spatiotemporal gas-solid distribution of the two-phase flow structure at time scale.

B.7 References

- [1] J.F. Davidson et al. (Eds.), Fluidization, 2nd ed., Academic Press, London, 1985.
- [2] J.E. Johnson, J.R. Grace and J.J. Graham, Fluidized-bed reactor model verification on a reactor of industrial scale, *A.I.Ch.E. J.*, 33(1986), 619 – 627.
- [3] M. Pell, Gas fluidization, Elsevier Sciences Publishers B.V., Amsterdam, 1990.
- [4] D. Kunii and O. Levenspiel, Fluidization Engineering, 2nd ed., Butterworth-Heinemann, Boston M.A., 1991.
- [5] R. Toei, and R. Matsuno, The coalescence of bubbles in the gas-solid fluidized bed, in: A.A.H. Drinkenburg (Eds.), Proc. Int. Symp. on Fluidization, Netherlands Univ. Press, Amsterdam, 1967.
- [6] M. Aoyagi and D. Kunii, Importance of dispersed solids in bubbles for exothermic reactions in fluidized beds, *Chem. Eng. Comm.*, 1(1974), 191-197.
- [7] J.R. Grace, Generalized models for isothermal fluidized bed reactors, Recent Advances in Engineering Analysis of Chemically Reacting System, John Wiley & Sons, New York, 1984, 237-255.
- [8] A.R. Abrahamson and D. Geldart, Behaviour of gas-fluidized beds of fine powders: Part II, voidage of the dense phase in bubbling beds, *Powder Technol.*, 26(1980), 47-55.

- [9] J. Chaouki, A. Gonzalez, C. Guy and D. Klvana, Two-phase model for a catalytic turbulent fluidized-bed reactor: application to ethylene synthesis, *Chem. Eng. Sci.*, 54(1999), 2039-2045.
- [10] Yu. A. Buyevich and Sh. K. Kapbasov, Random fluctuations in a fluidized beds, *Chem. Eng. Sci.*, 49(1994), 1229-1243.
- [11] J. H. Li, L. X. Wen, W. Ge, H. P. Cui and J. Q Ren, Dissipative structure in concurrent-up gas-solid flow, *Chem. Eng. Sci.*, 53(1998), 3367-3379.
- [12] A. Marzocchella, R. C. Zijerveld, J. C. Schouten and C.M. van den Bleek, Chaotic behavior of gas-solids flow in the riser of a laboratory-scale circulating fluidized bed, *A.I.Ch.E. J.*, 43(1997), 1458-1468
- [13] D. Musmarra, M. Poletto, S. Vaccaro and R. Clift, Dynamic waves in fluidized beds, *Powder Technol.*, 82(1995), 255-268.
- [14] D. Bai, A.S. Issangya and J.R. Grace, Characteristics of gas-fluidized beds in different flow regimes, *Ind. Eng. Chem. Res.*, 38(1999), 803-811.
- [15] H.P. Cui, J.H. Li, M. Kwauk, H. Zh. An, M. Chen, Zh. M. Ma and G.F. Wu, Dynamic behaviors of heterogeneous flow structure in gas-solid fluidization, A special issue of *Powder Technol.*, in press, 1999.

- [16] J. H. Li, L. X. Wen, G. H. Qian, H. P. Cui, M. Kwauk, J.C. Schouten and C.M. van den Bleek, Structure heterogeneity, regime multiplicity and nonlinear behavior in particle-fluid systems, *Chem. Eng. Sci.*, 51(1996), 2693-2698.
- [17] Z.L. Lehmann, *Testing statistical hypothesis*, 2nd ed., John Wiley & Sons, New York, 1986.
- [18] L. Reh and J. Li, Measurement of voidage in fluidized beds by optical probes, in: P. Basu, M. Horio, and M. Hasatani (Eds.), *Circulating Fluidized Bed Technology III*, Pergamon, Oxford, 1991, 163-170.
- [19] R.V. Hogg and E.A. Tanis, *Probability and statistical inference*, 3rd Ed., Macmillan, New York, 1977.

Table B.1 Size distribution of the bed materials

FCC		Sand	
Size(μm)	Percentage(%)	Size(μm)	Percentage(%)
20	1	90	2.2
40	7	180	4.36
80	50	250	5.84
105	22	417	28.7
149	20	595	16.5
		850	20.0
		1000	30.0

Table B.2 The values of parameters in Eqs. (B.27-B.31) ($r/R = 0$)

	FCC	Sand
$A_{f(1)}$	0	0.466
$A_{f(2)}$	1.00	0.534
$A_{f(3)}$	0.62	0.413
$A_{void-b(1)}$	0.784	1.0
$A_{void-b(2)}$	-0.139	-0.146
$A_{void-b(3)}$	0.272	4.439
$A_{var-b(1)}$	0.112	0.065
$A_{var-b(2)}$	-0.116	-0.017
$A_{var-b(3)}$	0.047	1.57
$A_{void-e(1)}$	ϵ_{mf}	$\epsilon_{mf} + 0.20$
$A_{void-e(2)}$	0.00061	-0.059
$A_{void-e(3)}$	-0.262	0.429
$A_{var-e(1)}$	0.025	0.086
$A_{var-e(2)}$	-0.02	-0.0408
$A_{var-e(3)}$	0.152	0.074

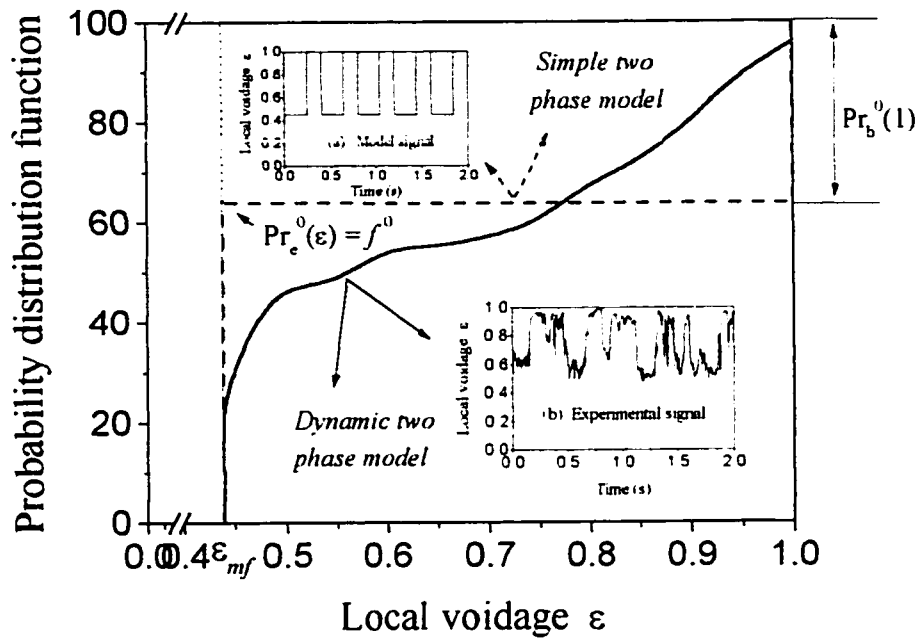


Figure B.1 Probability distribution model of the local voidage ϵ

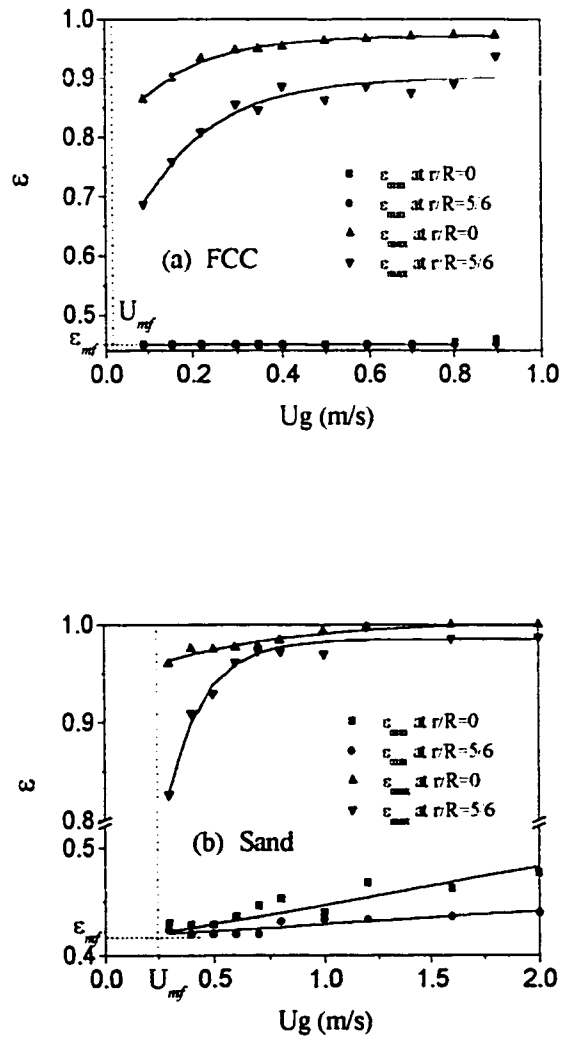


Figure B.2 Change in the minimum voidage of the emulsion phase, ϵ_{min} , and the maximum voidage of the bubble phase, ϵ_{max} , with U_g for FCC and sand particles ($r/R = 0$ and $r/R = 5/6$)

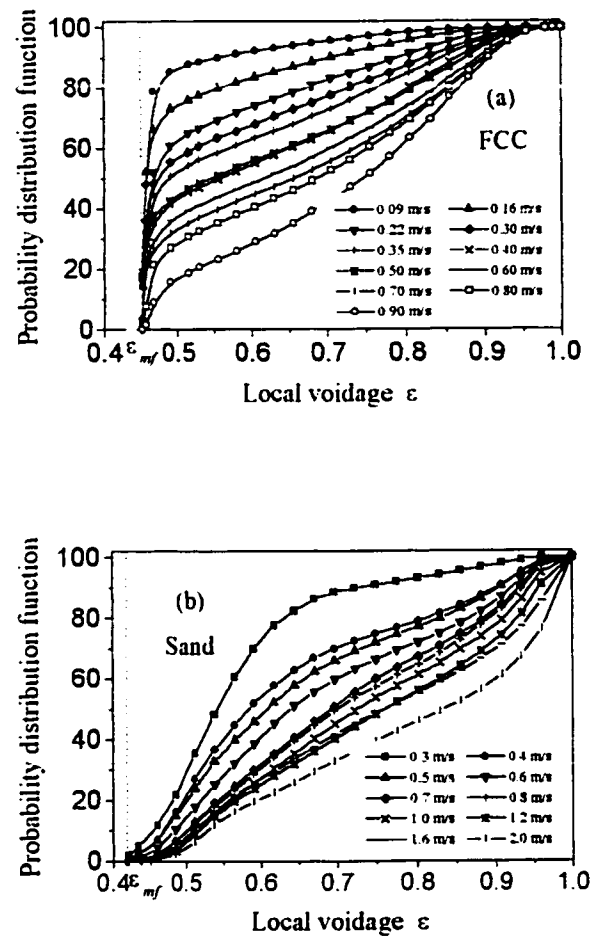


Figure B.3 Evolution of the probability distribution function of the local voidage with U_g at $r/R = 0$. (a) FCC; (b) sand

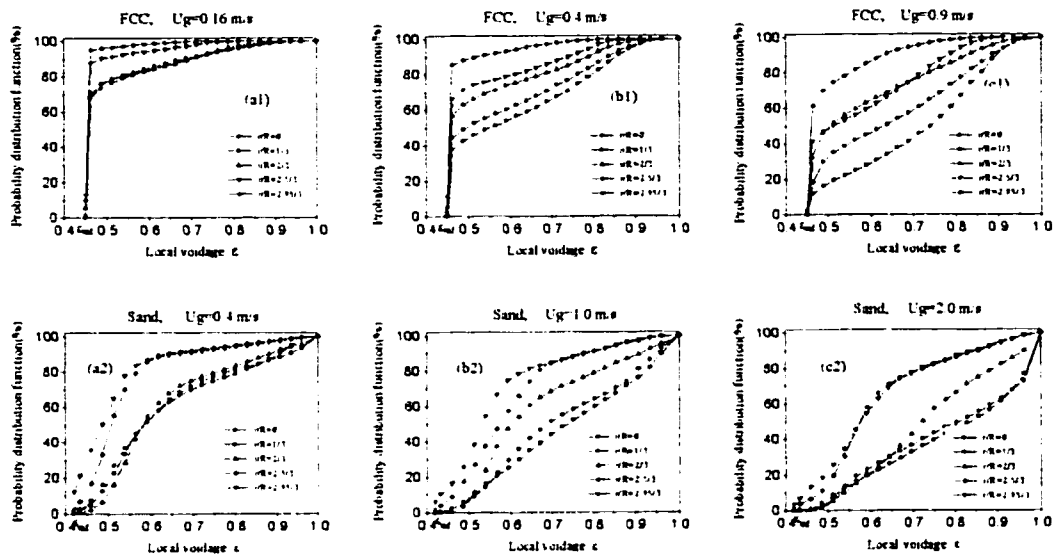


Figure B.4 Comparison between the probability distribution functions of the local voidage at different radial positions and different U_g . (a1), (b1), (c1) FCC; (a2), (b2), (c2) sand

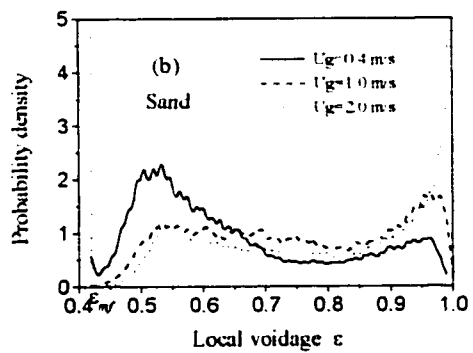
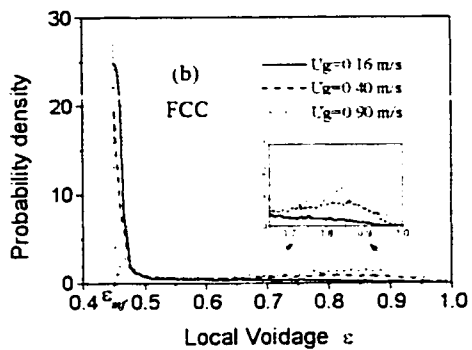


Figure B.5 Change in the probability density function of the local voidage with U_g at $r/R =$

0. (a) FCC; (b) sand

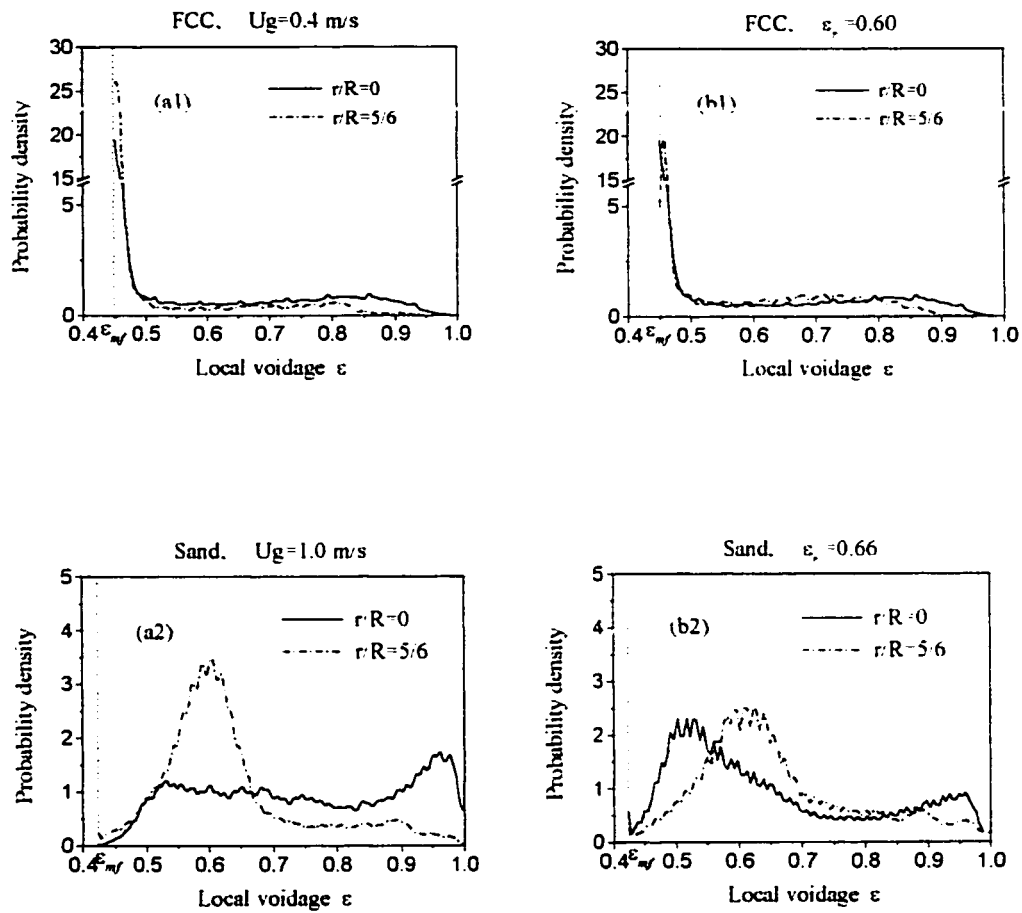


Figure B.6 Comparison between the probability density functions of the local voidage at different radial positions. (a1), (b1) FCC; (a2), (b2) sand; (a1), (a2) for the same U_g ; (b1), (b2) for the same time-averaged voidage

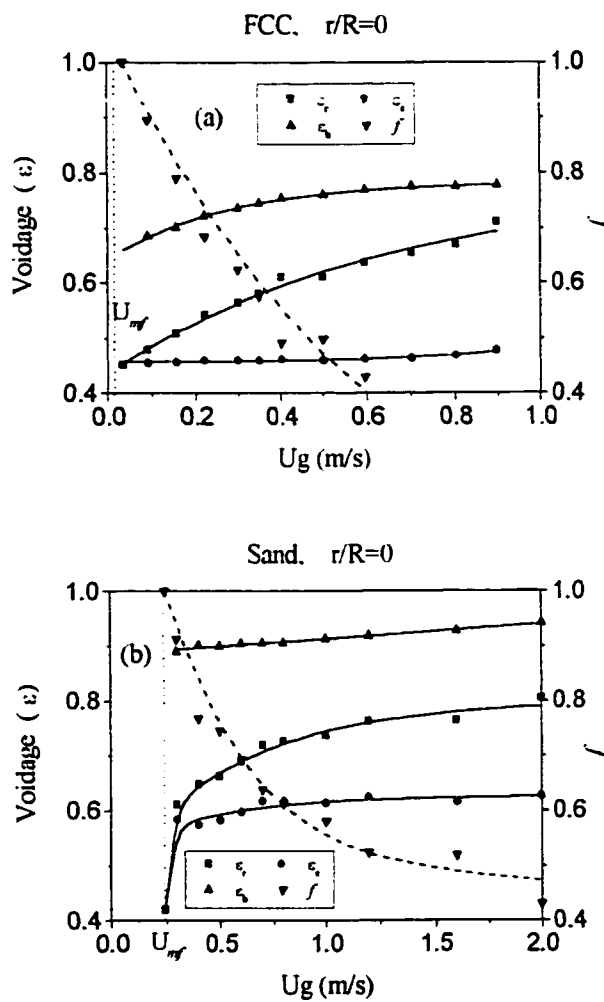


Figure B.7 Change in the emulsion phase fraction, the time-averaged voidage, and the mean voidages of the bubble phase and the emulsion phase with U_g at $r/R = 0$; (a) FCC; (b) sand

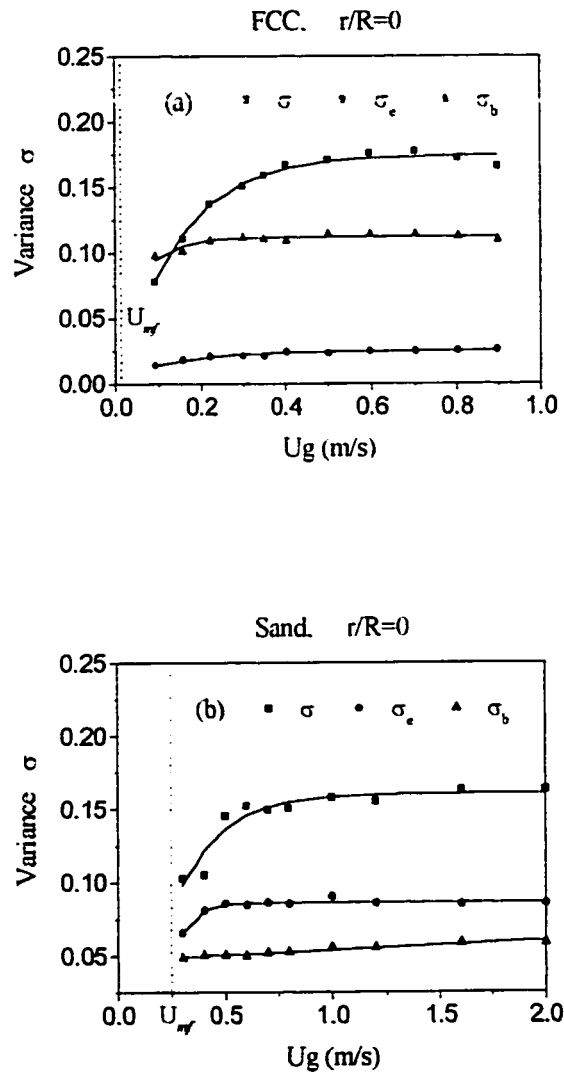


Figure B.8 Change in the mean variance of voidage fluctuations, and the variances of voidage fluctuations in the emulsion phase and the bubble phase with U_g at $r/R=0$. (a) FCC; (b) sand

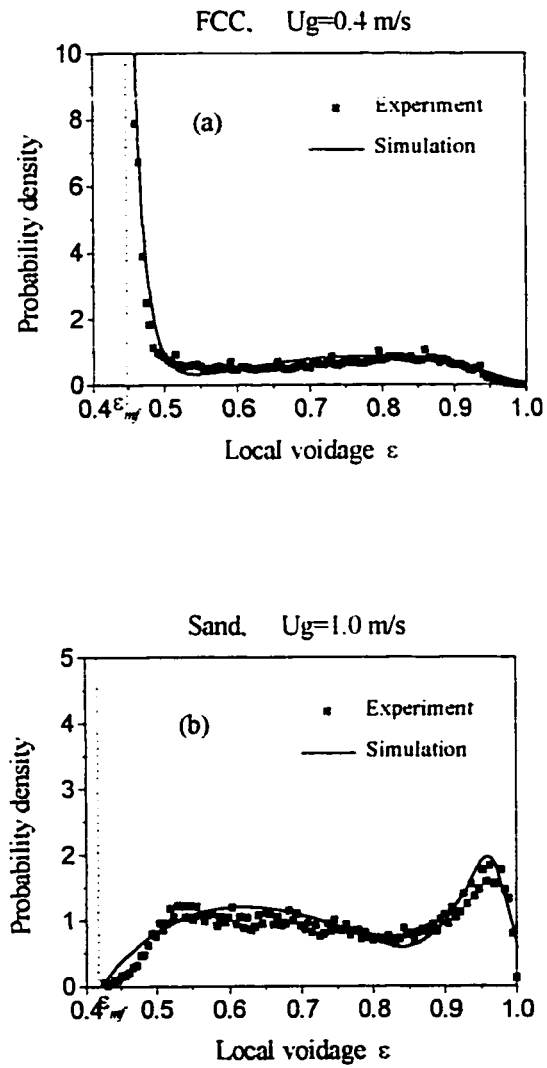


Figure B.9 Comparison between experimental and simulated probability density functions of the local voidage ($r/R = 0$)

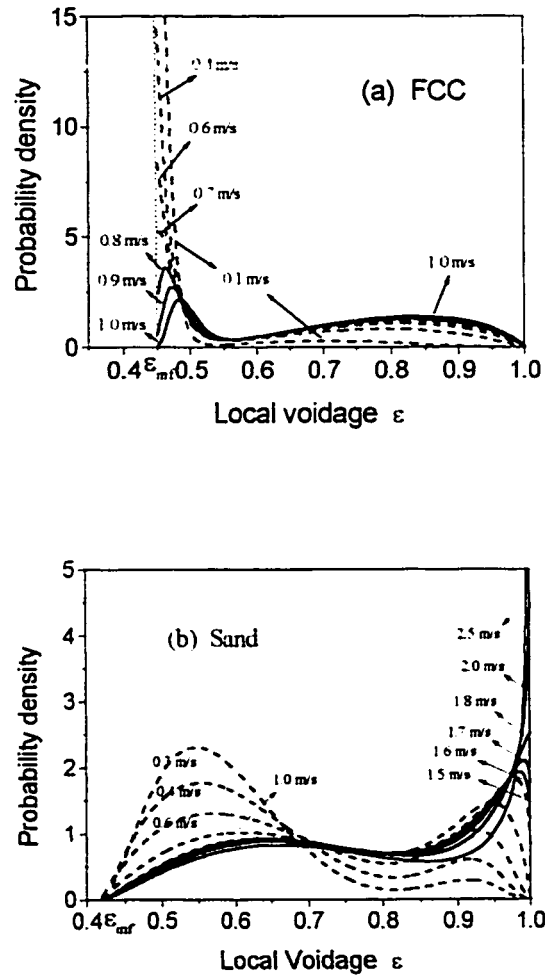


Figure B.10 Changes in the probability density function of the local voidage with increasing gas velocity ($r/R=0$; dash line: bubbling regime; line: turbulent regime)

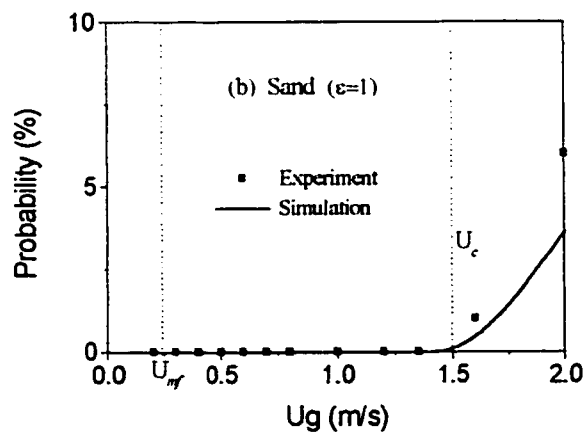
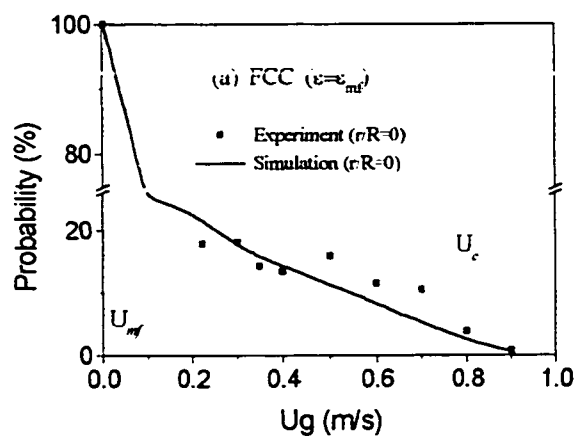


Figure B.11 Changes in the probability of the local voidage $\epsilon=\epsilon_{mf}$ for the FCC particles and of the local voidage $\epsilon=1$ for the sand particles.

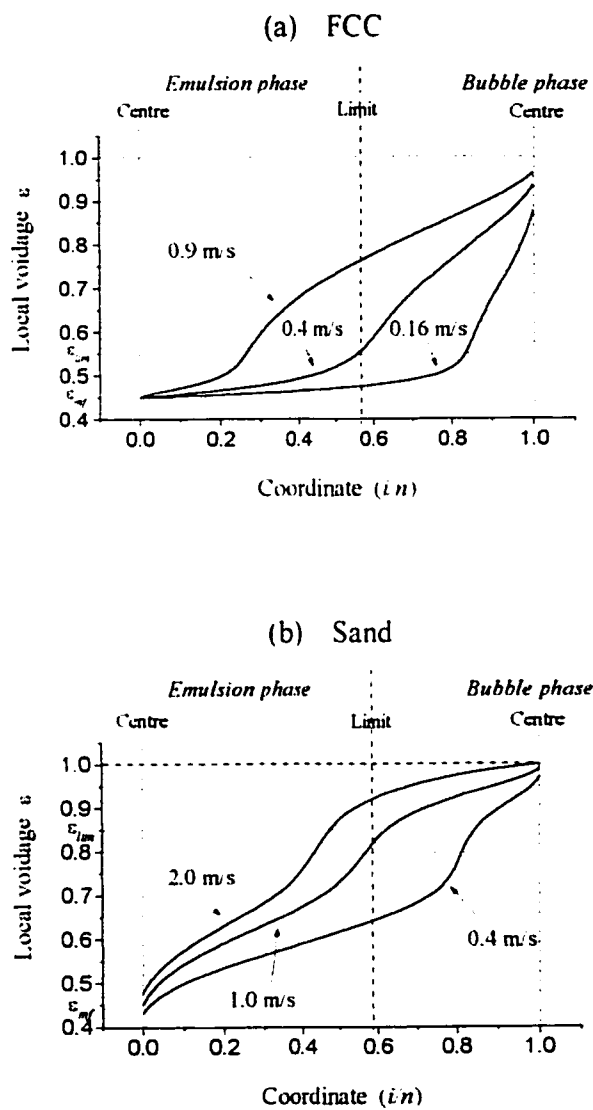


Figure B.12 Spatiotemporal voidage distribution between two centres of an emulsion phase element and its neighboring bubble phase at time scale ($t/R = 0$)

APPENDIX C : ON THE DISTRIBUTION OF GAS AND SOLIDS BETWEEN BUBBLE AND EMULSION IN FLUIDIZED BEDS

C.1 Abstract

This paper is devoted to quantitative understanding of the dynamic two-phase flow structure in the fluidized beds by the analysis of gas and solid volume fraction distributions in both bubble and emulsion phases. Experiments were carried out in an air-fluidized bed with FCC (Geldart A) and irregular sand (Geldart B) particles at different gas superficial velocities. A cross-optical fibre probe was used to measure the dynamic local particle concentration. The minimum probability method was introduced to identify the division between the emulsion phase and the bubble phase. The analysis of experimental data showed that the structures of bubble and emulsion phases possessed different dynamic behaviors for the two particle types. With increasing the gas superficial velocity, both the voidage and the variance of voidage fluctuations in each phase increases exponentially. The voidage fluctuations were more intense in the bed core than near the wall. Gas and solid volume fraction distributions in the two phases were shown to depend strongly on gas velocity, particle properties and radial position. A balance of the gas in the bubble and in the emulsion phases was observed for both the particles employed in this work. This gas balance occurred at different gas superficial velocity for different bed positions. The ratios of gas distributions in the two

phases showed a core-annulus distribution structure with a wider core for FCC particles than that of the sand. It was also shown that the bubbles contain more particles close to the centre for the FCC particles with respect to the sand particles at the studied conditions.

C.2 Introduction

Heterogeneous flow structure of the gas-solid fluidized beds show dynamic changes in both the dimension of cluster/bubble and the particle concentration (Cui et al., 1999a). The particles presented in the bubbles and the amount of gas in the emulsion phase greatly influence the practical operation of the fluidized beds. Dynamic behavior of the flow structure determines the complexity of gas-solid interaction in the bed. Heat and mass transfer and reaction exist not only at the bubble-emulsion interface, but also inside the two phases. It is necessary to understand the dynamic structure of each phase in order to quantify the complicated dynamic flow pattern and the reaction rate in the fluidized beds. The traditional simple two-phase models often neglect the effect of the presence of particles in the bubbles and the excess gas in the emulsion phase and only assume existence of the emulsion phase at minimum fluidization and solid-free bubbles. The cross-sectional average voidage $\bar{\epsilon}$ and the time-averaged voidage ϵ_t at a local position were commonly used to summarize the complicated two-phase flow structure. However, it is known that neither $\bar{\epsilon}$ nor ϵ_t can express the structure of the bubble and emulsion phases well and are sufficient to evaluate the complex gas-solid interactions in and between the two phases properly.

Therefore, more attempts are required to further understand the two-phase flow structure of such reactors and to optimize the design of the related process. In this paper, we studied the fluctuation properties of voidage in bubble and emulsion phases separately, and analysed the gas and solid volume fraction distributions in each phase in order to understand the dynamic two-phase flow structure of the fluidized beds.

C.3 Experiments

Experiments were carried out in a fluidized bed of 152 mm inside diameter and 1.5 m height at ambient temperature and pressure. Air was introduced into the bed through a nozzle type distributor placed above a stainless steel porous plate. The bed materials were either FCC particles ($\rho_p = 1673 \text{ kg/m}^3$, $d_p = 70 \text{ }\mu\text{m}$; Geldart A) or irregular sand particles ($\rho_p = 2650 \text{ kg/m}^3$, $d_p = 385 \text{ }\mu\text{m}$; Geldart B). The size distribution of solids is given in Table C.1. The static height of the bed was 300 mm. Different gas superficial velocities were employed, covering both bubbling and turbulent fluidization regimes. The transition gas velocity between bubbling and turbulent regime, determined by analyzing the pressure fluctuations of the bed, was found to be 0.77 m/s for FCC and 1.50 m/s for sand particles.

A cross-optic fiber probe (Reh and Li, 1991), with a defined measurement volume by its two cross fiber bunches of 0.8 mm in diameter, was placed at an axial position of 150 mm above the distributor and successively at different radial positions ($r/R = 0, 1/6, 1/3, 1/2, 2/3, 5/6$,

5.5/6, 5.9/6) to measure instantaneous particle concentration. PV-4A Particle Velocity Analyzer made by the Institute of Chemical Metallurgy, Chinese Academy of Sciences, was employed to obtain time series of dynamic voidage, and also served for the light resource and A/D transducer. More than 64,000 data were acquired with a sampling frequency of 488 Hz under various operating conditions.

C.4 Results and Discussion

C.4.1 Dynamic Flow Structure

The two-phase flow in the fluidized beds shows a complex dynamic behavior with various local voidages from ε_{mf} to 1 and a continuous gas-solid distribution between the two extremum (ε_{mf} and 1) (Cui et al., 1999b). Figure C.1 a, b shows that the dynamic flow structure is considerably different for different types of particles. However, it is traditionally assumed that the emulsion phase shows only the voidage of the minimum fluidization, ε_{mf} , and no particle presents in the bubble phase. The dynamic two-phase flow structures were often described with the local time-mean voidage, ε_r , expressed as follows

$$\varepsilon_r = f\varepsilon_{mf} + (1-f) \quad (\text{C.1})$$

where f^0 is the ideal dense phase fraction. Such a description can't reflect the actual process properly. In order to improve the dynamic two-phase flow structure, we identified the dynamic behavior in each phase separately, calculated the average of the voidages in each phase, and used them instead of ε_{mf} and 1 for emulsion and bubble phases, respectively. The time-averaged voidage, ε_r , can then be expressed as

$$\varepsilon_r = f\varepsilon_e + (1-f)\varepsilon_b \quad (\text{C.2})$$

where, f is the emulsion phase fraction, and ε_e and ε_b are the mean voidages of emulsion phase and bubble phase, respectively. Properties of the dynamic bubble and emulsion phases can therefore be further analyzed accordingly.

C.4.2 Partition of Two Phases

Since the heterogeneous flow structure exhibited a continuous gas-solid distribution between the voidages ε_{mf} and 1, an effective method has to be established first to discriminate the bubble phase from the emulsion phase. Further statistical analysis showed that the continuous gas-solid distribution exhibits a double-peak probability density function of the local voidage, from ε_{mf} to 1. Examples of such distributions are shown in Figures C.2 a, b. The peak at the left corresponds to the emulsion phase, whose average local voidage is about ε_{mf} for the FCC and about $\varepsilon = 0.55 (> \varepsilon_{mf})$ for the sand particles, at $r/R = 0$. The peak at the

right corresponds to the bubble phase, whose average local voidage is about $\varepsilon = 0.85$ (< 1) for the FCC particles and about $\varepsilon = 0.95$ (< 1) for the sand particles, at $r/R = 0$.

We thus introduced the minimum probability method to identify the exact partition between the emulsion phase and the bubble phase from such dynamic structure, that is, to take the local voidage point with the minimum probability density between two peaks (ε_{div}) as the limit between bubble and emulsion. This limit was found to be dependant on the operating conditions, position in the bed, and particle properties, and can be expressed as

$$\varepsilon_{div} = f(U_g, r/R, d_p, \rho_p, \dots) \quad (\text{C.3})$$

At $r/R = 0$, the average voidage of the boundary between the two phases, ε_{div} , is 0.56 for FCC and 0.81 for sand in the studied operating conditions. For different types of particles, the partition is different due to different dominant mechanism of the gas-solid interaction. As shown by the dashed lines in Figure C.3, the dense phase fraction, f , is different from the ideal dense phase fraction f^0 . The value of f is lower than f^0 for the FCC particles while it is higher than f^0 for the sand particles under various operating conditions. The dense phase fraction can be correlated as

$$f = (A_{f(1)} + A_{f(2)}(U_g - U_{mf}))f^0 \quad (\text{C.4})$$

where

$$f^0 = \frac{1 - \varepsilon_r}{1 - \varepsilon_{mf}} \quad (\text{C.5})$$

$(A_{r(1)}, A_{r(2)}) = (0.95, 1.17)$ for FCC and $(A_{r(1)}, A_{r(2)}) = (1.29, 0)$ for sand at $r/R = 0$. By using the above partition, the structure of bubble and emulsion phases can be better investigated.

C.5 Voidage Fluctuations in Two Phases

Properties of the voidage fluctuations in each phase was studied to understand the dynamic structure in the emulsion and bubble phases. The mean voidages and the variances of voidage fluctuations for each phase were calculated from the experimental data as follows,

$$\varepsilon_e = \frac{1}{n_1} \sum_{i=1}^{n_1} \varepsilon_{e(i)} \quad \text{and} \quad \varepsilon_b = \frac{1}{n_2} \sum_{j=1}^{n_2} \varepsilon_{b(j)} \quad (\text{C.6})$$

$$\sigma_e = \sqrt{\frac{1}{n_1} \sum_{i=1}^{n_1} (\varepsilon_{e(i)} - \varepsilon_e)^2} \quad \text{and} \quad \sigma_b = \sqrt{\frac{1}{n_2} \sum_{j=1}^{n_2} (\varepsilon_{b(j)} - \varepsilon_b)^2} \quad (\text{C.7})$$

where, σ_e and σ_b are the variances for voidage fluctuations in emulsion phase and bubble phase, respectively. Figures C.3 and C.4 show the mean voidage and variance of the voidage fluctuations obtained from the experimental data for the two types of the particles. For both particles, the mean voidage of the bubble phase ϵ_b were considerably lower than unity, indicating that a large amount of particles present within the bubbles. The presence of particles in the bubbles is more considerable for the FCC particles ($\epsilon_b < 0.8$). The mean voidages of the emulsion phase, ϵ_e , were far away from that of the minimum fluidization for sand particles, indicating that more gas enters the emulsion than that of the minimum fluidization. This value is very close to ϵ_{mf} for the FCC particles. Voidage fluctuations, both in emulsion phase and in bubble phase, change with operating conditions. An increase in U_g results in increasing all three kinds of voidages (the voidage of bubble phase, ϵ_b , the voidage of emulsion phase, ϵ_e , and the time-averaged voidage, ϵ_r) as well as increasing the bubble phase fraction ($1 - f$), as shown in Figure C.3. Figure C.4 illustrates that with increasing U_g , the variance of the voidage fluctuations in each phase increases exponentially. The variance of the bubble phase, σ_b , for FCC particles increases sharply at lower gas velocities due to the large amount of particles presented in bubbles. The variance of the emulsion phase, σ_e , for sand particles exhibits the similar sharp change at lower gas velocities due the large amount of gas presented in the emulsion phase. As a result, they led to a sharp exponential increase in the total variance σ . The fluctuations for the whole two-phase and each of the two phases also depend on the radial position. Figure C.4 also shows that the voidage

fluctuations are more intense and the variance is higher in the bed core than those near the wall.

Voidage fluctuations in each phase are different for the two particles, as shown in Figure C.3 and Figure C.4. For the FCC particles, a change in U_g hardly affects the voidage of the emulsion phase, ϵ_e . However, it causes a larger amount of particles enter into bubbles. As a result, the bubbles with relatively low voidage ($\epsilon_b < 0.8$) and high variance, σ_b , could be observed which greatly influence the motion of the bubbles and also the gas-solid interactions in the bed. Nevertheless, when increasing U_g from U_{mf} , the sand particles exhibited an abrupt increase in ϵ_e and a nearly linear increase in the voidage of bubbles, ϵ_b , which indicates that a lot of gas has entered and diluted the emulsion phase. It is worth mentioning that for the FCC particles the fluctuation intensity in bubble phase mainly influenced the fluctuation intensity of the overall two-phase structure while for the sand particles the fluctuations in emulsion phase mainly influence the fluctuation intensity of the two-phase structure. All these changes in the voidage fluctuations could be correlated as

$$\epsilon_b = A_{void-b(1)} + A_{void-b(2)} e^{\frac{(U_g - U_{mf})}{A_{void-b(3)}}} \quad (C.8)$$

$$\epsilon_e = A_{void-e(1)} + A_{void-e(2)} e^{\frac{(U_g - U_{mf})}{A_{void-e(3)}}} \quad (C.9)$$

$$\sigma_b = A_{\text{var-b}(1)} + A_{\text{var-b}(2)} e^{\frac{(U_g - U_{mf})}{A_{\text{var-b}(3)}}} \quad (\text{C.10})$$

$$\sigma_e = A_{\text{var-e}(1)} + A_{\text{var-e}(2)} e^{\frac{(U_g - U_{mf})}{A_{\text{var-e}(3)}}} \quad (\text{C.11})$$

where, at $r/R = 0$, for the FCC particles,

$$\begin{pmatrix} A_{\text{void-b}(1)} & A_{\text{void-b}(2)} & A_{\text{void-b}(3)} \\ A_{\text{void-e}(1)} & A_{\text{void-e}(2)} & A_{\text{void-e}(3)} \\ A_{\text{var-b}(1)} & A_{\text{var-b}(2)} & A_{\text{var-b}(3)} \\ A_{\text{var-e}(1)} & A_{\text{var-e}(2)} & A_{\text{var-e}(3)} \end{pmatrix} = \begin{pmatrix} 0.784 & -0.139 & 0.272 \\ \varepsilon_{mf} & 0.00065 & -0.262 \\ 0.112 & -0.116 & 0.047 \\ 0.0259 & -0.0253 & 0.1413 \end{pmatrix} \quad (\text{C.12})$$

and for the sand particles

$$\begin{pmatrix} A_{\text{void-b}(1)} & A_{\text{void-b}(2)} & A_{\text{void-b}(3)} \\ A_{\text{void-e}(1)} & A_{\text{void-e}(2)} & A_{\text{void-e}(3)} \\ A_{\text{var-b}(1)} & A_{\text{var-b}(2)} & A_{\text{var-b}(3)} \\ A_{\text{var-e}(1)} & A_{\text{var-e}(2)} & A_{\text{var-e}(3)} \end{pmatrix} = \begin{pmatrix} 1 & -0.146 & 4.439 \\ \varepsilon_{mf} + 0.20 & -0.059 & 0.043 \\ 0.065 & -0.017 & 1.57 \\ 0.086 & -0.0408 & 0.074 \end{pmatrix} \quad (\text{C.13})$$

Furthermore, gas and solid volume fraction distribution in the two phases were studied to quantitatively evaluate the gas-solid mixing in the two phases, and also to help in optimization of the operating process in gas-solid fluidized beds.

Furthermore, gas volume and solid volume distributions in two phases were studied to evaluate the gas-solid mixing and help to optimize the reaction process in gas-fluidized beds.

C.6 Gas Distributions in Two Phases

Total gas volume per unit volume of the bed was divided into two parts: one in the emulsion phase and another in the bubble phase. The ratio of the gas volume in the emulsion phase to the unit bed volume was defined as the bed voidage of emulsion phase, ϵ_{ge} , and the ratio of the gas volume in the bubble phase to the unit bed volume was defined as the bed voidage of bubble phase, ϵ_{gb} , i.e.,

$$\epsilon_{ge} = f\epsilon_e \quad (\text{C.14})$$

$$\epsilon_{gb} = (1-f)\epsilon_b \quad (\text{C.15})$$

and

$$\varepsilon_r = \varepsilon_{ge} + \varepsilon_{gb} \quad (\text{C.16})$$

A similar trend in the bed voidage was observed with a change in U_g for FCC and sand particles, as shown in Figure C.5. While increasing U_g , the bed voidage of the bubble phase, ε_{gb} , increases gradually as a larger amount of gas contributes to forming bubbles, and, therefore, the bed voidage of the emulsion phase, ε_{ge} , decreases gradually. At a certain superficial gas velocity, these two bed voidages became equal to each other (0.31 m/s for the FCC, 0.82 m/s for the sand, at $r/R = 0$), exhibiting a gas balance between the two phases, as shown in Figures C.5 a1, a2, b1. Such changes in the two bed voidages also show different for two particle types. For the sand particles a large amount of gas contributes to diluting the emulsion phase, while forming bubbles in the early bubbling regime. As a result, the bed voidage of emulsion phase, ε_{ge} , increases although its phase fraction, f , reduces. This fact explains why the time-averaged voidage increases sharply at low U_g , as shown in Figures C.5 a2, b2. After a transition gas velocity (about 0.32 m/s, at $r/R = 0$), developing bubbles is in full dominance, and the dense phase fraction gradually decreases with only a little change in the voidage, ε_r . Consequently, the bed voidage of the emulsion phase begins to decrease gradually, while the bed voidage of the bubble phase increases gradually with an increase in the bubble phase fraction. Nevertheless, for the FCC particles, the bed voidage of the emulsion phase monotonously decreases with increasing U_g .

For the two particles, the two bed voidages and their change with U_g depend strongly on the position in the bed, as illustrated in Figures C.5 a1, b1 and Figures C.5 a2, b2. They change faster on the core than near the wall with increasing U_g . Figure C.6 illustrates the gas velocities at which the two phases (bubble and emulsion) possess the equal gas volumes at different bed positions for the two particle types. The balance of the gas distribution in the two phases occurs at higher superficial gas velocity at radial positions close to the wall. Such a balance can be met in the bubbling fluidization regime at $r/R < 3/4$ for the FCC and $r/R < 1/2$ for the sand.

The ratio of gas distribution in the two phases (β_g) was further analyzed to understand the dependency of the gas distribution on both gas velocity and the bed position:

$$\beta_g = \frac{\varepsilon_{ge}}{\varepsilon_{gb}} \quad (\text{C.17})$$

The results showed that for both the FCC and sand particles the ratio β_g decreases with increasing U_g . Figure C.7 shows that there are fast changes in this ratio at low U_g (< 0.16 m/s for FCC; < 0.4 m/s for sand), corresponding to rapid exchanges in gas distribution between the two phases. As mentioned earlier, the ratio of gas distributions depends strongly on the radial position, suggesting a core-annulus structure. The value of β_g is low in the core and high near the wall. The wall restricts formation and development of the bubbles near itself. Thus, near the wall, the bubble phase shows a low phase fraction and low

voidage, and gas mainly presents the emulsion phase. Such a core-annulus gas distribution pattern in the two phases hinders the mixing and the reaction of the gas and solids well near the wall. Compared to the sand particles, β_g ratio for FCC particles show more definite core-annulus structure, with lower β_g ratio in the core and considerably higher ratios in the annulus section. The core section for FCC particles is wider (from $r/R = 0$ to about $r/R = 3/4$) compared to that of the sand (from $r/R = 0$ to about $r/R = 1/2$), as shown in Figures C.7 a, b. The ratio of the two bed voidages and their changes with U_g could be formulated as

$$\beta_g = \beta_{g0} + \frac{2\beta_{g1}}{\pi} \left(\frac{\beta_{g2}}{4(U_g - U_{mf})^2 + \beta_{g2}^2} \right) \quad (\text{C.18})$$

where, $(\beta_{g0}, \beta_{g1}, \beta_{g2}) = (0.3397, 3.7692, 0.08048)$ for FCC and $(\beta_{g0}, \beta_{g1}, \beta_{g2}) = (0.8625, 2.605, 0.12665)$ for sand, at $r/R = 0$.

C.7 Solid Distributions in Two Phases

Similarly, total solid volume per unit bed volume was divided into two parts. The ratio of the solid volume in the emulsion phase to the unit bed volume was defined as the bed solid volume fraction of the emulsion phase, ϕ_{pe} , and the ratio of the solid volume in the bubble phase to the unit bed volume defined as the bed solid volume fraction of the bubble phase,

ϕ_{pb} , i.e.,

$$\phi_{pe} = f(1 - \varepsilon_e) \quad (\text{C.19})$$

$$\phi_{pb} = (1 - f)(1 - \varepsilon_b) \quad (\text{C.20})$$

and

$$\phi_r = \phi_{pe} + \phi_{pb} \quad (\text{C.21})$$

The ratio of the bed solid volume fraction of the bubble phase to that of the emulsion phase was defined as the ratio of the solid distributions in the two phases

$$\beta_p = \frac{\phi_{pb}}{\phi_{pe}} \quad (\text{C.22})$$

By increasing U_g , the bubble phase fraction increases gradually, and more and more particles enter into the bubbles. As a result, the bed solid volume fraction in the bubble phase, ϕ_{pb} , gradually increases and the bed solid volume fraction in the emulsion phase, ϕ_{pe} , gradually decreases. These phenomena is shown in Figure C.8. For the sand particles, the bed solid volume fraction in the emulsion phase decreases sharply with increasing U_g at low gas velocities, mainly due to the large amount of gas which enters the emulsion phase. This change is rather gradual at high U_g , at which the bed solid volume fraction in the bubble phase is relatively low and nearly constant at higher U_g . However, for the FCC particles, the

bubbles contain more particles, leading to a relatively high bed solid volume fraction in the bubble phase, which is very close to the bed solid volume fraction of the emulsion phase at high gas velocities, as shown in Figure C.8 a. For both particles, the bed solid volume fractions in both emulsion and bubble phases also depend strongly on the radial position. At the same U_g , ϕ_{pe} shows the minimum and ϕ_{pb} shows the maximum at $r/R = 0$, indicating that gas has the strongest impact on solids at the bed centre.

Figure C.9 illustrates the ratio of the solid distributions in the bubble phase to those in the emulsion phase and their dependence on U_g and r/R . Such solid ratios gradually increase with increasing U_g and reaches the maximum at $r/R = 0$ for all gas velocities, indicating the intensive effect of gas on particles at this position. The changes in the ratio of the solid distributions in the two phases with U_g could be formulated by

$$\beta_p = \beta_{p0} + \beta_{p1} e^{\frac{(U_g - U_{mf})}{\beta_{p2}}} \quad (\text{C.23})$$

where, $(\beta_{p0}, \beta_{p1}, \beta_{p2}) = (0, 0.1024, -0.3513)$ for FCC and $(\beta_{p0}, \beta_{p1}, \beta_{p2}) = (0.218, -0.2156, 0.438)$ for sand at $r/R = 0$. Apparently, the solid ratio is higher for the FCC particles than for the sand particles, and the bubbles contain more particles in the case of FCC particles. Although the ratio of solid distributions in the two phases may depend on how to distinguish the bubble phase from the emulsion phase, there are considerable number of

particles in the bubbles for both types of particles, especially for FCC, as can be seen in Figure C.2. Particles in bubbles influence the motion of bubbles greatly, which should not be disregarded in quantification of the gas-solid interaction and the reaction in the fluidized beds.

C.8 Conclusion

The structures of the bubble and emulsion phases show different dynamic behaviors for the FCC particles and the sand particles. The voidages of the bubble phase are considerably lower than unity, especially for the FCC particles. The voidages of the emulsion phase are greatly higher than that of the minimum fluidization for the sand particles, but very close to ϵ_{mf} for the FCC particles. With increasing superficial gas velocity, both the voidage and the variance of voidage fluctuations in each phase increase exponentially. The fluctuation intensity of the overall two-phase structure was mainly influenced by the fluctuation intensity in the bubble phase for FCC but the fluctuation intensity in the emulsion phase for the sand particles. The voidage fluctuations were more intense in the bed core section than near the wall.

The gas and solid distributions in the two phases are shown to be strongly dependent on gas velocity, bed position and particle properties. Both gas and solid distributions in the emulsion phase decrease gradually, while those in the bubble phase increase gradually with

increasing gas velocity. A gas balance in the two phases was observed in the bed core regime for both particles in the studied conditions. The ratio of gas distributions in the two phases exhibits a core-annulus distribution structure, which is more obvious for the FCC particles than for the sand particles. More solids distribute in the bubble phase while closer to the bed centre. Bubbles exhibited higher ratio of particles for the FCC particles than for the sand particles.

C.9 References

Bai, D., Issangya, A.S. and Grace, J.R. (1999). Characteristics of gas-fluidized beds in different flow regimes. *Ind. Eng. Chem. Res.*, 38, 803-811.

Chaouki, J., Gonzalez, A., Guy, C. and Klvana, D. (1999). Two-phase model for a catalytic turbulent fluidized-bed reactor: application to ethylene synthesis. *Chem. Eng. Sci.*, 54.

Cui, H.P., Li, J.H., Kwauk, M., An, H.Zh., Chen, M., Ma, Zh.M., and Wu, G.F. (1999a). Dynamic behaviors of heterogeneous flow structure in gas-solid fluidization. *A special issue of Powder Technology to remember late Professor Soo*, submitted.

Cui, H.P., Mostoufi, N. and Chaouki, J. (1999b). Characterization of dynamic gas-solid distribution in fluidized bed. *Chemical Engineering Journal*, submitted.

Kunii, D. and Levenspiel, O. (1991). *Fluidization Engineering*, 2th Edition. Newton: Butterworth-Heinemann.

Li, J.H., Wen L.X., Ge W., Cui, H.P. and Ren J.Q. (1998). Dissipative structure in concurrent-up gas-solid flow. *Chem. Eng. Sci.*, 53(19), 3367-3379.

Li, J.H., Wen L.X., Qian G.H., Cui, H.P., Kwauk, M., Schouten, J.C. and van den Bleek C.M. (1996). Structure heterogeneity, regime multiplicity and nonlinear behavior in particle-fluid systems. *Chem. Eng. Sci.*, 51, 2693-2698.

Pell, M. (1990). *Gas fluidization*. Amsterdam: Elsevier Sciences Publishers B.V.

Reh, L. and Li, J. (1991). Measurement of voidage in fluidized beds by optical probes. *Circulating Fluidized Bed Technology III*, eds: Basu, P., Horio, M. and Hasatani, M., Pergamon, Oxford, 163-170.

Table C.1 Size distribution of the bed materials

FCC		Sand	
Size(μm)	Percentage(%)	Size(μm)	Percentage(%)
20	1	90	2.2
40	7	180	4.36
80	50	250	5.84
105	22	417	28.7
149	20	595	16.5
		850	20.0
		1000	30.0

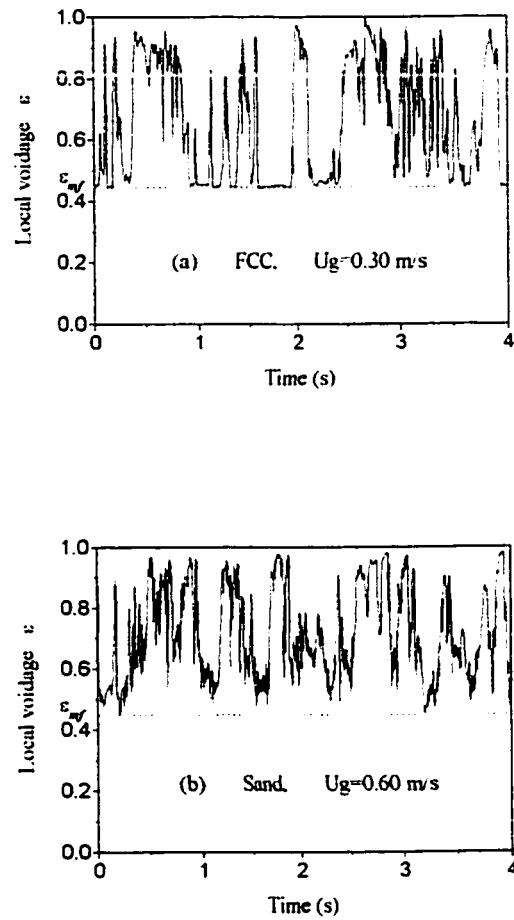


Figure C.1 Comparison of the voidage fluctuations for the FCC and sand particles ($r/R=0$).

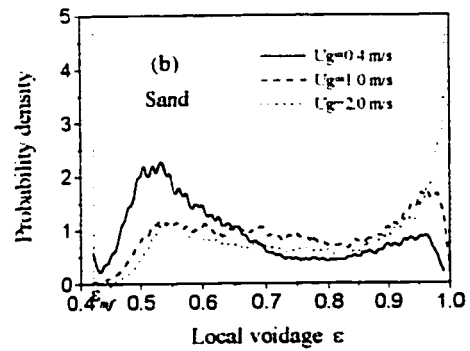
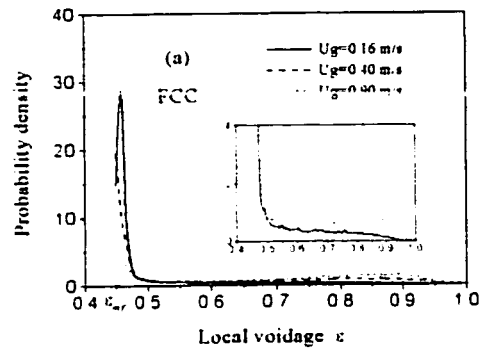


Figure C.2 Changes in the probability density functions of local voidages with U_g ($r/R=0$; a for the FCC; b for the sand).

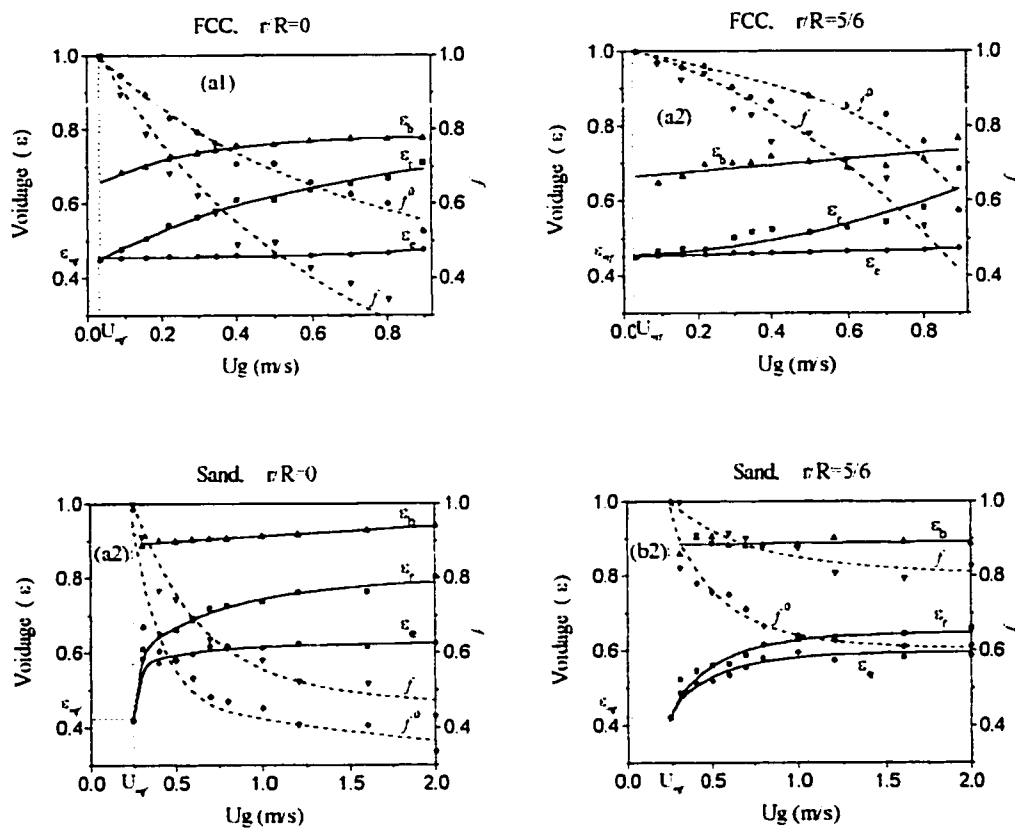


Figure C.3 Changes in the emulsion phase fraction, the time-averaged voidage, and the mean voidages of bubble phase and emulsion phase with U_g and r/R (a1, b1 FCC; a2, b2 for the sand).

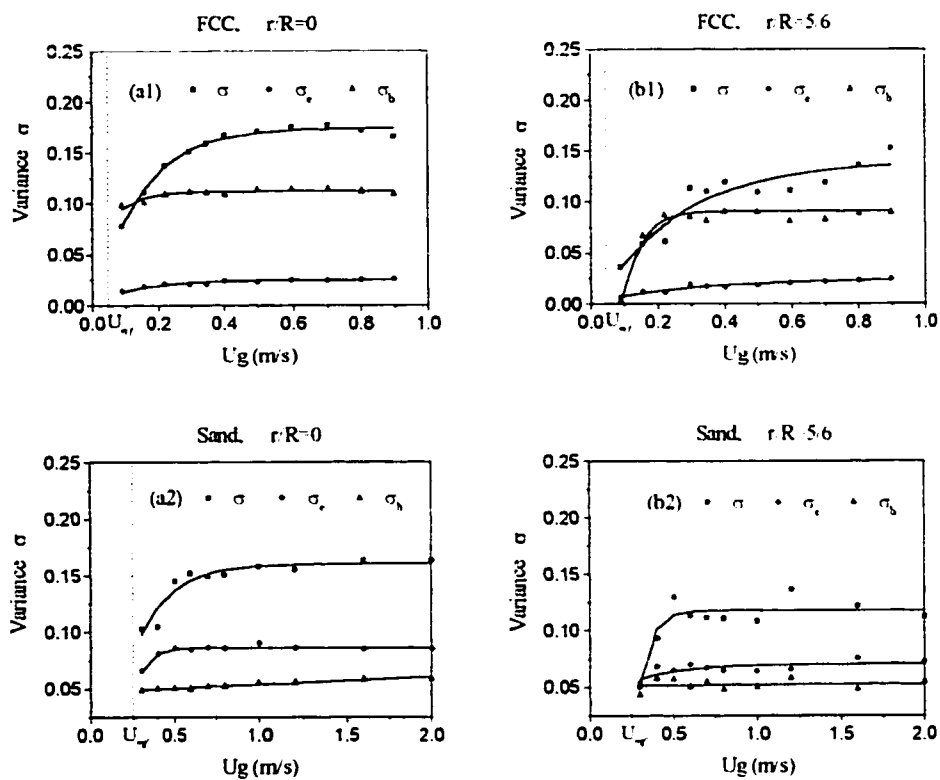


Figure C.4 Changes in the mean variances of voidage fluctuations, and the variance of voidage fluctuations in emulsion phase and bubble phase with U_g and r/R (a1, b1 for the FCC; a2, b2 for the sand).

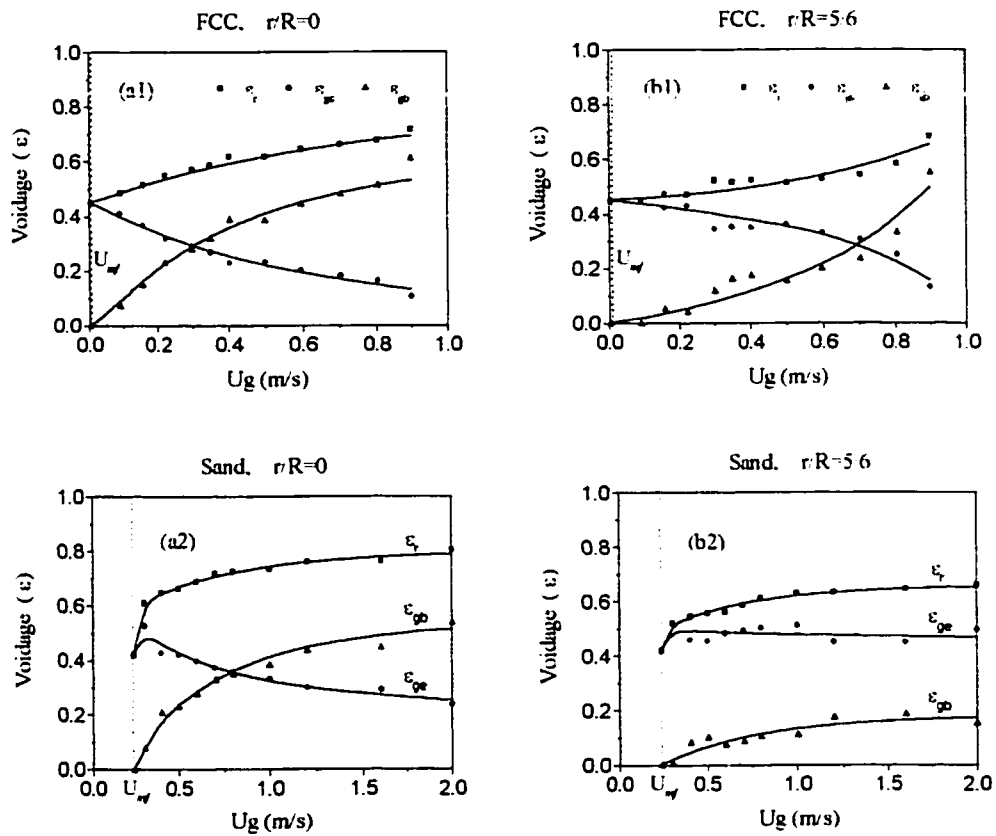


Figure C.5 Changes in the time-mean voidages ϵ_r , and the two bed voidages with U_g and r/R (a1, b1 for FCC; a2, b2 for sand)

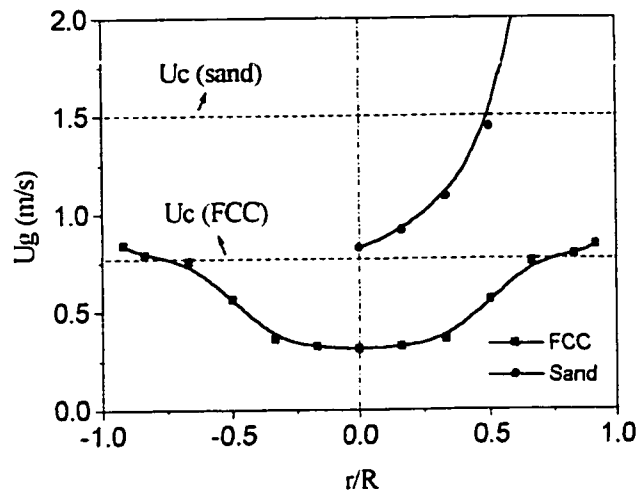


Figure C.6 Superficial gas velocities for the equal gas distribution between two phases at different bed positions for two particles

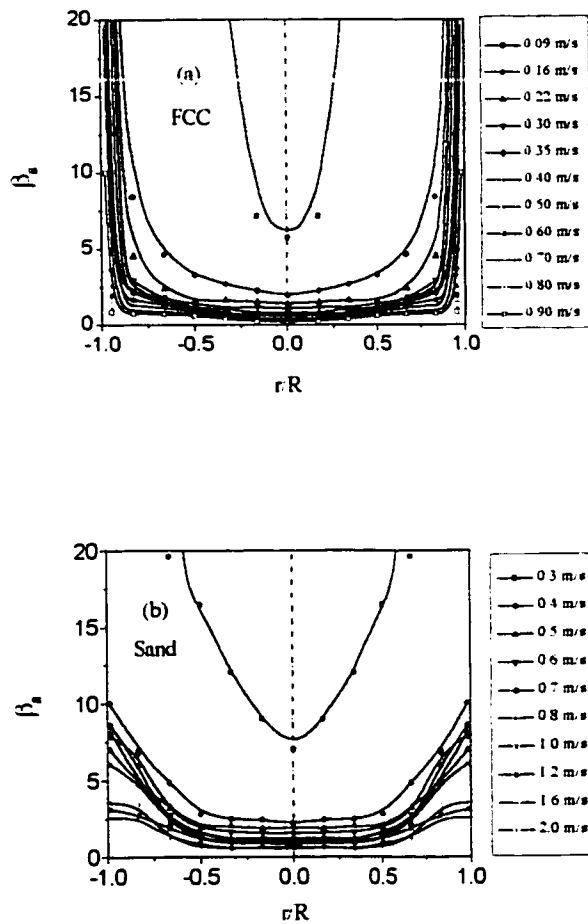


Figure C.7 Ratio of bed voidages of emulsion phase to those of bubble phase and the dependence on U_g and bed positions (a for the FCC; b for the sand).

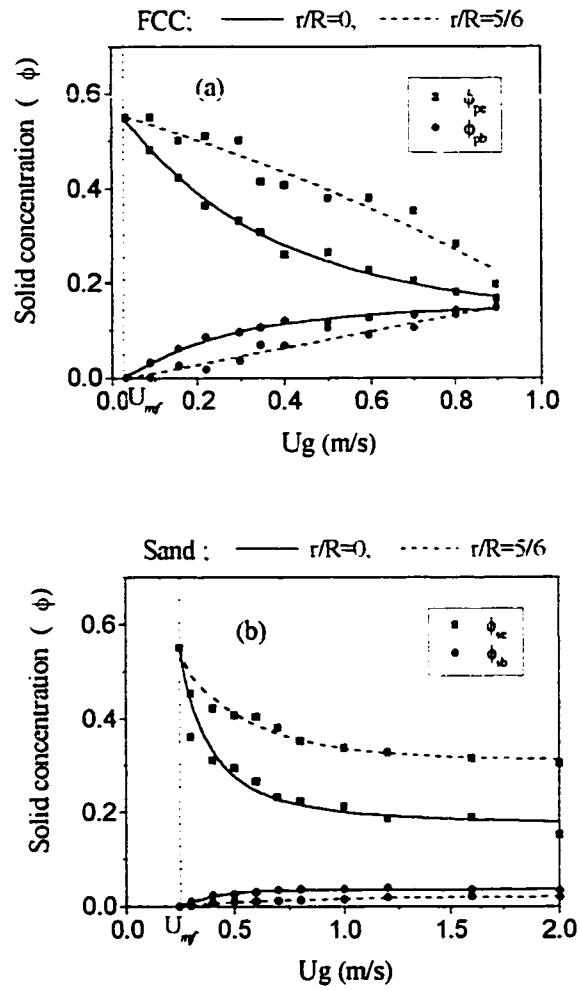


Figure C.8 Changes in bed solid volume concentrations of emulsion phase and bubble phase with U_g (a for the FCC; b for the sand).

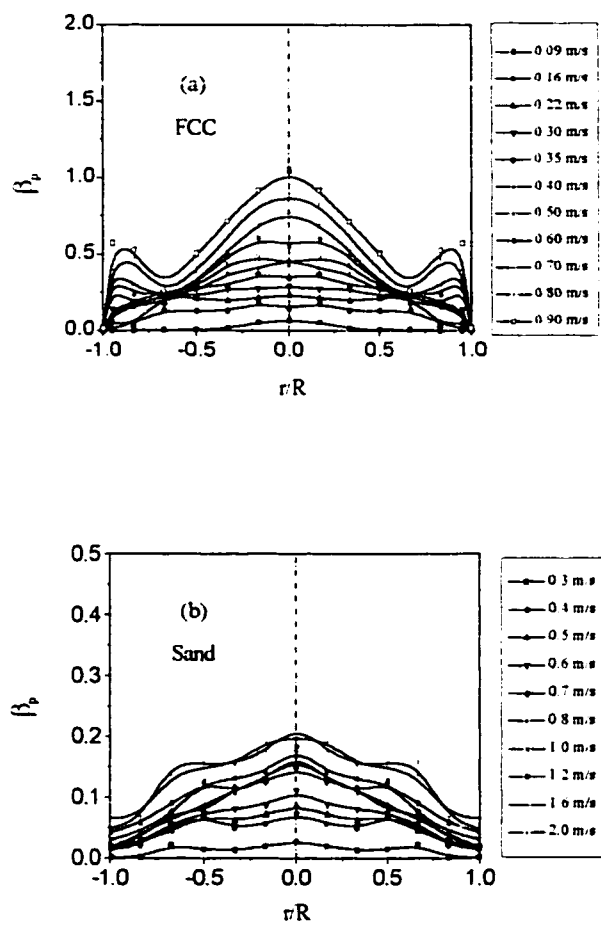


Figure C.9 Ratios of solid distributions of bubble phase to those of emulsion phase (a for the FCC; b for the sand).